THE

MER DE GLACE

WHERE THE CREEP OF GLACIERS

WAS FIRST STUDIED

CREEP AND FRACTURE OF ICE
AND
SURFACE STRAIN MEASUREMENTS ON GLACIERS AND SEA ICE

by

DOUGAL J. GOODMAN B.A.

A dissertation submitted for the degree of
Doctor of Philosophy
in the University of Cambridge

Christ's College,
Cambridge

March 1977

CREEP AND FRACTURE OF ICE
AND
SURFACE STRAIN MEASUREMENTS ON GLACIERS AND SEA ICE

by

DOUGAL J. GOODMAN B.A.

A dissertation submitted for the degree of
Doctor of Philosophy
in the University of Cambridge

Christ's College,
Cambridge

March 1977

PREFACE

This thesis is an account of my work while a research student in the Physics and Chemistry of Solids Group, Cavendish Laboratory, University of Cambridge in the period October 1973 to March 1977 under the direction of my supervisor Professor D. Tabor.

The thesis describes my original work except where acknowledgement has been made in the text. It does not exceed 60,000 words in length and has not been or is being submitted to any other University for any degree or other qualification.

D. J. Goodman

March 1977

D.J. Goodman

SUMMARY

The thesis is divided into two parts. Part I examines the creep and fracture properties of polycrystalline ice, while part II outlines a new technique for surface strain measurements on glaciers and sea ice.

The possible creep mechanisms (collapse, proton rearrangement controlled glide, lattice resistance controlled glide, and diffusional creep) in polycrystalline ice are critically reviewed and discussed. Constitutive equations for each mechanism are presented and used to construct a diagram, or deformation mechanism map, which illustrates on axes of homologous temperature and normalised stress, the regimes where each mechanism dominates over the others. The diagram is used to suggest the possible creep mechanisms in the Antarctic ice sheet at Byrd station, and in an ice shelf.

Glen's picture of a unique barrier to dislocation motion in the ice lattice due to the random proton arrangement is quantified, and the statistical results obtained are found to agree with those of the Whitworth, Paren, and Glen model. The results for the dislocation velocity as a function of stress, show that it is likely that proton rearrangement close to the dislocation is faster than the average in the lattice.

The stress required to make a single crack, of known dimensions, in an ice block propagate is discussed in terms of Irwin fracture toughness concepts. Preliminary results from experiments to measure the stress intensity factor at failure, K_{1c}, and the crack extension force, G, are also given.

Part II presents the results from a number of field experiments, in which continuous observations of surface strain changes on sea ice, glaciers, and in a rock tunnel very close to a sliding glacier were made. The results show that a geophysical wire strainmeter can be successfully used to make rapid determinations of the strain rates on the surface of glaciers and sea ice. The data collected show large amplitude strain changes (5×10^{-6}) in the sea ice in Bylot Sound, NW Greenland, due to long period waves in the bay (these may ultimately be responsible for the break-up of the ice; they have also been observed in data collected in Forteau Bay, Labrador presented here); surface strain

changes on the Barnes Ice Cap, Baffin Island; and possible stick-slip events between the glacier and its bedrock under the glacier d'Argentière in the French Alps. A design for a more portable instrument (which uses an Invar rod as a length standard) is also given.

ACKNOWLEDGEMENTS

Professor D. Tabor, my supervisor, has given me constant encouragement and been infinitely patient in allowing me to follow an independent line of research somewhat outside the work of his group. I am grateful for this freedom; I have learnt much by making my own mistakes.

I also thank Dr L.M. Brown (who was my supervisor while Professor Tabor was away) for his guidance.

The direction of my work has been strongly influenced by Prof. M.F. Ashby, of the Department of Engineering, who first suggested that I should construct a deformation map for ice. This has provided a framework in which to explore the creep properties of ice, and led to my interest in dislocation motion. The statistical model described in Chapter three, was the result of prolonged discussions with Dr H.J. Frost, also of the Department of Engineering. Dr Frost was responsible for writing the Fortran program used to plot the deformation maps. I am also grateful to Drs. Whitworth, Paren, Glen and Homer (University of Birmingham) for helpful discussions.

I owe much thanks to Dr G. de Q. Robin, Director of the Scott Polar Research Institute for allowing me to use the facilities of the Institute. Access to the library and use of an office have kept me in touch with the ice literature, and given me the opportunity to meet many workers from abroad who have called in to enjoy the warm and friendly atmosphere of the Institute. I have enjoyed many discussions with Dr. Robin on glacier sliding, and sea ice. I thank him for his permission to analyse the data collected by the SPRI sea ice group in Labrador in 1975.

The strain programme was the result of discussions with Dr. R. Bilham (then Department of Geodesy and Geophysics, and now at Lamont Doherty Observatory) while I was an undergraduate. It was his efforts, and those of Alistair Allan (SPRI) which enabled me to put my ideas into practice. Alistair Allan organised, and led the field trip to NW Greenland, and taught me much about the organisation of field work.

Dr. G. C. P. King (Department of Geodesy and Geophysics) continued to encourage and support my interest in the use of wire strainmeters in glaciology after Dr. Bilham had left. I am very grateful for his help, and in particular for coming with me to Argentière to install the strainmeters under the glacier.

The Barnes Ice Cap experiment would not have been possible without the field support arranged and organised by Dr G. Holdsworth (Dept. of Environment, Ottawa), and Keith Evans (Dept. Geodesy and Geophysics) who installed the strainmeters.

Professor R. Vivian kindly arranged access to the tunnels under the glacier d'Argentière. I have had fruitful discussions with him, and other members of his group.

John Beavan introduced me to the horrors of the University's IBM 370, and allowed me to use his programs to analyse the Labrador data after they had been digitised by Heather Woods and Brenda Burton.

I have enjoyed discussions about sea ice problems with Vernon Squire and Dr P. Wadhams of SPRI.

Denis Buckley worked very hard to build parts of the fracture apparatus and the four 1 m strainmeters.

G. Ballard spent long hours servicing the electronics for the strainmeters for which I am very grateful.

Many others have helped me with the strain experiments. I would like to thank John Horsfall, Russ Evans, Gareth John, Terry Ridings, and the members of the Cambridge East Greenland Expedition 1974.

I must thank those members of PCS, SPRI and BAS who have provided encouragement during the ups and downs of the past three-and-half years. Many thanks to Brian Briscoe, Andrew Briggs, Jacob Klein, Mike Steward, and Stephen Kreminzter of PCS, Kristin Hollick, Chris Neal, and Dave Meldrum of SPRI, and Chris Doake and Charles Swithinbank of BAS.

Last, but not least, I am very grateful to friends who have helped in the last few weeks by typing or checking for errors. Thanks to - Penny Butler, Chris Hope, Mike Grossbard, Ann Robinson and Elaine Lingham. Alan Peck printed the plates.

I was supported for three years by the Science Research Council, and between October 76 and February 77 by a grant from the Cambridge Philosophical Society. The Royal Society has made three generous grants for equipment and field expenses to support the strain work. Without this support much of the strain work described would not have been possible. My college, and the Philosophical Society have made contributions towards my travel expenses.

CONTENTS.

CHAPTER ONE

INTRODUCTION

Chapter 1

INTRODUCTION

1. OUTLINE OF THE THESIS.

The thesis is divided into two parts. Part I examines the creep and fracture properties of polycrystalline ice. Part II summarises the results from field experiments in Greenland, Canada, and France which were designed to evaluate a new method for the rapid determination of surface strain rates on glaciers and sea ice. How the different chapters relate to each other is shown in figure 1.01.

Part I relies heavily on the work of my predecessors in the Physics and Chemistry of Solids Group, P. Barnes and J. C. F. Walker (Barnes, 1968; Walker, 1970), who, by careful and painstaking experimental work, made an accurate description of how ice creeps over a wide temperature and stress range. This augmented the foundations laid down by Glen (1955) and Steinemann (1958) in the fifties. Their results are summarised in Barnes, Tabor and Walker (1971).

The book by Hobbs (1974) has provided an invaluable, comprehensive, and critical guide to the ice literature. The book by Fletcher (1970), and the review article by Glen (1974) have also been most useful.

In chapter two the possible creep mechanisms in polycrystalline ice are reviewed, and the constitutive equations given for each mechanism are used to construct diagrams or deformation mechanism maps (Ashby, 1972). The maps illustrate the creep behaviour over all feasible stresses and temperatures. An example is given in figure 1.02.

Strong support is given to Glen's model of dislocation motion in ice. Glen (1968) has pointed out that when a dislocation moves through the ice lattice Bjerrum (figure 1.03) or ionic defects are created unless the proton configuration is rearranged ahead of the dislocation. Other reviews (Weertman, 1973; Langdon, 1973) suggest that dislocation motion in ice is described by diffusion controlled climb. If the diffusion constant is independent of hydrogen fluoride doping (Blicks, Dengel and Riehl, 1966),

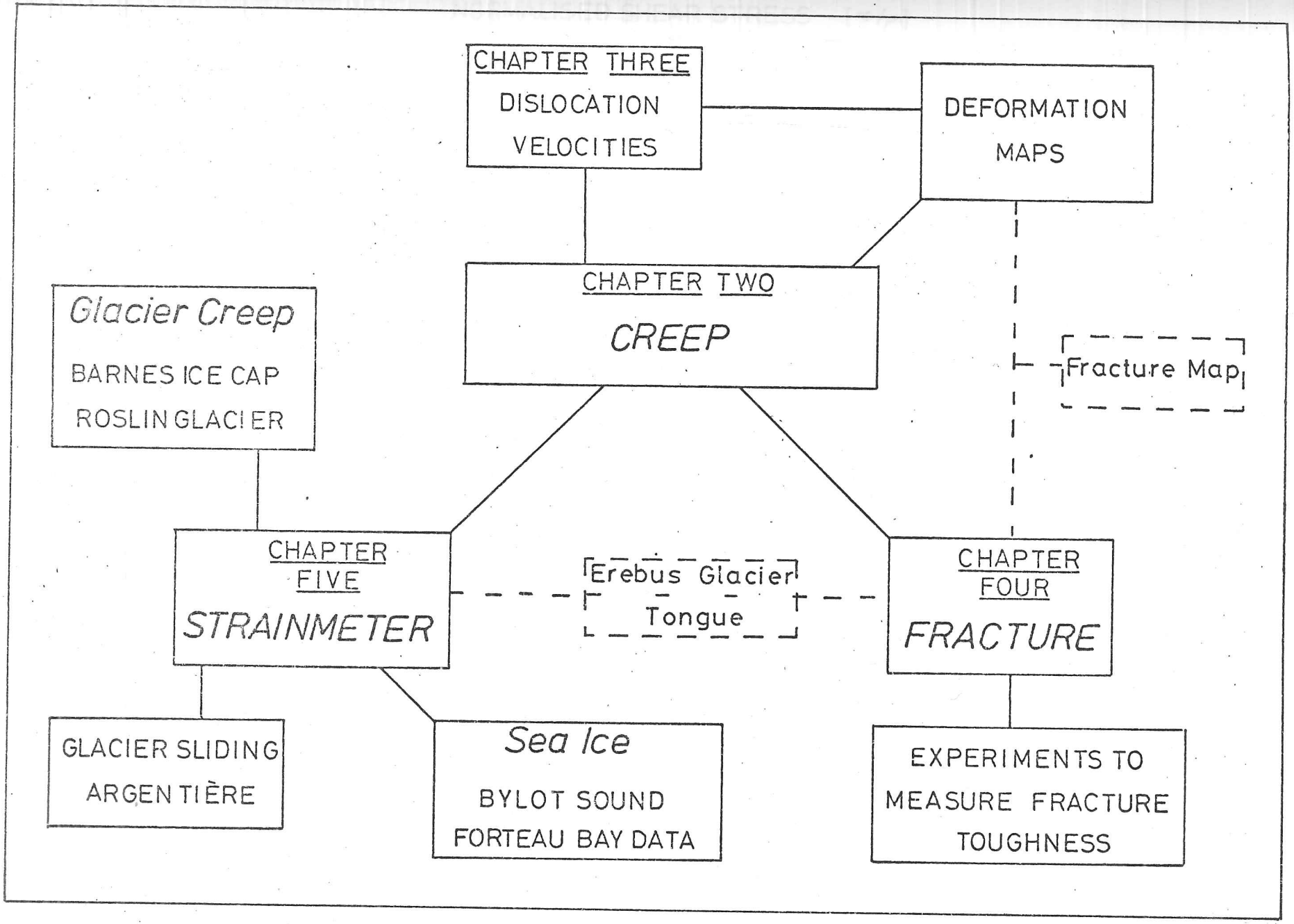

Figure 1.01; The relation of the different chapters to each other.
(the dashed lines show future work)

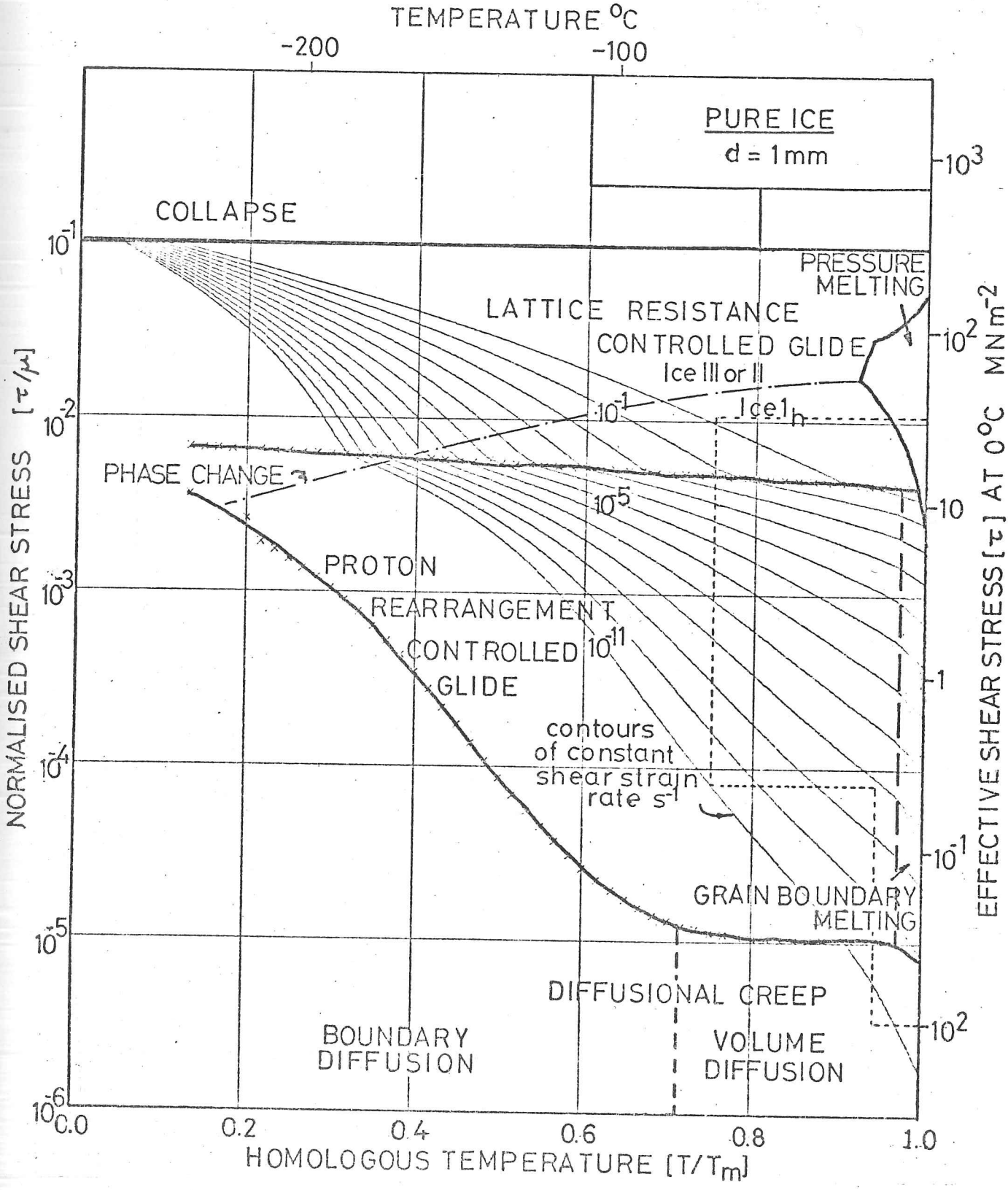

Figure 1.02; A Deformation Map for Ice. The constitutive equations used to construct the map are described in chapter two.

a climb controlled mechanism cannot account for the observation of Jones and Glen (1968; 1969) that HF doping enhances the creep rate. However the evidence is not conclusive for two reasons. Firstly because the activation energies for creep, diffusion, and electrical properties are more or less the same (which would suggest the same physical process operates), and secondly because a satisfactory quantitative model for Glen's picture does not yet exist. Whitworth, Paren, and Glen (1976) attempt to do this, but find it necessary to assume that the proton rearrangement rate close to the dislocation is faster than it is in the bulk of the ice. In chapter 3, a statistical calculation is presented which arrives at the same result as Whitworth et al by a different route.

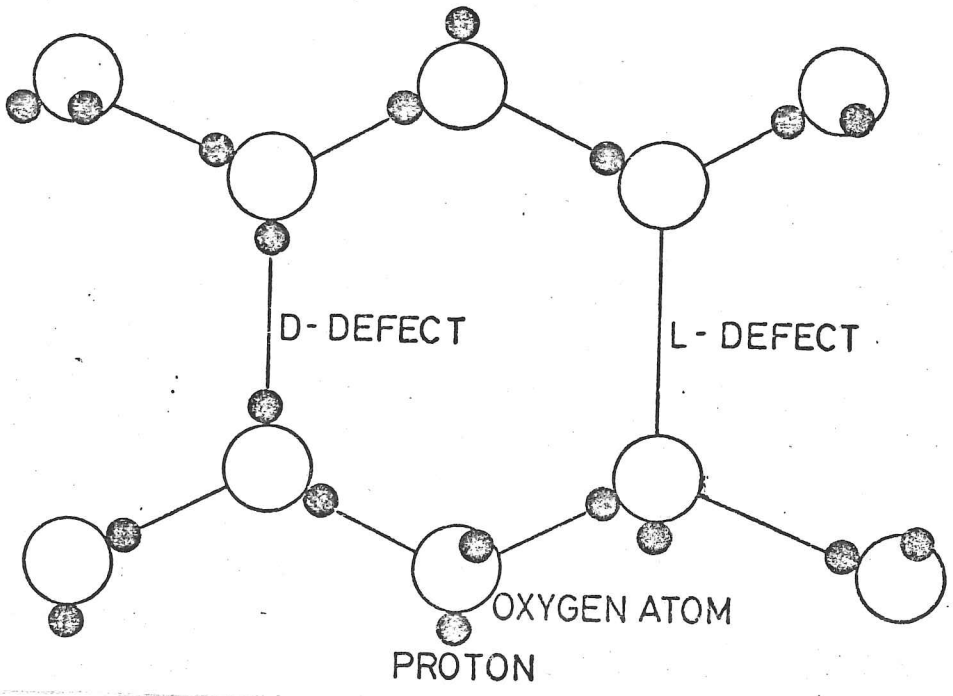

Figure 1.03; Bjerrum Defects. L - Defect (from the German Leer meaning empty) D - Defect (Doppelt meaning double).

In the construction of the map a semi-empirical equation based on Glen's model has been used. However the constants used in this equation have been deduced from the data of Barnes et al (1971), and predict strain rates for a given stress and temperature that are very close to those predicted by a diffusion based model. The deformation map can be no better than the data used to construct it.

The map, when compared with the map for Nickel, shows that ice is

surprisingly creep resistant. This reflects the unique barrier dislocations face when they move through the lattice. Glaciers made of Nickel on an imaginary planet with a surface temperature of 1600°K (a homologous temperature of 0.95 for Nickel) would have surface velocities of m s^{-1}.

When the stress on, or strain rate in, an element of ice is large, the response to the load is no longer creep controlled but is dominated by the initiation and propagation of cracks. What 'large' is depends on the applied hydrostatic pressure, temperature, and grain size. Chapter four discusses whether the concepts of a critical stress intensity factor, K_{1c}, can be applied to ice. The stress intensity factor is a description of the singularity at the crack tip (Lawn and Wilshaw, 1975), and has gained wide acceptance in the description of the fracture of metals. The preliminary results from several experiments to measure K_{1c} for ice are given.

The strain experiments on glaciers and sea ice described in part II, were motivated by a desire to obtain field data of the way cracks propagate through ice. However the experiments have been directed at perfecting a method for the rapid measurement of surface strain rates. The results obtained, however, do have some implications for the work described in part I. The data analysis from the measurements of strains in sea ice due to the action of waves in Labrador suggest that cyclic strains may decrease the modulus of the ice as the season progresses. A wave of 10 s period cycles the ice about a million times in a season. 10^6-10^8 cycles is roughly the fatigue life of most materials.

The method uses a geophysical wire strainmeter to continually monitor the distance between two points from 2 to 10 m apart. It can easily detect strain rates of the order of 10^{-7} s^{-1} on sea ice, and 10^{-7} day^{-1} on glaciers. Results are given from five field experiments in Bylot Sound, near Thule, NW Greenland; Forteau Bay, Labrador; the Roslin Glacier, east Greenland; the Barnes Ice Cap, Baffin Island; and the glacier d'Argentière, Mont Blanc, France. The experiment in Argentière measured the elastic strain changes in the rock just beneath the glacier. The strainmeters were located in a network of tunnels which run under the middle of the glacier where it

is about 80 m deep. The strainmeters detected what is thought to be strain events which are the result of the glacier freezing to its bed.

The design of a new strainmeter is given. This uses a 1 m Invar bar as a length standard. It has been built, and was taken to the North Pole in September 1976. Good results were not obtained, but it is at present in use on the sea ice off Newfoundland. The preliminary results from this site suggest that it is operating satisfactorily, and can detect strain changes due to waves passing underneath.

2. SOME USEFUL NUMBERS.

S.I. units have been used throughout this thesis except for day^{-1} in 10^{-6} strain day^{-1} which is found to be the most convenient unit to describe the glacier strain data.
Conversion tables for most units to S.I. are given in figure 1.05. To convert the units in the row into the units in the columns multiply by the factor shown at the intersection.

The discussion throughout the thesis, except for one short section in chapter two, is for polycrystalline ice I_h. The regimes of temperature and pressure where this form of ice exist are shown in the phase diagram shown in figure 1.06. For the convenience of the reader, a diagram of the ice I_h lattice is given in figure 1.04.

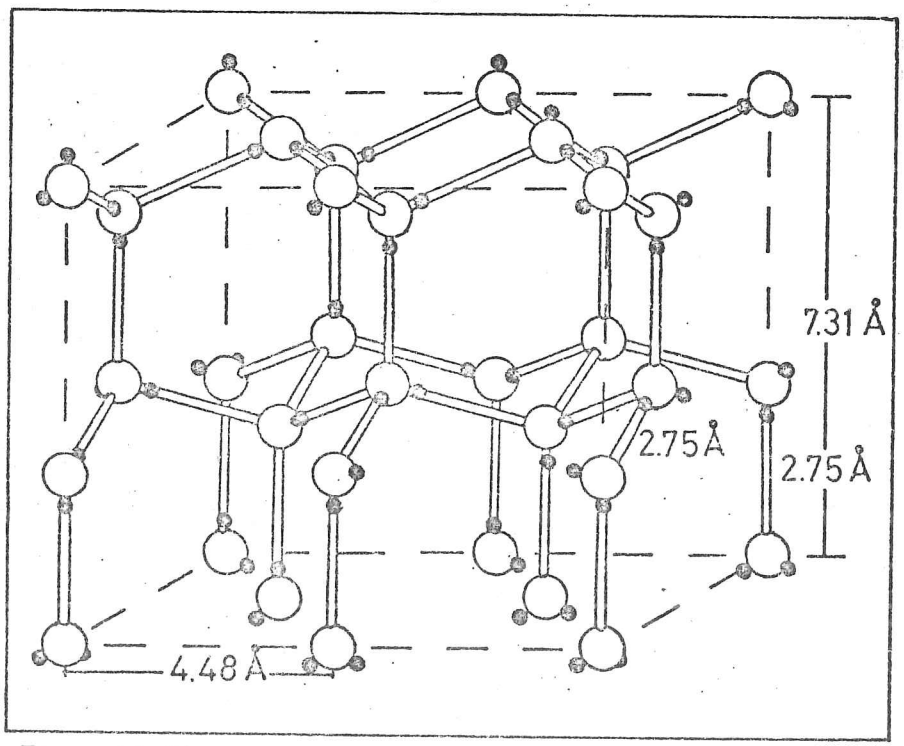

Figure 1.04; The Ice 1_h Lattice. (Fletcher, 1970)

Conversion table for stress and pressure

	MN m^{-2}	dyn cm^{-2}	psi	kgf cm^{-2}	kgf mm^{-2}	bar	ton in^{-2}
MN m^{-2}	1	10^{7}	145	10.2	0.102	10	6.35×10^{-2}
dyn cm^{-2}	10^{-7}	1	1.4×10^{-5}	1.02×10^{-6}	1.02×10^{-8}	10^{-6}	6.35×10^{-9}
psi	6.90×10^{-3}	6.90×10^{4}	1	7.03×10^{-2}	7.03×10^{-4}	6.90×10^{-2}	4.46×10^{-4}
kgf cm^{-2}	9.80×10^{-2}	9.80×10^{5}	14.2	1	10^{-2}	0.980	6.23×10^{-3}
kgf mm^{-2}	9.80	9.80×10^{7}	1.42×10^{3}	100	1	98.0	6.23×10^{-1}
bars	0.10	10^{6}	14.50	1.02	0.0102	1	6.35×10^{-3}
tons in^{-2}	15.75	1.57×10^{8}	2.24×10^{3}	1.61×10^{2}	1.61	1.57×10^{2}	1

Conversion table for fracture toughness

	MN·$m^{-3/2}$	N·$mm^{-3/2}$	k.s.i. $in^{1/2}$
MN·$m^{-3/2}$	1	31.6	0.89
N·$mm^{-3/2}$	3.16×10^{-2}	1	2.83×10^{-2}
k.s.i. $in^{1/2}$	1.12	35.4	1

Conversion table for specific energy

	J/mol	cal/mol	erg/atom	eV/atom
J/mol	1	0.239	1.66×10^{-17}	1.04×10^{-5}
cal/mol	4.18	1	6.94×10^{-17}	4.34×10^{-5}
erg/atom	6.02×10^{16}	1.44×10^{16}	1	6.25×10^{11}
eV/atom	9.63×10^{4}	2.305×10^{4}	1.6×10^{-12}	1

Conversion table for energy

	J	erg	cal	eV	BThU	ft lb_f
J	1	10^{7}	0.239	6.24×10^{18}	9.47×10^{-4}	0.737
erg	10^{-7}	1	2.39×10^{-8}	6.24×10^{11}	9.47×10^{-11}	7.37×10^{-8}
cal	4.18	4.18×10^{7}	1	2.61×10^{19}	3.96×10^{-3}	3.08
eV	1.60×10^{-19}	1.6×10^{-12}	3.83×10^{-17}	1	1.52×10^{-22}	1.81×10^{-19}
BThU	1.06×10^{3}	1.06×10^{10}	2.52×10^{2}	6.59×10^{21}	1	7.78×10^{2}
ft lb_f	1.36	1.36×10^{7}	3.24×10^{-1}	8.47×10^{18}	1.28×10^{-3}	1

Figure 1.05; S.I. Conversion Tables. To go from row to column multiply.

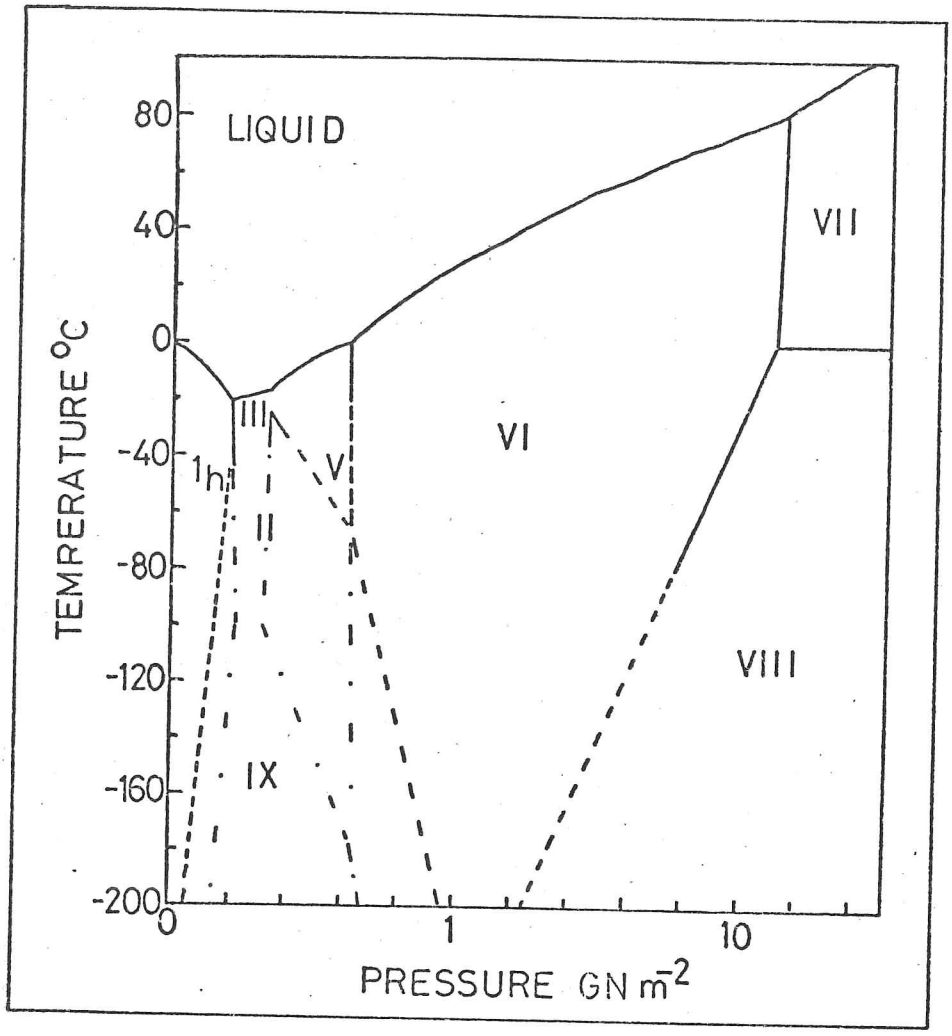

Figure 1.06; The phase diagram for ice.
(from Hobbs, 1974)

I hope the reader will enjoy the description and explanation of my work over the past three and half years. I apologise here for any errors or omissions that have 'crept' in.

PART I

THEORETICAL AND EXPERIMENTAL WORK

CHAPTER TWO

CREEP MECHANISMS IN POLYCRYSTALLINE ICE

CREEP MECHANISMS IN POLYCRYSTALLINE ICE.

1. INTRODUCTION.

For most common materials reasonable microscopic models exist to explain their creep behaviour. Often some of the constants in the constitutive equations which represent these models have been deduced empirically from creep experiments. However the models (of dislocation glide and creep, diffusional flow) are sufficiently successful to enable extrapolations to be made beyond the ranges of stress and temperature where the experiments were conducted. Ashby (1972) and later Frost and Ashby (1973), have used the available constitutive equations (which relate the strain rate to the stress, temperature, and crystalline structure) to construct diagrams to represent the creep behaviour, for a range of materials, over all feasible stresses and temperatures, and for structure variations such as grain size. Such a diagram for Nickel appears in figure 2.01. The diagram has axes of homologous temperature (T/T_m ; T_m is the melting temperature), and normalised shear stress, $\bar{\tau}/\mu$ ($\bar{\tau}$ is the effective shear stress; μ is the shear modulus - an appendix to this chapter relates $\bar{\tau}$ to other stress states and gives the temperature dependence of the modulus for ice). Plotted on the axes are the boundaries between different areas or fields in which each mechanism dominates, and contours of constant shear strain rate. Thus for a given temperature and stress (the most frequently met independent parameters) it is possible to see from the diagram what the dominant mechanism operating is, and the creep rate.

This approach has been adopted here to discuss the possible creep mechanisms in polycrystalline ice. The diagrams or deformation mechanism maps presented in section 3 are used to show where, in a temperature-stress space, the different mechanisms dominate, and the effect of changing the grain size. In section 4 an application of the maps to the creep of ice in an ice sheet is given.

The discussion is restricted to the secondary creep of an equiaxed, isotropic aggregate of ice grains. As is usual, the creep is assumed to be independent of the hydrostatic component of the stress, as has been found by experiment (Rigsby, 1958; Haefeli, Jaccard, and Quervain, 1968). Also it is assumed that the hydrostatic component is sufficiently large to prevent the initiation and propagation of cracks. The latter assumption is a severe one; in uniaxial tests for strain-rates greater than 10^{-4} s^{-1}, and stresses greater than 1 MN m^{-2} crack

motion begins to control the change of shape (Hawkes and Mellor, 1972; Gold, 1972). However it is possible to observe the ductile behaviour of ice at high strain rates in a hardness test or an extrusion experiment (Barnes, Tabor, and Walker, 1971; Kuon and Jonas, 1973). Beneath a hardness indenter or in an extrusion dye the hydrostatic component of the stress is large, and the size of the indentation or the force required to extrude the ice depends on the ductility of the ice (see however chapter 4 for a further discussion of this).

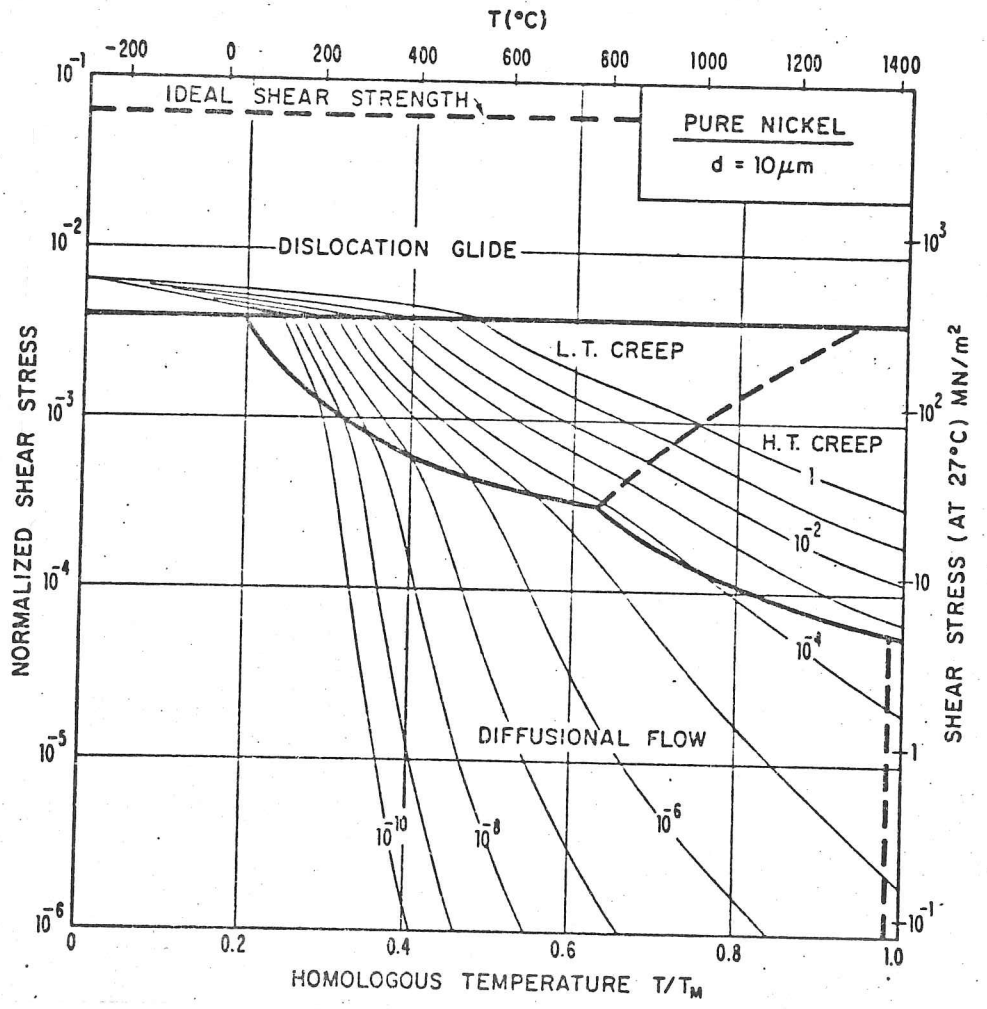

Figure 2.01; A Deformation Map for Nickel.
(from Frost and Ashby, 1973; contours of constant shear strain rate in s^{-1})

Five possible creep mechanisms are outlined; collapse, Peierls barrier or lattice resistance controlled glide, proton rearrangement controlled glide, diffusional creep (volume or Nabarro-Herring, and boundary or Coble creep), and other mechanisms, such as

recrystallisation, for which no satisfactory constitutive equation exist. All the mechanisms, with the exception of proton rearrangement controlled glide, are well documented in the literature on the creep of other materials (for a review see Frost and Ashby 1973). Glen (1968a,b) first pointed out that the peculiar structure of ice 1_h, with its random proton lattice, leads to a unique barrier to dislocation motion. Here this is termed 'proton rearrangement controlled glide': it is outlined in the next section, and a quantitive picture developed in chapter 3. However a satisfactory quantitative model still does not exist; a semi-empirical model is used to construct the map. The barrier exists because, if new bonds were made without regard to the proton configuration, highly energetic Bjerrum or Ionic defects would be formed (see chapter 1 for a discussion of these defects). In general there is insufficient energy available to form such defects; the bond is not made until the proton configuration is favourable.

Weertman, in a paper in 1963 and in his review of creep in 1973 (Weertman 1963, 1973) suggests two further mechanisms. Firstly he points out that proton configuration changes in the elastic strain field of a moving dislocation will lead to an energy loss similar to the rearrangement of interstitial atoms in the Eshelby-Schoek damping mechanism in steels. Secondly he suggests that diffusion controlled climb around forest dislocations could account for the observed creep behaviour if a sub-grain model is used (it is necessary to introduce the sub-grain so that the strain rate depends on the third power of the stress instead of the stress to a power of 4.5). He uses the equations already deduced for these mechanisms in other materials to show, that when suitable parameters for ice are used, these mechanisms could account for the single crystal creep behaviour (when the dislocation density is accounted for). It is our opinion that, although these mechanisms are perfectly feasible, the rate controlling process is the rearrangement of protons close to the dislocation so that when new bonds are formed they do not contain proton defects (the barrier exists whether the dislocation is gliding or climbing).

In an equiaxed polycrystalline aggregate, creep must involve slip on five independent slip systems if holes are not to appear on the grain boundaries - the Von Mises criteria for ductile flow (Kelly and Groves, 1970). It would be six if the volume were not conserved.

Slip systems which can produce different non-rotational strains are independent. Basal slip cannot provide five independent systems; thus non-basal slip must occur in a polycrystalline block which creeps to large strains. The two most likely systems are $\{10\bar{1}0\}\langle 1\bar{2}10\rangle$(prismatic) and $\{11\bar{2}2\}\ \frac{1}{3}\langle \bar{1}\bar{1}23\rangle$(pyramidal) from the etch pit observations of Muguruma and Higashi (1963). Slip on the basal and prismatic systems alone is also insufficient if climb is not allowed but the existance of pyramidal slip has not been confirmed. For small strains it may be possible for the unfavourably orientated grains merely to deform elastically, but at large strains another possibility, particularly above -10^{o}C, is the recrystallisation of such grains (strong fabric developments have always been observed in samples from bore-holes; Budd, 1972). It is hypothetically possible, given the rate equations for each slip system to deduce the polycrystalline creep equation (J. W. Hutchinson, personnel communication; see also Taylor 1956, Bishop and Hill 1951, Kocks 1958). Tegart (1964) discusses non-basal slip in terms of microscopic models of slip in hexagonal metals.

It has been suggested that grain boundary sliding is an independent creep mechanism (Langdon, 1973); we think that this is unlikely. Certainly grain boundary processes, as Barnes, Tabor and Walker (1971) suggest, are important within a few degrees of the melting point, but, if grains are to remain in complete contact with each other, changes of shape by dislocation glide or diffusion must occur and these will probably determine the creep rate.

2. CONSTITUTIVE EQUATIONS USED TO CONSTRUCT THE MAP.

2.1 Secondary Creep Data.

The constitutive equations which follow, and the diagrams they are used to construct, must, even though they are based on microscopic models which are inevitably incomplete, be a correct representation of the existing data. The deformation map can be no better than the data used to construct it.

Experiments by many workers to investigate the secondary creep of polycrystalline ice have recently been thoroughly reviewed by Hobbs (1974), and Weertman (1973). Table 2.01 lists the

Table 2.01; Polycrystalline Creep Data

Authors	Temperature Range °C	Uniaxial Stress Range MN m^{-2}	Grain Size mm	Activation Energy kJ mole^{-1}	Stress Exponent n	Equation used to fit the data	Experimental Technique
Glen (1955)	-13 to 0	0.01 to 0.1	~ 1	134	3.2	$\dot{\varepsilon}_i = A_1 \exp(-Q/RT)\sigma_i^n$	Uniaxial Compression
Steinemann (1958)	-22 to -2	0.06 to 1.6	~0.8	63 - 159			Uniaxial Compression
Barnes, Tabor and Walker (1971)	-8 to -2	0.1 to 10	~ 1	120	3.14	$\dot{\varepsilon}_i = A_2(\sinh\alpha\sigma_i)^n \times \exp(-Q/RT)$	Uniaxial Compression
	-14 to -8	0.3 to 10	~ 1	78.1	3.08		
	-22 to -14	0.3 to 10	~ 1	78.1	2.92		
	-45 to -8	0.3 to 10	~ 1	78.1	3.05		
Barnes (1968)	-11 to -2	0.3 to 30	1 to 3	147	4.4	$\dot{\varepsilon}_i = A_3\sigma_i^n \exp(-Q/RT)$	Hardness
Walker (1970)	-12 to 0	2 to 17	~ 1	150	3.9		Hardness
	-25 to -12	2 to 17	~ 1	72.5	4.4		
Schulz and Knappwost (1968)	-100 to -10	98 to 100	~ 1	-	-	-	Hardness
Butkovich (1954)	-50 to -5	17 to 55	-	-	-	-	Single Crystal Hardness
Kuon and Jonas (1973)	-20 to -3	5 to 35	~ 1	-	5.7	$\dot{\varepsilon}_i = A_4\sigma_i^n$	Extrustion
Mellor and Testa (1969a)	-61 to -10	1.2	~ 1	68.8	-		Uniaxial Compression
	-10 to 0	0.05 to 1.2		-			
Mellor and Testa (1969b)	-2	0.01 to 0.05	~ 1	-	1.8	$\dot{\varepsilon}_i = A_5\sigma_i^n$	Uniaxial Compression
Bromer and Kingery (1968)	-13 to -3	0.02 to 0.2	0.1 to 0.6	50.2	1	$\dot{\varepsilon}_i = \frac{20\,D\Omega}{3kT\,d^2}\sigma_i$ $D=D_o\exp(-Q/kT)$	Tensile Creep Tests
Butkovich and Landauer (1960)	-19 to -1	0.002 to 0.02	~ 3	59.9	0.86 to 1.1	$\dot{\varepsilon}_i = A_6\sigma_i^n \exp(-Q/RT)$	Constant stress Compression Tests
Gold (1973)	-40 to -5	0.1	3 to 5	64.9	2.04	$\dot{\varepsilon}_i = A_7 D\left(\frac{\sigma_i\Omega}{kT}\right)\left(\frac{\sigma_i}{E}\right)^{n-1}$	Constant stress Compression Test (Columnar Grained Ice)

In the equations $\dot{\varepsilon}_i$ is the uniaxial strain rate, σ_i the uniaxial stress, Q the activation energy, T the temperature, Ω atomic volume, R the Gas constant, k Boltzmann's constant, D_o the diffusion constant, d the grain size, and A_{1-7} and α are constants.

more significant papers. Some papers have been omitted because they have been superseded by others (Mellor and Smith, 1966; Dillon and Andersland, 1967) or because they deal more with 'strength' (Hawkes and Mellor, 1972). A wealth of data also exists of the creep properties of single crystals of ice (see Hobbs, 1974 for a review). The single crystal data is quite different from the polycrystalline data because slip can easily occur on the basal plane, and large changes in the dislocation density usually occur at the beginning of the test.

Data from the papers have been replotted onto axes of the map, homologous temperature and normalised stress; the plot is shown in figure 2.02 It is clear from the the table, and the data plot that the creep of ice has been studied only over a limited range of temperature close to the melting point (0.8 to 1.0 T/T_m; -50 to 0°C). This is unlike most creep data; for other materials it is often extremely difficult to obtain data at high homologous temperatures. Therefore it is not surprising that we think of ice as offering little resistance to creep compared to other materials at lower homologous temperatures. We shall see later that this view is misleading; ice is surprisingly creep resistant.

Hardness data has been included in the table and the plot following the work of Atkins, Silvério, and Tabor (1966) (see also the review of the hardness test by Tabor (1970). They show how the size of the indentation in a time dependent hardness test (where the indentation size depends on the loading time as well as the contact pressure) can be explained in terms of the creep behaviour of the material beneath the indenter. The strain field under the indenter is complex, and some parts of the material undergo strains much larger than those that could be obtained in a uniaxial test (cracks do not propagate because the hydrostatic component of the stress is also large). Tabor (1951) has shown that the mean equivalent uniaxial strain in a hardness test is 8%. To plot the hardness data with the uniaxial creep data, we assume here that the effective shear strain rate is $0.08 \times \sqrt{3} / t$,where t is the loading time, and the effective shear stress is $p/3\sqrt{3}$ from Tabor's relation that the hardness, p, is three times the uniaxial yield stress. Later we discuss the meaning of yield stress in the context of the creep of ice but for the purposes of plotting the data over six decades

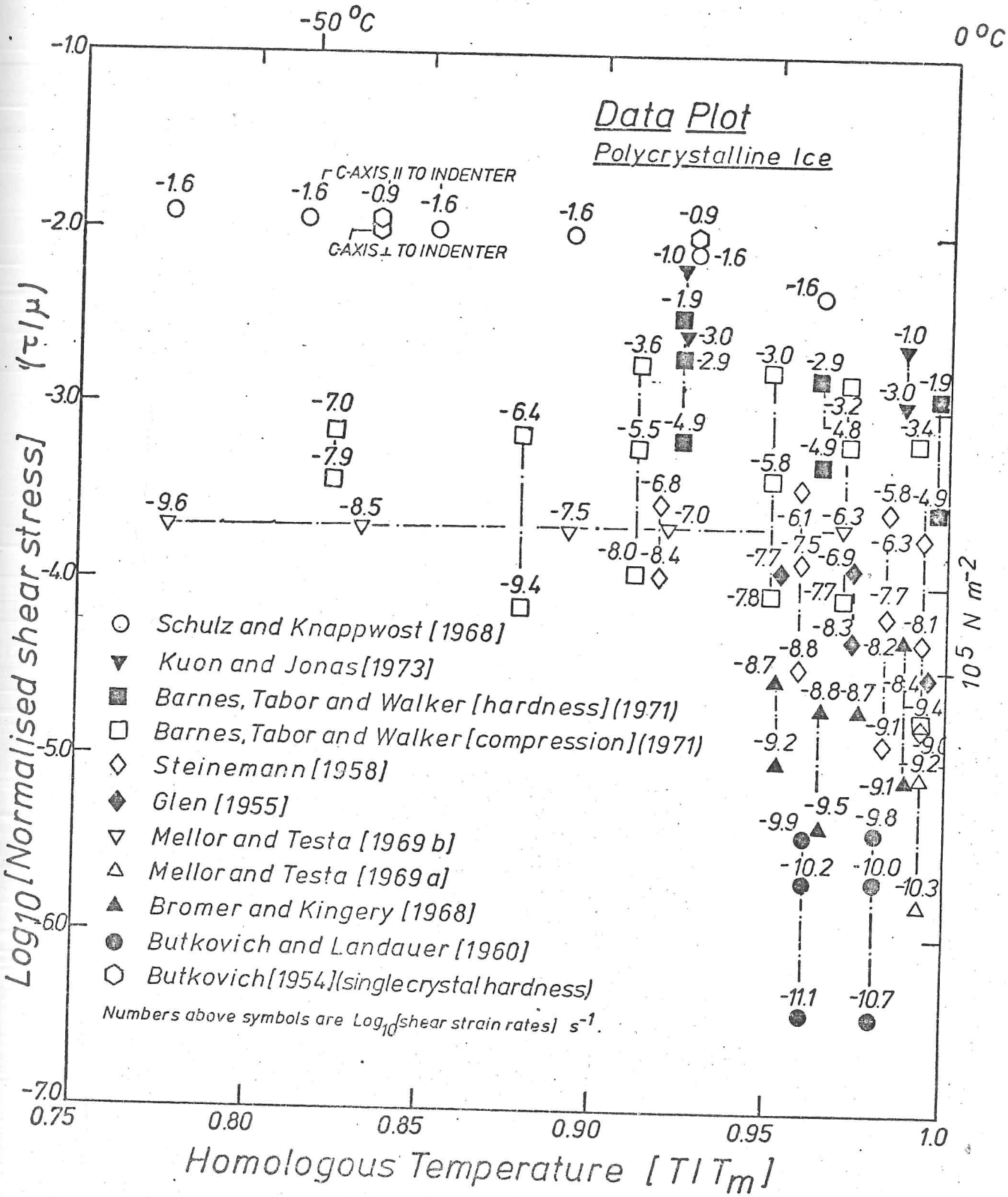

Figure 2.02; Secondary Creep Data for Polycrystalline Ice.

of stress these approximations are satisfactory. For clarification of the introduction of the $\sqrt{3}$'s see the appendix to this chapter. Tabor's relation holds as long as the elastic yielding of the hinterland beyond the plastically deformed region is not significant. This has to be taken into account when the yield stress is within a factor of hundred of the modulus (Tabor, 1970). This will occur for hardness tests at low homologous temperatures.

In many of the papers plotted in figure 2.02, no attempt was made to distinguish between transient and secondary creep. The most direct attempt to do this is in Barnes, Tabor and Walker (1971). They apply the Cottrell-Aytekin equation, which gives the strain, ϵ, at time t;

$$\epsilon = \epsilon_e + a_1 t^{\frac{1}{3}} + \dot{\epsilon}_s t \qquad 2.01$$

where a_1 is a constant, ϵ_e the elastic strain, and $\dot{\epsilon}_s$ the true secondary creep rate. They derive a value for a_1, and use it to subtract the transient creep component from their data. This is particularly important at low stresses, when the total strain rate is less than 10^{-7} s^{-1}, and secondary creep may never be established (Weertman, 1969).

In comparison with other materials, creep data for ice exists over a very small range of temperatures, and unusually, they are all at high homologous temperatures. The data given in table 2.01 and figure 2.02 show that the creep of ice can be represented empirically by an equation of the form;

$$\dot{\epsilon} = A \sigma^n \exp(-Q/RT) \qquad 2.02$$

where $\dot{\epsilon}$ is the strain rate, A a constant, σ the stress, Q the activation energy, and T the temperature. For uniaxial stresses between 0.1 and 1 MN m^{-2} ($\tau/\mu = 2 \times 10^{-5}$ to 2×10^{-4}) n is approximately 3; above these stresses n rises rapidly. Barnes et al (1971) represent this change by using a $(\sinh \alpha\sigma)^n$ function which has the property that at low stesses it reduces to $(\alpha\sigma)^n$, while at high stresses it goes to $\exp(n\alpha\sigma)$. At low stresses there is some indication of a decreased exponent. Q changes from ~80 kJ mol^{-1} to ~120 kJ mol^{-1} at about $-8^{\circ}C$ because recrystallisation and grain boundary effects become more important. Above $-2^{\circ}C$, at high stresses, pressure melting effects greatly enhance the apparent creep rate.

We now adopt a different point of view, and consider what microscopic mechanisms could be responsible for creep in ice.

2.2 Collapse.

The first mechanism considered is the simplest and the one most likely not to occur. For any crystalline solid there is an upper bound to the shear stress it will support defined by the shear strength of the perfect lattice. Above this stress the lattice fails completely, below, if no other mechanisms were possible, it would behave elastically. Precise values of the stress have been computed many times; every value depends strongly on the model chosen to represent the force law between the atoms. All calculations lead to a value which is between $\mu/10$ and $\mu/20$ (Kelly, 1966). Here we have taken the upper bound, and assumed that collapse occurs when $\hat{\tau}$ equals $\hat{\tau}_{th}$, with $\hat{\tau}_{th}$ equals 0.1μ. Thus the constitutive equation is;

$$\dot{\gamma}_c = \infty \qquad \hat{\tau} \geq \hat{\tau}_{th}$$
$$\dot{\gamma}_c = 0 \qquad \hat{\tau} < \hat{\tau}_{th} \qquad 2.03$$

It is independent of the grain size and the impurity content.

2.3 Proton Rearrangement Controlled Glide.

Glen (1968) pointed out that, as was mentioned in the introduction, dislocations in a hydrogen-bonded lattice with a random arrangement of protons face a unique barrier to their motion. This barrier exists because, if the dislocation were to move with the protons frozen in position, many of the new bonds formed would contain either no protons (a L-type Bjerrum defect) or two protons (a D-type Bjerrum defect); every Bjerrum defect pair formed requires 0.64 eV of energy (Hobbs, 1974). If the protons were randomly arranged, a defect would be formed, on average, on every other bond. The situation is shown in figure 2.02 which is an adaption of Glen's orginal figure. Glen calculated the stress required to move the dislocation in this way. He equated the energy needed per unit length of the dislocation ($0.34/ab^2$ eV m^{-1}; where a is the interatomic distance parallel to the dislocation) to the work done by a shear stress, τ, acting on the slip plane if the dislocation moves

one Burger's vector, b (τb^2). This gives a value for the shear stress of

$$\tau = \frac{0.34 \times 1.6 \times 10^{-19}}{2ab^2} \qquad 2.04$$

with $a = \frac{\sqrt{3}}{2}$ b, and b = 4.5×10^{-10} m this gives

$$\tau = 340 \text{ MN m}^{-2} \qquad (\tau/\mu = 0.09)$$

We can see that this value is of the same order as the ideal shear strength described in the last section. If the proton on the D - defect were allowed to tunnel to the L -defect (which would require no energy) two Ionic defects would be formed (H_3O^+ and OH^-). These are even more energetic than the Bjerrum defect pair (0.98 eV instead of 0.64 eV; quoted in Glen 1968), and so this is unlikely to happen.

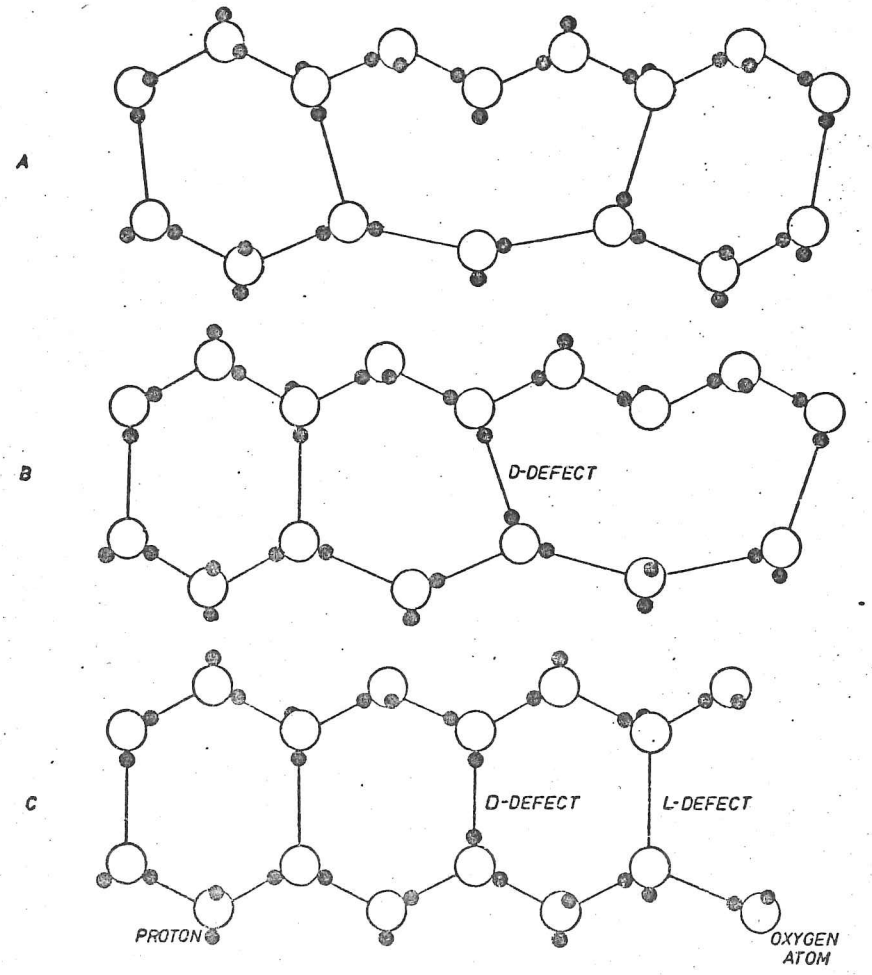

Figure 2.02; If the proton arrangement is 'frozen', the motion of the edge dislocation shown in A will create a pair of Bjerrum defects.

At high homologous temperatures, 340 MN m^{-2} is much greater than the stresses at which creep is observed to occur. If we suppose that dislocation motion is responsible for the change of shape (diffusional flow is shown below to be very slow), the dislocations must move without the creation of proton defects. A dislocation advances, when a stress exists on the slip plane, by throwing forward a double kink pair, the kinks separate and eventually annihilate with kinks of opposite sign (see figure 2.04).

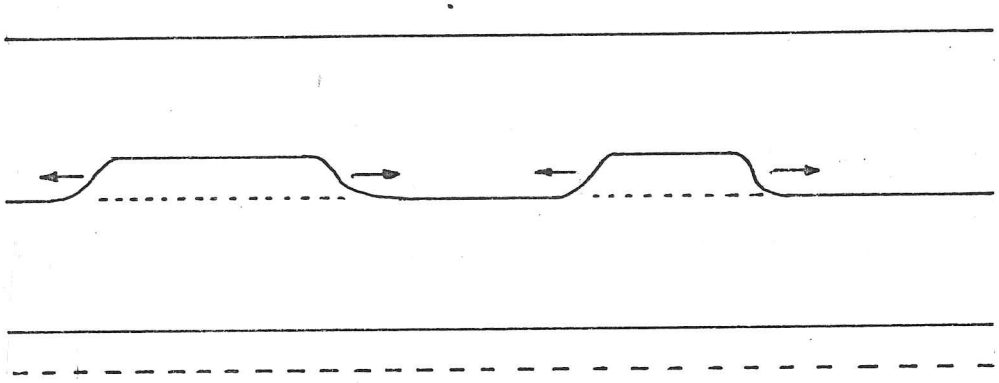

Figure 2.04; Dislocations advance by the motion of kinks.

As the kink propagates it waits for the proton configuration to become favourable. Proton rearrangement is continually occuring as Bjerrum and Ionic defects (which exist in thermal equilibrium with the lattice) diffuse through the lattice; at high stresses the large local stress field close to the dislocation may induce rearrangement (the reasons for believing this are discussed in the next chapter and in Whitworth, Paren, and Glen, 1976; Frost, Goodman, and Ashby, 1976).

Evidence in support of the existance of proton rearrangement controlled glide comes from the observations of the changes in the mechanical properties when small amounts of impurities, in particular hydrogen fluoride, which change the proton defect concentration are added to the ice. Jones and Glen (1968, 1969b), and Nakamura and Jones (1973) observed that in single crystals of ice, deformed in tension with the basal plane at 45° to the tensile axis, the stress required to deform the crystal at a constant strain rate after the initial

yield drop was an order of magnitude less than that for pure ice at $-70^{\circ}C$ for 3 p.p.m. of HF, but the effect was much less marked at $-11^{\circ}C$. The activation energy observed was 32 kJ mol^{-1} for the HF doped ice compared to 66 kJ mol^{-1} for the pure ice. This is consistent with the picture that the HF is added substitionally to the lattice adding one L-defect for each atom; the mean time between proton rearrangements would then be controlled by the extrinsic concentration of L-defects which would lead to an enhanced dislocation velocity for a given stress and a reduced activation energy (the L-defect activation energy for mobility instead of formation and mobility; 22 kJ mol^{-1} instead of 55 kJ mol^{-1}, Fletcher 1970). The results from the addition of NH_4OH, which would add D-defects, are inconclusive; both softening and hardening have been observed.

The above observations can only be used in support of Glen's model instead of the more usual rate controlled by dislocation climb (Weertman 1973) if the HF does not also change the self-diffusion rates (which control the rate of climb). Between $-3.5^{\circ}C$ and $-30^{\circ}C$, for doping levels of 10^{-5} to 5×10^{-3} mol $litre^{-1}$ (0.2 to 90 p.p.m.) of HF Blicks, Dengel and Riehl (1966) observed no effect in the diffusion rates of tritium which is believed to diffuse at the same rate as H_2O molecules (Fletcher 1970). HF doping does increase the static dislocation density (Jones and Gilra 1972) but this should only affect the maximum stress obtained in a constant strain rate test (Johnston 1962).

Although a satisfactory quantitative picture for the proton rearrangement controlled glide does not yet exist, it is possible to derive a semi-empirical constitutive equation by assuming that the time between proton rearrangements has a temperature dependence which is the same as the Bjerrum defect formation and diffusion rates; it is then possible to calculate the velocity of a kink on the dislocation line for a given normalised stress, $\hat{\tau}$, on the slip plane by a statistical argument (Whitworth, et al, 1976; Frost, et al, 1976; and chapter 3). This calculation leads to the result that

$$v_{dis} = A_1 \hat{\tau} \exp\left(- \frac{F_f + F_m}{kT} \right) \qquad \tau < 10 \text{ MN m}^{-2} \qquad 2.05$$

where A_1 is a constant, F_f and F_m are the activation energies for the formation and mobility of a L or D defect, k is Boltzmann's constant,

T the temperature, and $\hat{\tau}$ the stress. The value calculated for A_1 does not agree with the X-Ray topograph measurements of Fukuda and Higashi (1969, 1973) who measured dislocation velocities as a function of stress, probably because there is an decrease in the time between the proton rearrangements close to the dislocation. For stresses below 10 MN m^{-2} the equation correctly predicts that the velocity is proportional to the stress, however it does not give the gradually increasing dependence on the stress observed by Maï (1976), and which is expected from the creep data. Therefore purely empirically we have assumed that the stress dependence of the dislocation velocity can be represented by

$$v_{dis} = a_3 \hat{\tau} \exp\left(- \frac{F_f + F_m}{kT} \left(1 - \frac{\hat{\tau}}{\hat{\tau}_o} \right) \right) \qquad 2.06$$

where a_3 and $\hat{\tau}_o$ are constants. The dislocation velocity is related to the creep rate by Orowan's equation;

$$\dot{\gamma}_{prg} = \rho \, b \, v_{dis} \qquad 2.07$$

where ρ is the mobile dislocation density, b the Burger's vector. There are a variety of arguments to show that ρ is proportional to the stress squared (see for example Kocks, Argon and Ashby 1973), this gives;

$$\boxed{\dot{\gamma}_{prg} = a_o \hat{\tau}^3 \exp\left(- \frac{F_f + F_m}{kT} \left(1 - \frac{\hat{\tau}}{\hat{\tau}_o} \right) \right)} \; * \qquad 2.08$$

where a_o is another constant. Note that the equations are in terms of the normalised stress $\hat{\tau}$ which equals τ/μ ; using this removes the temperature dependence of the modulus from the pre-exponential constant a_o . The values of a_o and $\hat{\tau}_o$ have been calculated from the creep data of Barnes, Tabor and Walker (1971). In figure 2.05 the data from Barnes et al's paper is compared with secondary creep curves computed from equation 2.08. The values of the constants used to construct the curves are;

F_m = 22.2 kJ mol^{-1} (0.23 eV) (Fletcher 1970)
F_f = 32.8 kJ mol^{-1} (0.34 eV) (Fletcher 1970)
a_o = 1.72 x 10^{15} s^{-1}
$\hat{\tau}_o$ = 0.0149

When $\hat{\tau}$ is considerably less than $\hat{\tau}_o$ ($\tau \lesssim 3$ MN m^{-2}), the equation reduces to the more familiar equation first used by Glen (1955).

* boxed equations are used in section 3 to construct the deformation maps.

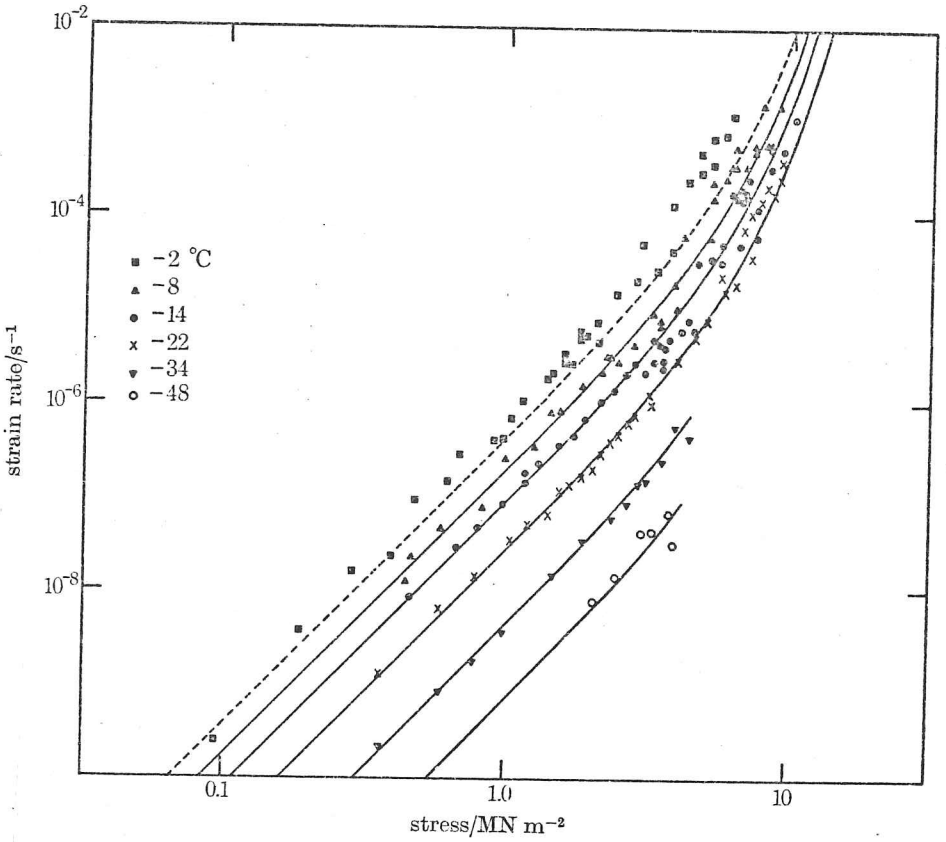

Secondary creep rate plotted against the applied stress on logarithmic coordinates. The curves are calculated sinh functions based on all the experimental points between −8 and −48 °C. It can be seen that the calculated curve for −2 °C (shown as a broken line in the figure) lies well below the experimental points obtained at −2 °C, indicating that the ice is creeping faster than would have been predicted by extrapolation from lower temperatures.

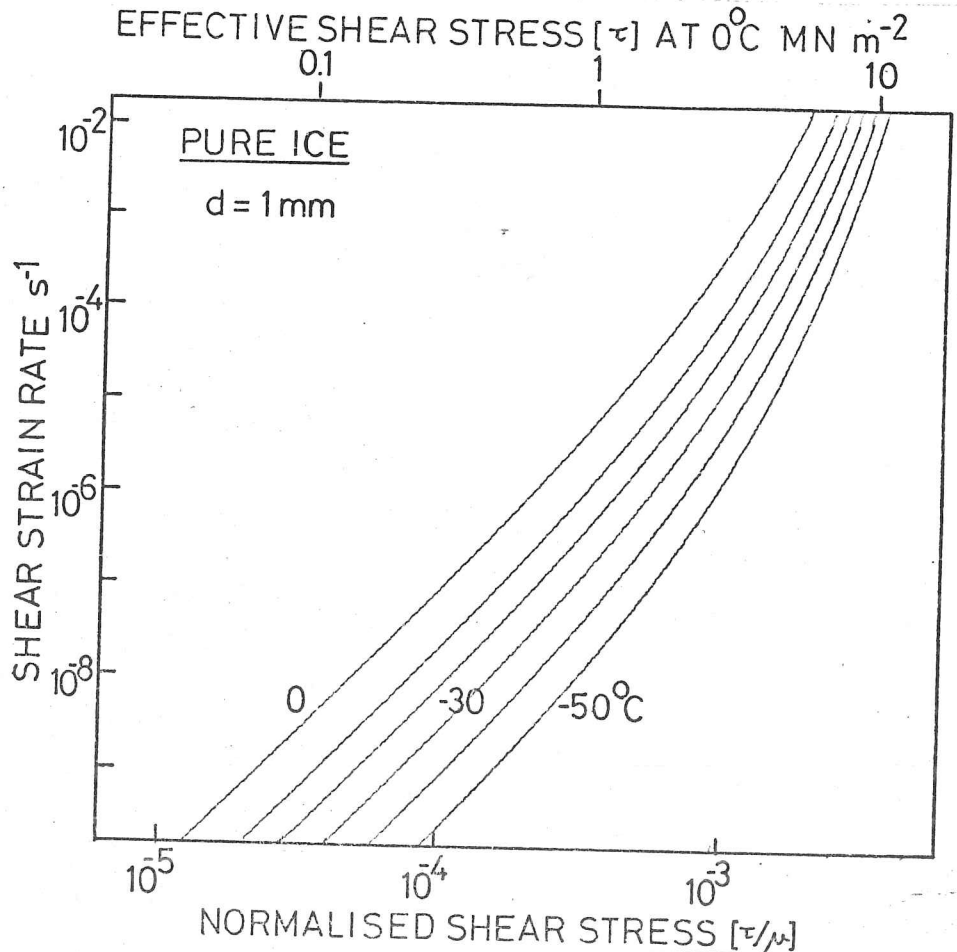

Figure 2.05; Upper diagram - data from Barnes, Tabor and Walker (1971), lower diagram - creep curves calculated from equations 2.08 and 2.23.

$$\dot{\gamma}_{prg} = a_o \hat{\tau}^3 \exp\left(- \frac{F_f + F_m}{kT} \right) \qquad \hat{\tau} \ll \hat{\tau}_o \qquad 2.09$$

An alternative choice of equation, which would fit the data almost as well would be;

$$\dot{\gamma}_{prg} = a'_o \hat{\tau}^2 \sinh\left(\frac{\hat{\tau}}{\tau'_o} \right) \exp\left(- \frac{F_f + F_m}{kT} \right) \qquad 2.10$$

where a'_o and τ'_o are constants. The sinh represents the effect of stress induced switching; at low stresses it closely approximates to its argument again giving equation 2.09; while at high stresses it has the form $\exp\left(\frac{\hat{\tau}}{\tau'_o} \right)$ which gives;

$$\dot{\gamma}_{prg} = a_o \hat{\tau}^2 \exp\left(- \frac{F_f + F_m}{kT} \left(1 - \frac{\hat{\tau}}{\hat{\tau}_o} \right) \right) \qquad 2.11$$

which is rising less rapidly with the stress than equation 2.08, although the stress in the exponential will dominate its behaviour

The most disconcerting feature of Glen's model, which he himself has pointed out, is its inability to predict the large difference in stress required to produce the same strain rate on the basal and non-basal systems. Proton rearrangement should affect them both equally. In a constant strain rate test (3×10^{-6} s^{-1}) at $-19^{\circ}C$ for crystals orientated first to favour basal slip then to prevent it, Higashi, Mae, and Fukuda (1968) observed that the stress required on the non-basal system was about one hundred times that on the basal system. The ratio of shear moduli on prismatic to basal planes is 1.14.

2.4 Lattice Resistance Controlled Glide.

If equation 2 is extrapolated to stresses between 10^{-3} and 10^{-2} of the modulus, the strain rate predicted is found to agree much less well with the data (the hardness tests of Schulz and Knappwost, 1968; Butkovich, 1954; Barnes, Tabor and Walker (1971), and the extrusion tests of Kuon and Jonas, 1973). The creep rate is too fast. We can see that equation 2.08 will do this because the normalised shear stress, $\hat{\tau}$, cannot be greater than 0.015 (the value $\hat{\tau}$ of at $0^{\circ}K$), but from figure 2.02 we can see some data points exist for $\hat{\tau}$ greater than 0.01 (if the interpretation of the hardness tests in terms of creep is

correct). Further at $0^{o}K$, when no proton rearrangement is possible, the yield stress must be that given by Glen (1968) for the yield stress on a slip plane, 340 MN m^{-2} ($\hat{\tau} \sim 0.09$) multiplied by the appropriate Taylor factor. The Taylor factor relates the yield stress of a polycrystalline specimen to the yield stress on the slip planes; in this case we have taken the Taylor factor to be 1.67 (Kocks, 1970), and therefore the yield stress at $0^{o}K$ would be 568 MN m^{-2} ($\hat{\tau} = 0.142$). Equation 2.11 is extremely sensitive to the value chosen for $\hat{\tau}_{o}$, and would not represent the data of Barnes et al (1971) if the value was set at 0.142.

When the data of Schulz and Knappwost (1968) is replotted onto axes of $\log_{10}$ (normalised stress) versus reciprocal temperature (figure 2.06), and the data fitted to the equation

$$\dot{\gamma} = a\hat{\tau}^{n} \exp\left(-\frac{F'_{p}}{RT}\right) \qquad 2.12$$

where a and n are constants, F'_{p} is the activation energy, the gradient is

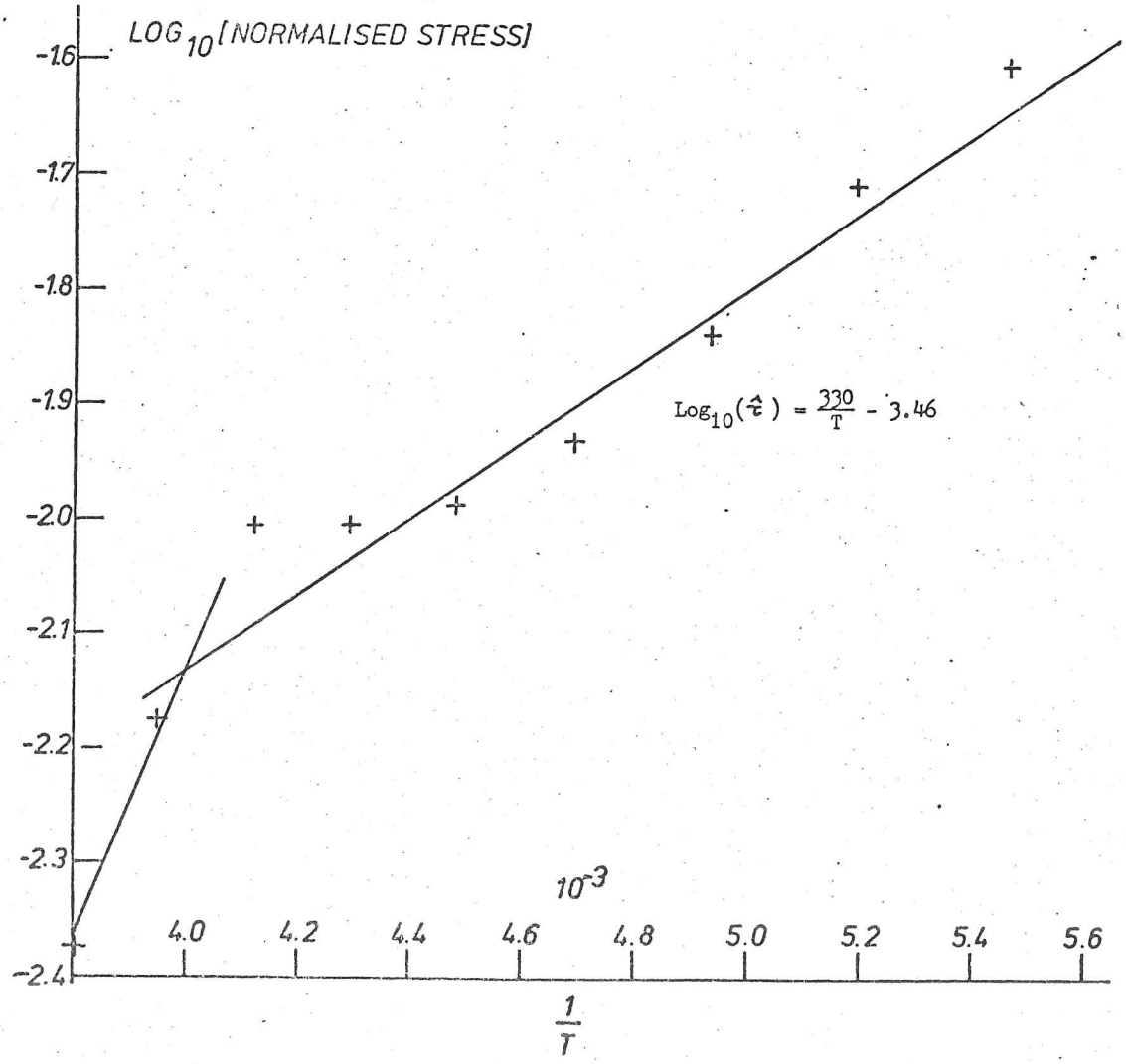

Figure 2.06; The data of Schulz and Knappwost (1968) replotted on axes of $\hat{\tau}$ and 1/T.

constant (because in a hardness test the strain rate is constant) and gives the ratio F'_p/n. In this case

$$\frac{F'_p}{n} = 6.32 \text{ kJ mol}^{-1}$$

for temperatures below $-30^{\circ}C$. A reasonable value for n is 5.7 from the extrusion data of Kuon and Jonas (1973), which suggests $F'_p \sim 36$ kJ mol^{-1}. This is much less than the activation energy for proton rearrangement controlled glide, although the value derived is very dependent on the choice of n . A lower activation energy could be accounted for by the existence of impurities which add proton defects; proton rearrangement would then only depend on the activation energy for motion of L or D defects, which is 26.1 kJ mol^{-1}(Fletcher, 1970). However, Nakamura and Jones (1973) comment, from their study of the effects of impurities on the creep of single crystals, that HF doping has less effect on the mechanical properties at low temperatures, and high strain rates. Thus it is unlikely that impurities can account for the reduced activation energy in this case. Further hardness tests at low temperatures on HF doped ice would soon resolve this point.

The above observations suggest that, at low homologous temperatures and high strain rates, another mechanism, slower than proton rearrangement controlled glide, becomes rate controlling. This is very likely, because firstly there must be a lower limit to the time in which proton rearrangements can occur (below the limit the dislocation is forced to create proton defects to move), and secondly the directional nature of the bonding in the lattice resists dislocation glide (the Peierls barrier). Lattice resistance controlled glide or Peierls barrier controlled glide is well documented in the literature (Guyot and Dorn, 1967; Kocks, Argon and Ashby, 1973). We put the effect of the creation of defects into the lattice resistance controlled model by assuming the dislocation faces a free energy barrier whose height is determined by the formation of a single Bjerrum defect (which must be a lower bound to the height). The energy for the formation of a single Bjerrum defect is $(F_f) \sim 32.8$ kJ mol^{-1} (0.34 eV), (Fletcher 1970), is close to the activation energy calculated from the Schulz and Knappwost data (but this should be treated with caution because the value of n is not well known).

The dislocation will take up a position of minimum free energy

parallel to the Peierls 'hills'. The dislocation advances by the formation, by thermal activation aided by the applied stress, of bulges or double kink pairs along its length, which subsequently drift together and annihilate (figure 2.07). The rate at which bulges are formed is assumed to control the dislocation velocity. All the models for the Peierls mechanism described by Guyot and Dorn (1967) or Kocks et al (1973) calculate, from an assumed force law between the molecules, the energy required to form a bulge, and use this to predict the rate of formation of bulges. It is in fact not the height of the barrier which is important but its shape; the shape determines the minimum force required to extend the dislocation into the next potential well.

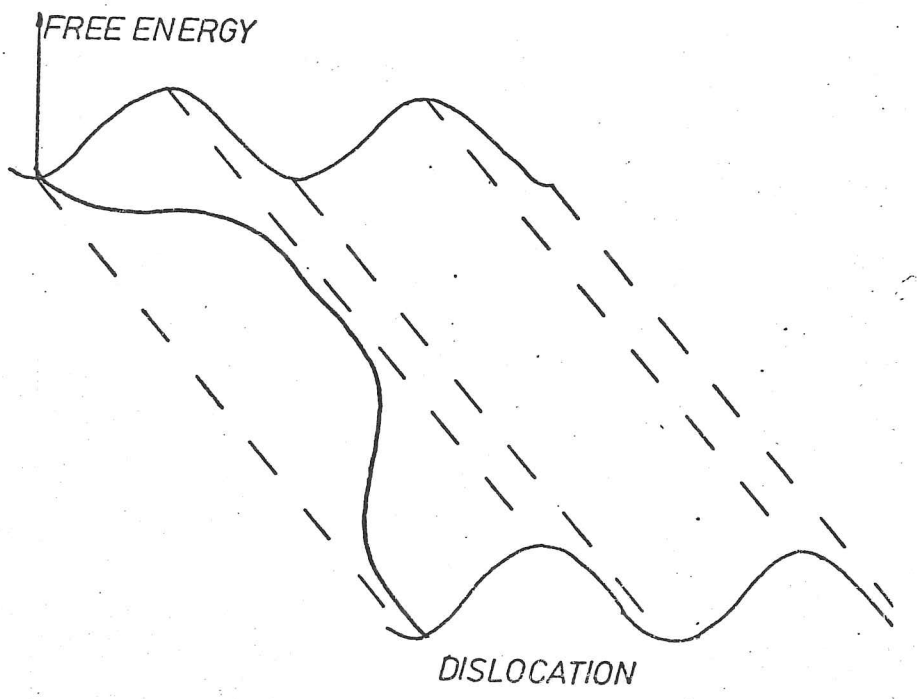

Figure 2.07; The free energy of the dislocation is a function of position when the directional nature of the bonding is taken into account. The free energy barrier here is assumed to represent both the bonding effect and the likelihood that proton defects are formed when the dislocation advances at low homologous temperatures and high strain rates.

All the models for lattice resistance controlled glide lead to an equation of the same form;

$$\dot{\gamma}_p = a_p \hat{\tau}^2 \exp\left(- \frac{F_p}{RT} \left(1 - \frac{\hat{\tau}}{\hat{\tau}_p} \right)^r \right)^s \qquad 2.13$$

where a_p, r, s, and $\hat{\tau}_p$ are constants, F_p is the height of the free energy hill, and $\dot{\gamma}_p$ is the shear strain rate for this mechanism.

Kocks et al (1973) discuss the possible values for r and s and show that the equation is insensitive to their choice; the preferred values are r equals 3/4 and s equals 4/3. The $\hat{\tau}^2$ in front of the exponential follows in the same way from the mobile dislocation density as in equation 2.08. The value of a_p, 10^{11} s^{-1}, has been fixed by obtaining the best fit to the data shown in figure 2.02. This is the same as Frost and Ashby (1973) found for other materials. At 0^oK $\hat{\tau}$ equals $\hat{\tau}_p$, which, as was shown earlier, is 0.1409 (548 MN m^{-2}).

Thus the constitutive equation adopted for lattice resistance controlled glide in ice is;

$$\boxed{\dot{\gamma}_p = a_p \hat{\tau}^2 \exp\left(- \frac{F_p}{RT} \left(1 - \frac{\hat{\tau}}{\hat{\tau}_p} \right)^{\frac{3}{4}} \right)^{\frac{4}{3}}} \qquad 2.14$$

with

F_p = 32.8 kJ mol^{-1}
a_p = 10^{11} s^{-1}
$\hat{\tau}_p$ = 0.1409 (548 MN m^{-2})

The existence of this mechanism in ice could be tested by creep tests at temperatures below -50^oC over a wide temperature range (at least 40^oC) under a hydrostatic pressure to prevent cracks forming. Alternatively hardness tests could be carried out to extend the data obtained by Schultz and Knappwost; however the formation of cracks under the indenter does occur and may affect the interpretation (see chapter 4). The addition of impurities which change the proton defect concentration should have no effect.

2.5 Diffusional Creep Mechanisms.

Self diffusion has been well studied in ice (for a review see Hobbs, 1974). From experiments which observed the motion of H^3, H^2, and O^{18}, it is found that the water molecule diffuses as a whole; however it is still not clear whether mass transport is controlled by the

motion of vacancies (Ramseier, 1967) or by the motion of interstitials (Onsager and Runnels, 1969). Here we are not concerned with the precise mechanism of diffusion, but only that, when a chemical potential gradient exists between two sites, mass transport by diffusion will occur. If $\underline{\text{grad}}\ \mu_p$ is the chemical potential gradient, $\underline{J}$, the flux of molecules, is given by Fick's law;

$$\underline{J} = -\frac{1}{\Omega}\left(\frac{D}{kT}\right)\underline{\text{grad}}\ \mu_p \qquad 2.15$$

where k is Boltzmann's constant, T the temperature, Ω the atomic volume (we have set Ω to b^3, where b is the Burger's vector), and D is the diffusion constant. D depends exponentially on the temperature through the relation;

$$D = D_o \exp\left(-\frac{F_{vol}}{RT}\right) \qquad 2.16$$

where D_o is a constant, R is the gas constant, and F_{vol} the activation energy for diffusion.

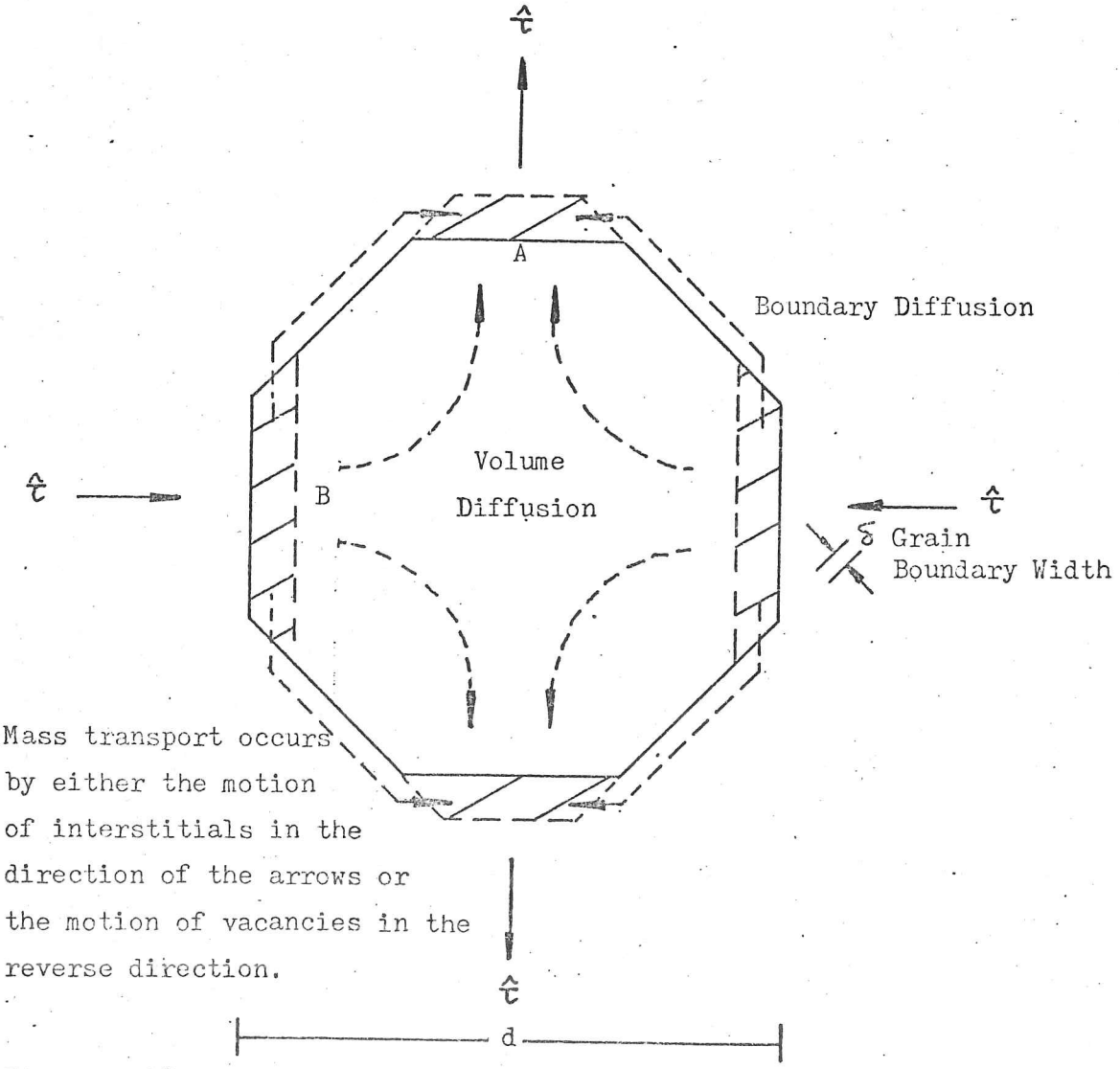

Figure 2.08; Volume or Boundary Diffusion can change the shape of a grain.

When a shear stress is applied to an aggregate of grains, a chemical potential gradient exists between the grain boundaries and it will change its shape by self diffusion (Nabarro, 1948; Herring, 1950). Consider the grain shown in figure 2.08; the stresses drawn are equivalent to shear stresses acting on planes at 45° to the axes shown. If μ is the shear modulus, a molecule on grain boundary A in the figure has a chemical potential which is less than that for a molecule on grain boundary B by an amount $2\Omega\mu\hat{\tau}$. Then, if a_g is a constant determined by the geometry, the flux of molecules between grain boundary B to grain boundary A is;

$$J = \frac{a_g D_{vol}}{kT\ d} \Omega\mu\ \hat{\tau} \qquad 2.17$$

where d is the grain size. Each molecule displaces the grain boundary by an amount Ω/A, where A is the area of the grain boundary, and for a flux J the number of molecules reaching the grain boundary per second is J x A. Therefore the shear strain rate, in this simple case, is;

$$\dot{\gamma}_{vol} = a_g \frac{D_{vol}}{kTd^2} \Omega\mu\ \hat{\tau} \qquad 2.18$$

Thus, for volume diffusion, the strain rate is proportional to the stress, and inversely proportional to the grain size squared.

Alternative diffusion paths, which are faster than volume diffusion, also exist. On the grain boundary, or within the core of a dislocation, the concentration of vacancies or interstitials is not determined by thermal activation; consequently the activation energy for diffusion will depend only on the migration energy. However the cross sectional area of these diffusion paths is very much smaller than that for volume diffusion (for grain boundary diffusion it scales as δ/d, where δ is the 'width' of the grain boundary, assumed here to be twice the Burger's vector, 2b) Then by a similar argument the shear strain rate for boundary diffusion is;

$$\dot{\gamma}_{bd} = a'_g \frac{\Omega D_{bd}}{kT\ d^2} \frac{\delta}{d} \mu\ \hat{\tau} \qquad 2.19$$

The strain rate in this case is, again, proportional to the stress but is now inversely proportional to the grain size cubed (Coble, 1963). The diffusion constant, D_{bd}, has a different activation energy compared to that for volume diffusion. Data does not exist which will give either D_{ob}, the pre-exponential or the activation energy F_{bd} in the equation

$$D_{bd} = D_{ob} \exp(- \frac{F_{bd}}{RT}) \qquad 2.20$$

Here we have assumed D_{ob} equals D_{ov}, and F_{bd} equals 0.6 F_{vol}. These arbitrary assumptions have been made so that creep by diffusion around the grain boundaries, which almost certainly occurs, can be included on the deformation map.

Raj and Ashby (1971) have reanalysed diffusional creep. They calculate the rate at which grain boundary sliding can occur when void growth is not permitted on the boundary. If sliding is allowed on some grain boundaries, other grains must change their shape (figure 2.09, from Raj and Ashby). They find the shear strain rate when the change of shape is by diffusion either around or between the grain boundaries. For grains which are equiaxed, their calculation yields;

$$\boxed{\dot{\gamma}_{dif} = \frac{42\Omega\mu}{kTd^2} \left[D_{vol} + \frac{\pi\delta}{d} D_{bd} \right] \hat{\tau}} \qquad 2.21$$

where $\dot{\gamma}_{dif}$ is the shear strain rate for grain boundary sliding with diffusional accommodation, and the other symbols have been defined above. The equation has been used to represent diffusional creep on the deformation map. The numerical values used for the constants are given in Table 2.02; D_{ov} (9.13×10^{-4} m^2 s^{-1}), and F_{vol} (59.4 kJ mol^{-1}, 0.62 eV) have been taken from the tritium diffusion measurements of Ramseier (1967). The temperature dependences of D_{vol}, and D_{bd} are given in equations 2.16 and 2.20.

Bromer and Kingery (1968) made observations of the creep of polycrystalline ice in tension at low stresses in an effort to detect diffusional creep. They observed a linear dependence of strain rate on the stress, and that the strain rate was inversely proportional to the grain size (volume diffusion), but the diffusion constant calculated from the creep data was two orders of magnitude greater than that observed

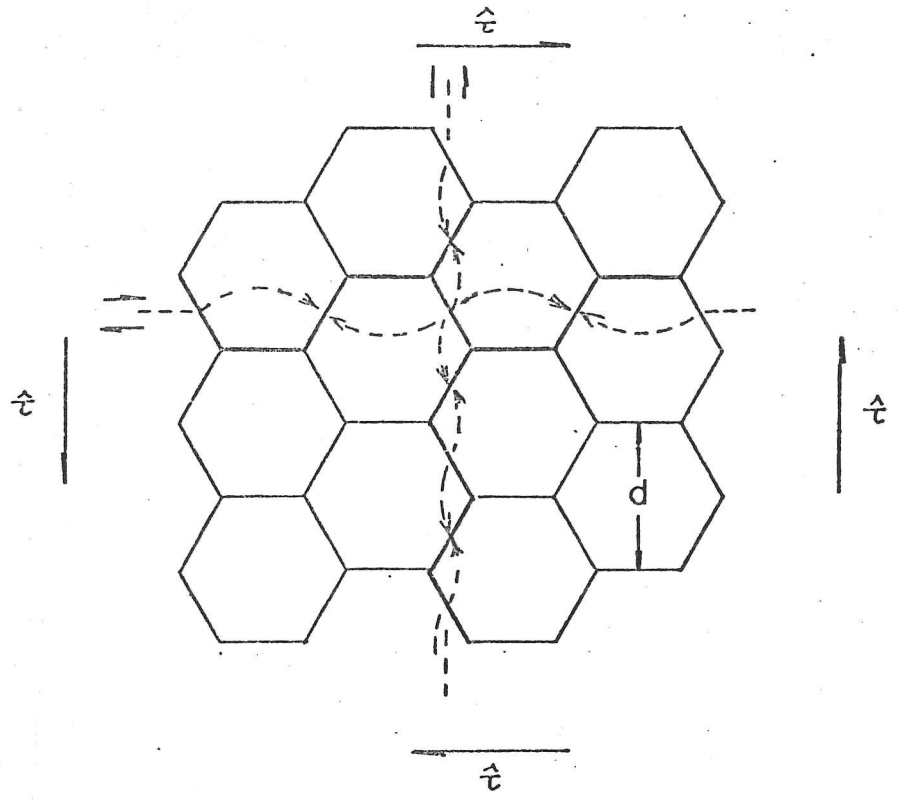

Figure 2.09; Grain boundary sliding with diffusional accommodation (from Raj and Ashby, 1971).

in the diffusion studies of Itagaki (1966) or Dengel and Riehl (1963). At $-10^{\circ}C$, when the normalised shear stress was 10^{-5} (0.03 MN m^{-2}), and for a grain size of 3.5 mm, Bromer and Kingery observed a minimum shear strain rate of 8.5×10^{-10} s^{-1}; equation 2.21 predicts a shear strain rate, if the data from table 2.02 is inserted, for the same conditions of 4.0×10^{-12} s^{-1} (96% volume diffusion). Bromer and Kingery suggest the discrepancy is due to enhanced diffusion in a wide region close to the grain boundary; I think this is unlikely. To obtain agreement between Bromer and Kingery's data and equation 2.21, it would be necessary to assume a grain boundary width of $10^{4}b$ (5 μm), which is clearly unlikely. A possible explanation for Bromer and Kingery's results could be the existence of an alternative mechanism, Harper-Dorn creep (Harper and Dorn, 1957), in which the dislocation density in equation 2.07 no longer depends on the stress, and so the strain rate for proton controlled rearrangement glide would depend linearly on the stress in equation 1.08. However Butkovich and Landauer (1960, with d equals 3 mm, and a range of τ from 0.01 to 0.001 MN m^{-2}), and Mellor and Testa (1969b, with d equals 1 mm, and a range of τ from 0.03 to 0.006 MN m^{-2}) in their creep tests do not find a linear dependence of strain rate on the stress.

Weertman (1969) has suggested that the data from the creep experiments described above were dominated by transient creep effects. He suggests that it is necessary for a creep strain of at least 1 % to occur before transient effects disappear; at a strain rate of 10^{-8} s^{-1} this would take at least a year. However, if it were feasible to prepare specimens with a very small grain size and in some way inhibit grain growth, it might be possible to observe diffusional creep at higher strain rates. The stresses, temperatures, and grain sizes where diffusional creep is likely to be observed are illustrated in the deformation maps in section 3. For a temperature of $-10^{o}C$, a normalised stress of 10^{-5}, and a grain size of 0.1 mm, the shear strain rate predicted by equation 2.21 is 1.2×10^{-8} s^{-1} (40 % volume diffusion).

In an ice shelf (a floating ice mass creeping under its own weight) the stresses may be sufficiently low, and the strains sufficiently large to establish true secondary creep for linear flow by diffusion (given a small enough grain size) to be faster than proton rearrangement controlled glide. However all observations on ice shelves to date (Thomas, 1973a, on the Brunt; Dorrer, 1971, on the Ward Hunt; Budd, 1966, on the Amery) have found that the proton rearrangement glide mechanism (Glen's flow law) equation satisfactorily predicts the strain rate, probably because the grain size is, in each case, too large. Gow (1963) observed from a core taken from the Ross Ice Shelf that the grain size increased linearly with depth with a minimum value of about 2 mm.

In Nabarro-Herring or Coble creep each grain suffers the same strain change as its neighbour. Another, quite different picture, is to assume some grains deform much more than others (by diffusion through the grain or around the grain boundary), and grains are allowed to exchange their neighbours. Ashby and Verrall (1973) have derived a constitutive equation to represent this, and use it to explain deformation behaviour at high strains (so called super-plasticity). The equation predicts a strain rate which is seven times faster than equation 2.21 but has the same form;

$$\dot{\varepsilon}_{sup} = \frac{300\,\Omega\mu}{kT\,d^2}\left[D_{vol} + \frac{3.3\,\delta}{d}D_{bd}\right]\left[\hat{\tau} - \frac{0.72\,\Gamma}{d}\right] \qquad 2.22$$

where the symbols have the same meaning as before, and Γ is the grain

boundary surface energy (because d is usually greater than 1 mm, Γ/d is much less than $\frac{\sigma}{2}$). There is insufficient evidence to show whether this mechanism, or that represented by equation 2.21 operates. In constructing the deformation maps we have chosen to use equation 2.21 as the constitutive equation for diffusional flow.

All the diffusional mechanisms described lead to the destruction of fabric (a prefered orientation of the c-axes); dislocation glide on the other hand will lead to the creation of a pronounced fabric. In the upper layers of an ice sheet (where we might expect diffusional flow to be faster than dislocation glide), the fabric is usually not well developed. Gow(1968) remarks that in the core obtained from the bore-hole at Byrd station a marked increase of fabric occured below 900 m. These remarks are expanded in the case study on the Byrd borehole in section 4.

Ashby (1972) discusses the introduction of the atomistic nature of the grain boundary, and the possibility that the grain boundary may not be a perfect source or sink of vacancies. Both effects will make equations 2.21 and 2.22 upper bound solutions to the creep rates.

2.6 Recrystallization, Pressure Melting and Other Mechanisms.

Recrystallization can affect the creep in two ways. Firstly repeated grain growth or dynamic recrystallization can remove grains which are unfavourably orientated for slip on the basal plane or as an accommodation mechanism as other grains change their shape by dislocation glide or diffusional creep; secondly the new grains have a much lower dislocation density, and consequently have a lower creep resistance. Yet, although recrystallization has been carefully observed and is well documented (Glen, 1955; Steinemann, 1958; Rigsby, 1960; Shumskiy, 1958; Wakahama, 1964; Watanabe and Oura, 1968; Duval, 1972; and Kamb, 1958, 1972) a satisfactory constitutive equation to represent its effect on creep does not exist. Kamb (1972), who discusses his results from combined compression and torsion experiments (between -5° and 0°C) in great detail, finds that the fabric depends on total strain rather than time or stress and develops progressively over the strain range 0.04-0.3. In a simple

shear test, a sample with an initially random c-axis distribution was found, after a stationary fabric had been established by recrystallisation, to consist of two maximum densities of c-axes (one at the pole of the shear plane, and the other 20° away from the shear direction). Dynamic recrystallisation is responsible for the acceleration of the creep after the secondary or steady state stage in a creep test when the strain is greater than a few per cent (Steinemann, 1958).

Barnes et al (1971) observed, in both their compression and hardness tests, that the creep rate above -8°C was much higher than that which would be predicted from their creep data obtained below this temperature. They suggest that this is due to melting on the grain boundaries, because first the same effect is not observed in single crystals, and secondly good thermodynamic arguments (Frank and Nye, 1973), and some experimental data (by nuclear magnetic resonance) exist to show that water may be found on the grain boundaries. The melting of the grain boundary naturally reduces its resistance to sliding, but this in itself does not constitute a separate mechanism as Langdon has suggested (Langdon, 1973). The sliding serves only to make the accommodation of changes of shape of other grains (by dislocation glide or diffusional creep) easier.

To derive an equation to represent their data, Barnes et al used the same equation which they had used to represent their data below -8°C, but with a much increased activation energy (120 kJ mol^{-1}) and a pre-exponential adjusted to give agreement between the two equations at -8°C. This represented the data satisfactorily, and we have used this purely empirical approach to plot the creep data above -8°C by using an equation of the form (taken from equation 2.11);

$$\dot{\gamma}_{gb} = a_o \hat{\tau}^3 \exp\left(-\frac{2(F_f+F_m)}{RT}\left(1-\frac{\hat{\tau}}{\hat{\tau}_o}\right)\right)\exp\left(-\frac{(F_f+F_m)}{R \times 265}\left(1-\frac{\hat{\tau}}{\hat{\tau}_o}\right)\right) \quad 2.23$$

where the symbols have been explained above. We have chosen to make the activation energy twice that for proton rearrangement controlled glide.

Above -3°C Barnes et al observed a very rapid fall off in hardness which they attributed to pressure melting because the point at which fall off occurred could be predicted over a range of 10^8 in loading times from the depression of freezing point by pressure melting.

For the temperatures and stresses we are considering here it is necessary to consider the complete phase diagram (see chapter 1, or Fletcher, 1970; Hobbs, 1974). If it is assumed that, beneath a hardness indenter, the mean hydrostatic pressure, p, is two thirds of the indentation stress, p_h, (Tabor, 1970) then it is possible to derive a relation between the equivalent normalised shear stress under the indenter and pressure-temperature relations from the phase diagram representing phase changes. As an example, consider the Liquid-Ice 1_h-Ice III triple point. From Fletcher (1970) this is at a temperature of $-22.0^{\circ}C$, and a pressure of 207 MN m^{-2}; if σ_h is the indentation pressure or hardness, then the mean pressure, $\bar{p}$, is

$$\bar{p} = \frac{2}{3}\sigma_h \qquad 2.24$$

but the mean normalised shear stress, $\langle\hat{\tau}\rangle$, is given by (a relation used in the discussion of hardness results above)

$$\langle\hat{\tau}\rangle = \frac{1}{3\sqrt{3}}\frac{\sigma_h}{\mu} \qquad 2.25$$

which implies that pressure melting effects occur at $-22^{\circ}C$ when

$$\langle\hat{\tau}\rangle \geq \frac{1}{2\sqrt{3}}\frac{p}{\mu} \qquad 2.26$$

Using this approach the phase diagram can be translated onto axes of normalised shear stress (in a hardness test), and homologous temperature. This has been done on the deformation maps given in the next section; it can be seen that pressure melting effects or the phase change from Ice 1_h to Ice III or II are only apparent for $\hat{\tau}$ greater than 3×10^{-3}. For the purposes of the discussion in section 2.4 on lattice resistance controlled glide, and because of lack of experimental creep data at low temperatures, any difference between the mechanical properties of Ice 1_h and Ice III or II has been ignored. From observations of the hardness at temperature within a few degrees of the melting point, Barnes et al showed, by observing how the hardness changed for indenters of different thermal conductivity that regelation processes were important.

It is inevitable that the discussion has overlooked other feasible deformation mechanisms. In b.c.c. and hexagonal metals particularly at low homologous temperatures or high strain rates (where

five independent slip systems are not available) twinning occurs when a stress is applied. Twinning is the co-operative reshuffling of parallel atomic planes to form a new lattice of a different crystallographic orientation (Kelly and Groves, 1970), and it is quite feasible that it can occur in ice, although it has not been plotted on the deformation mechanism maps. Other variants of the mechanisms previously described may also occur, for instance diffusional creep between sub-grains. When creep and hardness data have been collected over a much wider range of temperatures and stresses than that shown in figure 2.02, other mechanisms, for which no account has been taken, may be discovered.

3. THE MAPS.

3.1 Construction of the Maps.

In equations 2.03, 2.08, 2.14, 2.21, and 2.23 constitutive equations for the shear strain rate as a function of stress, temperature, and grain size for the different mechanisms described have been stated. A total strain rate can be computed by adding the slower of the shear strain rate for proton rearrangement controlled glide, $\dot{\gamma}_{prg}$, or lattice resistance controlled glide, $\dot{\gamma}_p$, to the strain rate predicted from diffusion creep, $\dot{\gamma}_{dif}$. When the temperature is greater than $-8^{\circ}C$, the equation for proton rearrangement controlled glide (equation 2.08) is replaced by equation 2.23 to include the effects of grain boundary melting and recrystallization. Addition of the strain rates linearly is a first approximation to enable the maps to be constructed; different mechanisms may interact with each other. Thus the total shear strain rate, $\dot{\gamma}_t$, is given by equation 2.27.

$$T < -8^{\circ}C$$

$$\dot{\gamma}_t = \dot{\gamma}_c + \dot{\gamma}_{dif} + \begin{bmatrix} \dot{\gamma}_{prg} \\ \text{or} \\ \dot{\gamma}_p \end{bmatrix}$$

$$T \geq -8^{\circ}C \qquad 2.27$$

$$\dot{\gamma}_t = \dot{\gamma}_c + \dot{\gamma}_{dif} + \dot{\gamma}_{gbm}$$

Table 2.02 gives the data which has been used in the equations to calculate $\dot{\gamma}_t$.

Table 2.02

Data used to construct the Deformation Mechanism Maps.

Atomic Volume	Ω	3.27×10^{-29} m^3	(b^3)
Burger's Vector	b	4.52×10^{-10} m	1
Melting Temperature	T_m	273.15 ^oK	1
Shear Modulus (Adjusted to 300^oK)	μ	2.91 GN m^{-2}	2
Temperature Dependence of the Modulus	$\frac{d\mu}{dT}$	1.29×10^{-3} $^oK^{-1}$	2
Pre-exponential for Lattice Diffusion	D_{ov}	9.13×10^{-4} m^2 s^{-1}	3
Activation Energy for Lattice Diffusion	F_{vol}	59.4 kJ mol^{-1}	3
Pre-exponential for Boundary Diffusion	D_{ob}	9.13×10^{-4} m^2 s^{-1}	*
Activation Energy for Boundary Diffusion	F_{bd}	38.3 kJ mol^{-1}	*
Width of Boundary Diffusion Path	δ	9.04×10^{-10} m	(2b)
Pre-exponential for Proton Rearrangement Controlled Glide	a_o	1.72×10^{15} s^{-1}	4
Activation Energy for Proton Rearrangement Controlled Glide	$F_m + F_f$	54.2 kJ mol^{-1}	1
Pre-exponential for Lattice Resistance Controlled Glide	a_p	10^{11} s^{-1}	*
Activation Energy for Lattice Resistance Controlled Glide	F_f	32.3 kJ mol^{-1}	*
Normalised Flow Stress at 0^oK for Proton Rearrangement Controlled Glide	$\hat{\tau}_o$	0.0149	4
Normalised Flow Stress at 0^oK for Lattice Resistance Controlled Glide	$\hat{\tau}_p$	0.1409	*
Ideal Shear Strength	$\hat{\tau}_{th}$	0.10	*

1 - Fletcher (1970), 2 - Dantl (1968), 3 - Ramseier (1967)
4 - Barnes, Tabor and Walker (1971), * - estimated.

For grain sizes of 0.1 mm, 1 mm, and 10 mm, the variation of $\dot{\gamma}_t$ as a function of temperature and stress has been used to plot contours of constant shear strain rate on axes of homologous temperature and normalised stress. Other lines have been drawn on the diagram, or deformation mechanism map, to separate the fields in the stress-temperature space where each mechanism is rate controlling. These have been calculated by finding the stress and temperature where the predicted strain rates for each mechanism are equal. The plots were drawn with a FORTRAN programme written by H.J. Frost (personal communication). The resultant diagrams are shown in figure 2.10a, b, and c. It should be recognised that the creep and hardness data used to construct the maps exist over only a small range of stress and temperature, and the maps can only be as good as the data used to construct them.

The maps show six seperate fields; collapse, lattice resistance controlled glide, proton rearrangement controlled glide, diffusional creep, and pressure melting. Diffusional creep has been further sub-divided into boundary and volume diffusion. Above $-8^{\circ}C$, the proton rearrangement controlled glide field has been divided to represent the effects of grain boundary melting and recrystallization. A box, which represents the extent of the data plotted in figure 2.02, has also been drawn. If the stress, temperature, and grain size in a sample of ice is known, it is possible from the maps to deduce the strain rate and the dominant creep mechanism.

If the maps in figure 2.10 are compared with the map for Nickel shown in figure 2.01, the important differences in creep behaviour between ice and a metal can be seen. First creep mechanisms which appear on the Nickel map, L.T. and H.T. creep (diffusion controlled climb around obstacles) are absent from the ice maps; secondly ice is surprisingly creep resistant (because of the unique barrier to dislocation motion). At a homologous temperature of 0.8, and a normalised stress of 3×10^{-4}, Nickel has a strain rate of 10^{-2} s^{-1} (1% in 1 s) compared to 10^{-9} s^{-1} (1% in four months) for ice. Lastly, Nickel at room temperature (a homologous temperature of 0.2) has a well defined yield stress; as the stress is increased nothing happens until the normalised stress reaches about 5×10^{-3}, when many contours of constant strain rate are crossed, and 'yield' would be observed. On the other hand, at temperatures close to $0^{\circ}C$, where ice is used as an engineering material, contours of constant

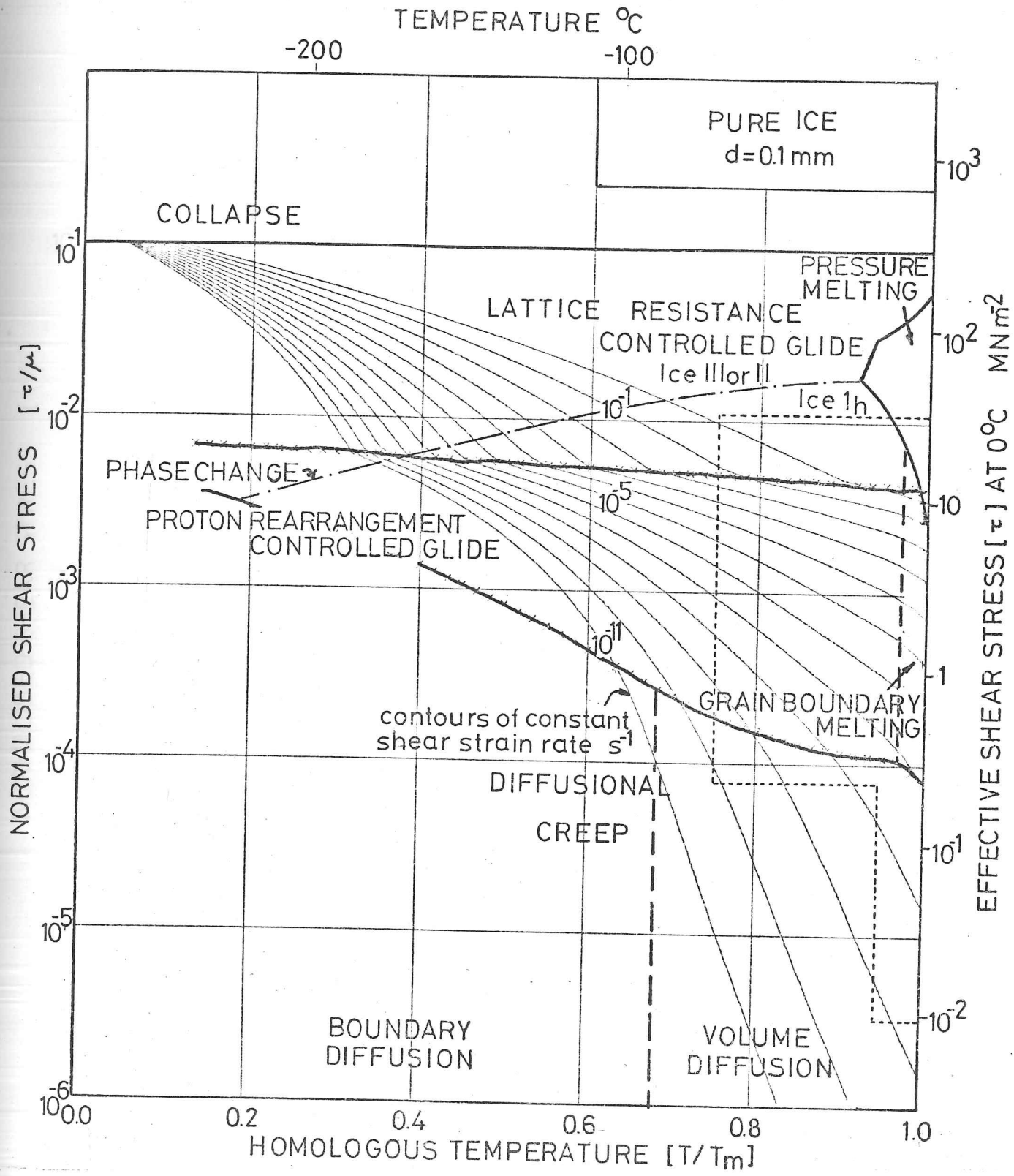

Figure 2.10a; Deformation Mechanism Map for Polycrystalline Ice of 0.1 mm grain size.

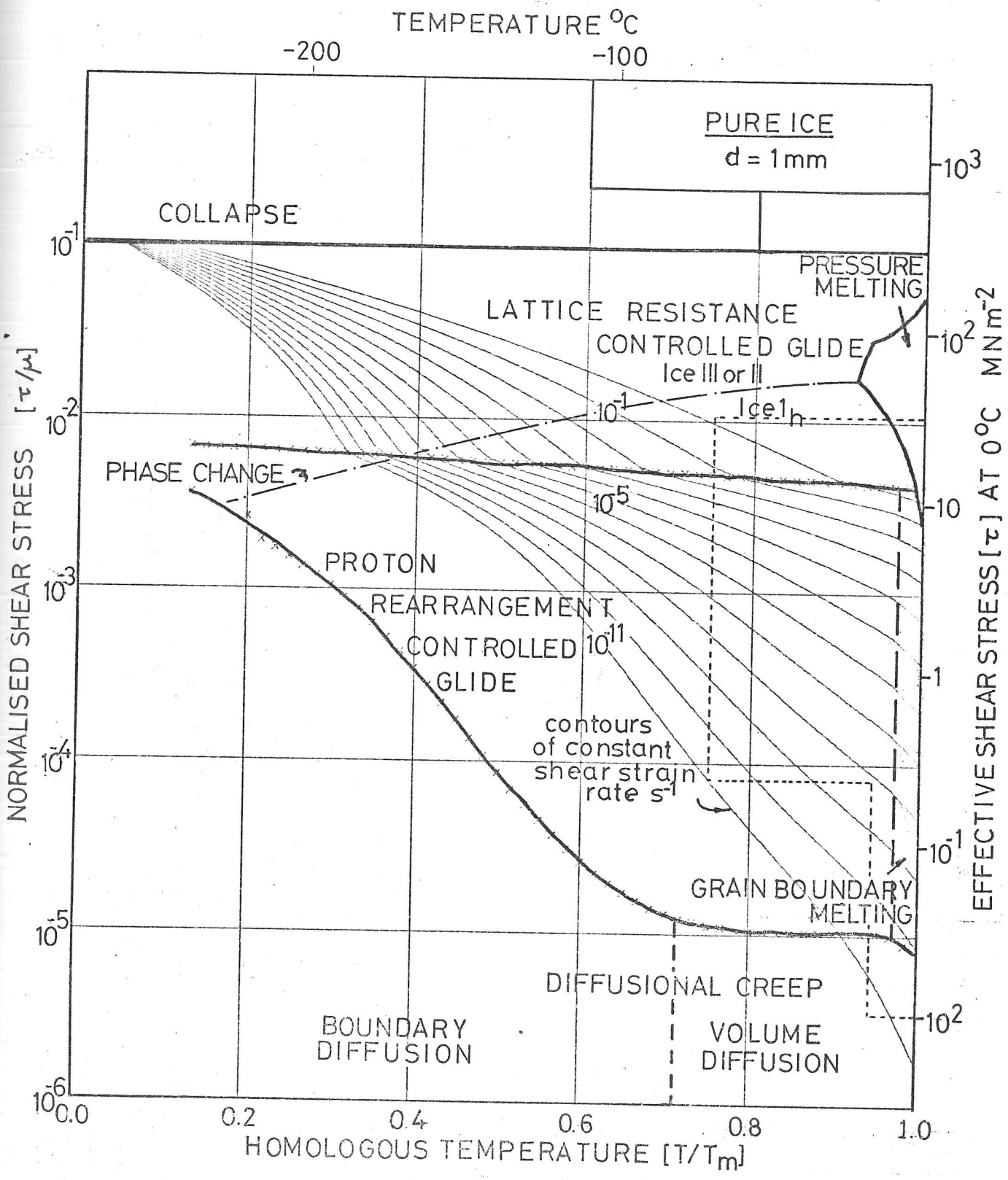

Figure 2.10b; Deformation Mechanism Map for Polycrystalline Ice of 1 mm grain size.

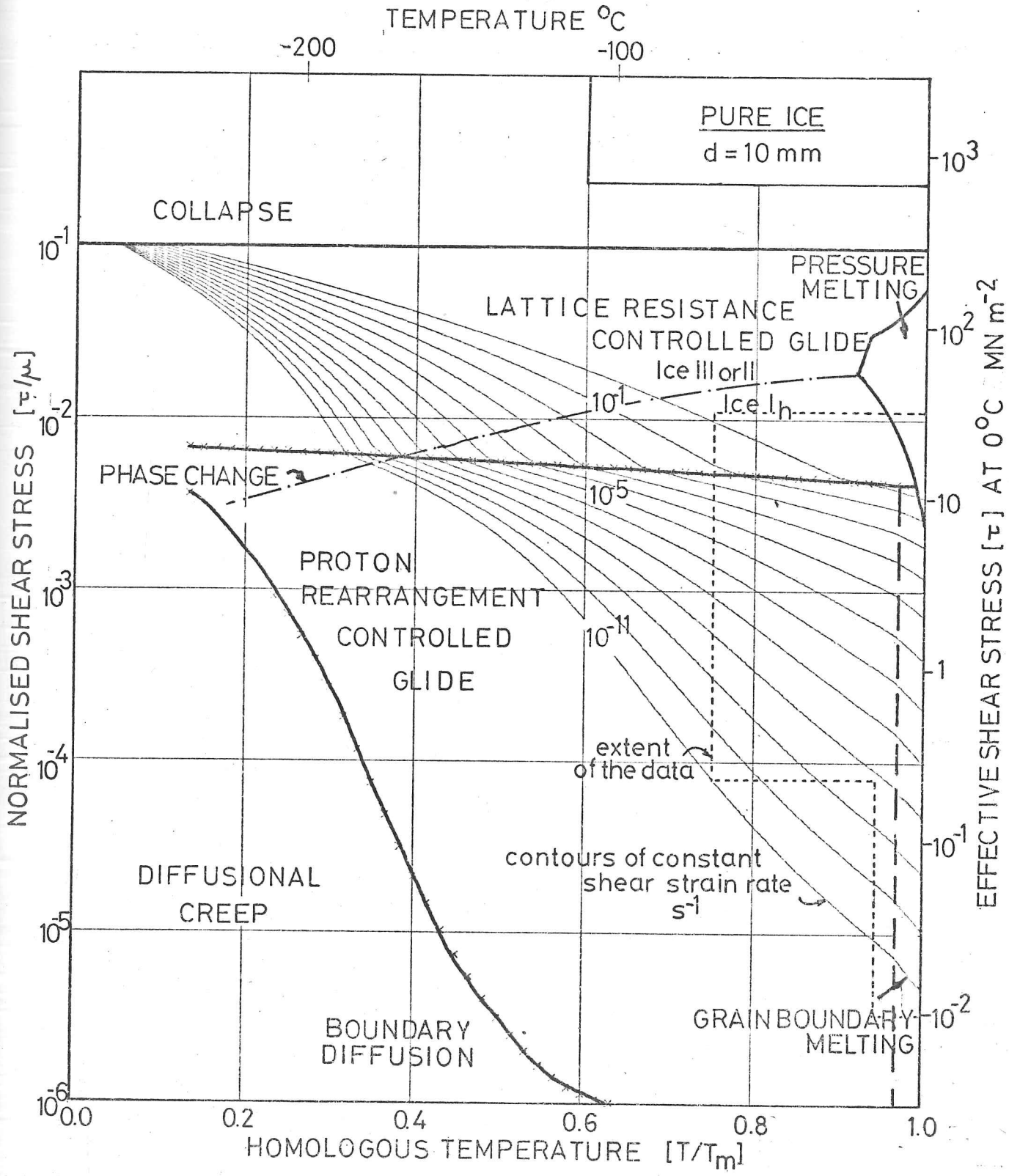

Figure 2.10c; Deformation Mechanism Map for Polycrystalline Ice of 10 mm grain size.

strain rate are crossed very slowly when the stress is increased. Thus, at temperatures close to its melting point, ice does not have a well defined 'yield' stress.

It will be most interesting, when they become available, to compare the ice maps with those for other materials such as Silicon and Germanium. Silicon and Germanium have high Peierls barriers, and an open lattice structure, and consequently their mechanical properties should be similar, using the normalisations adopted for the maps, to those of ice.

The maps can also be plotted with axes of shear strain rate, and normalised stress with curves of constant temperature. Such a plot has already been used in figure 2.05. Further plots on these axes are shown in figure 2.11. Reproduced in the same figure is a diagram by Budd (1969), which he deduced purely empirically from a selection of field and laboratory creep data. By comparing the figures, the significance of changing the grain size can be appreciated. Budd for his calculations for the whole Antarctic ice sheet required a flow law which depended only on stress and temperature, and assumed the grain size variation was not important.

4. CASE STUDIES.

In this section two simple examples of the use of the maps are given. The possible creep mechanisms, and strain rates are deduced for firstly the Antarctic Ice Sheet at Byrd station (80° 01'S, 119° 32'W), and secondly for the spreading of ice shelves (large floating ice masses which creep under their own weight).

4.1 Byrd Borehole.

Figure 2.12 is a profile of the Antarctic ice sheet taken from Budd, Jensson, and Radok (1971), which extends along a flowline through Byrd station. The ice sheet is in a dynamic equilibrium; although snow continually accumulates on the surface, the ice creeps out radially from shear stresses created by its own weight, and mass is lost at the edges by calving of icebergs and ablation so that the overall profile is stationary.

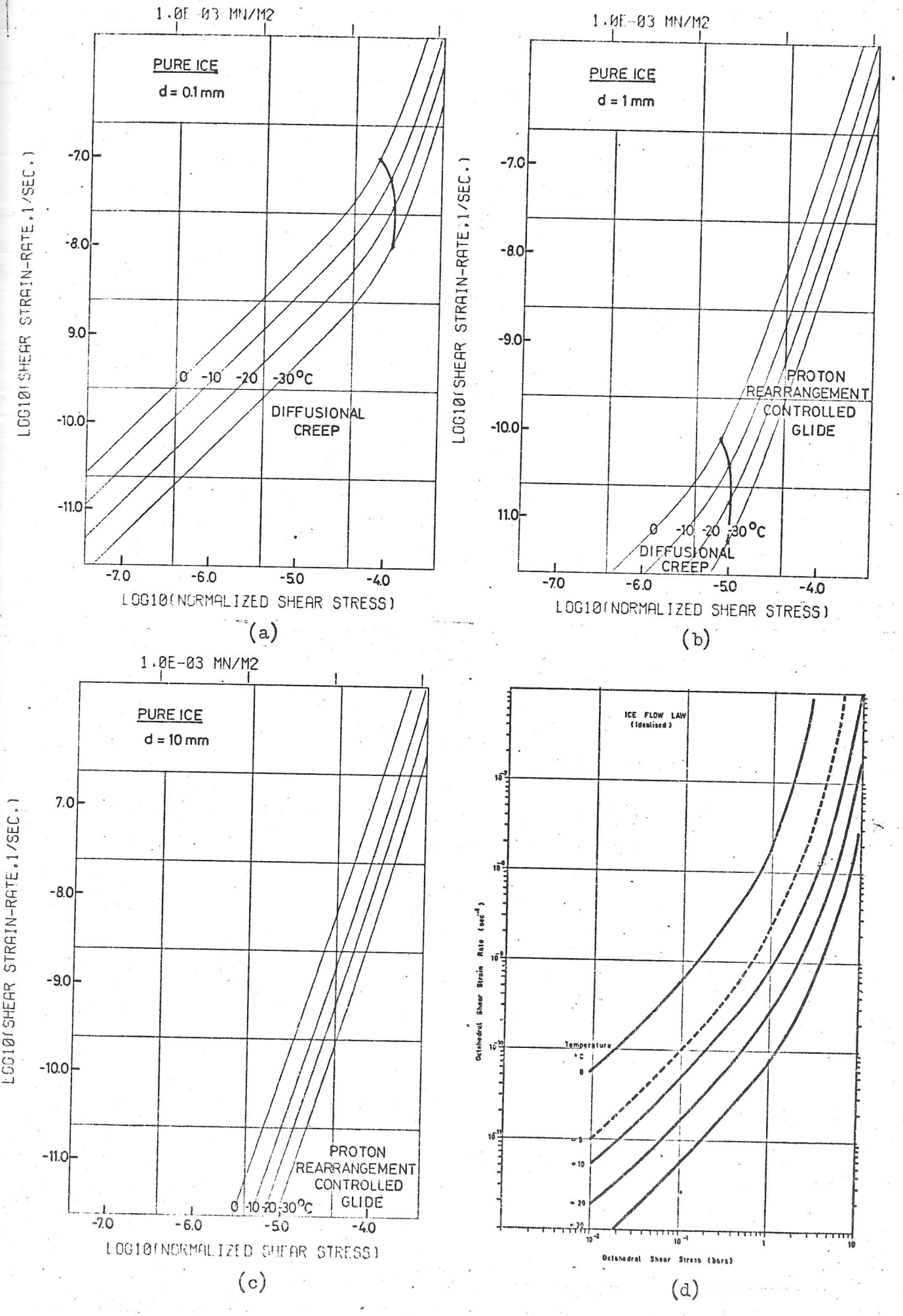

Figure 2.11; Constant Temperature Plots. (d) is reproduced from Budd (1969).

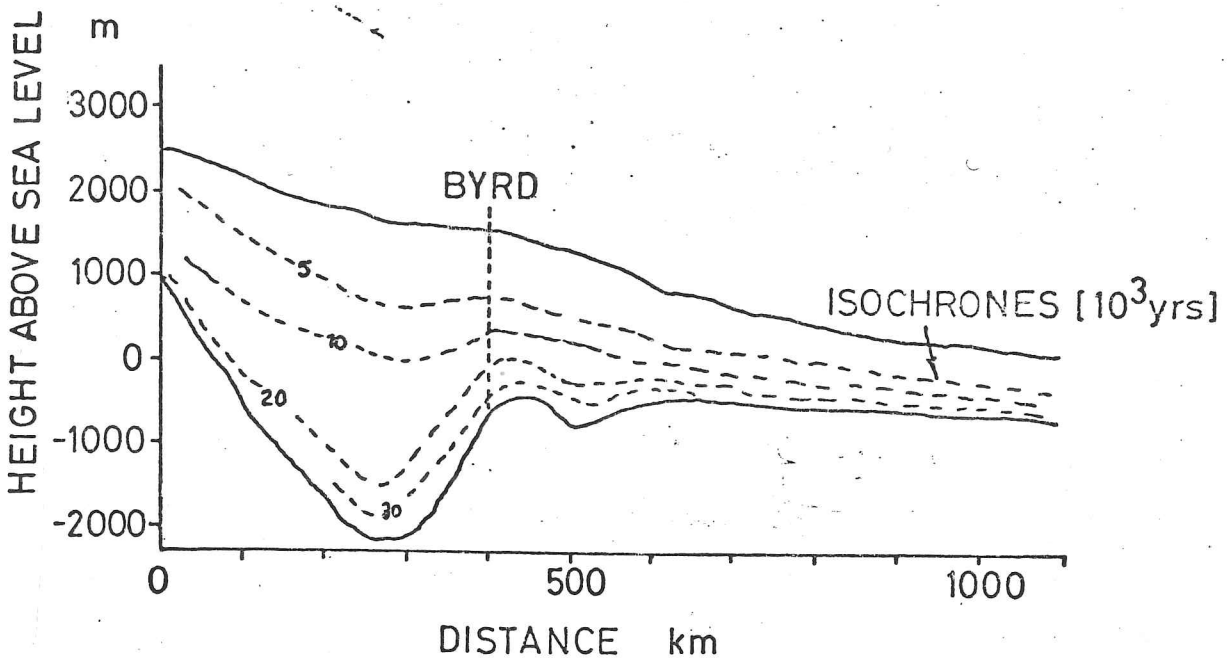

Figure 2.12; A profile of the Antarctic Ice Sheet along a flowline through Byrd station.

In the 1967-68 season, a borehole was drilled through the ice sheet to bedrock, a distance of 2164 m. Temperature sensors were lowered down the hole, and a temperature profile measured (Gow, Ueda, and Garfield, 1968); the core extracted has provided a comprehensive picture of the fabric development and grain size through the ice sheet (Gow, 1970; 1976). An order of magnitude estimate of the shear stresses in the ice sheet at Byrd station can be made by assuming simple shear due only to the surface slope. The stresses are then given by (Paterson, 1969);

$$\tau = \rho g h \alpha \qquad 2.28$$

where ρ is density, g the acceleration due to gravity, h the depth, and α the surface slope. The surface slope has been taken as 0.0022 rads from the contour maps given by Budd et al (1971).

The temperature and shear stress profiles have been used to plot the temperature-stress regime of the Byrd borehole on an enlarged

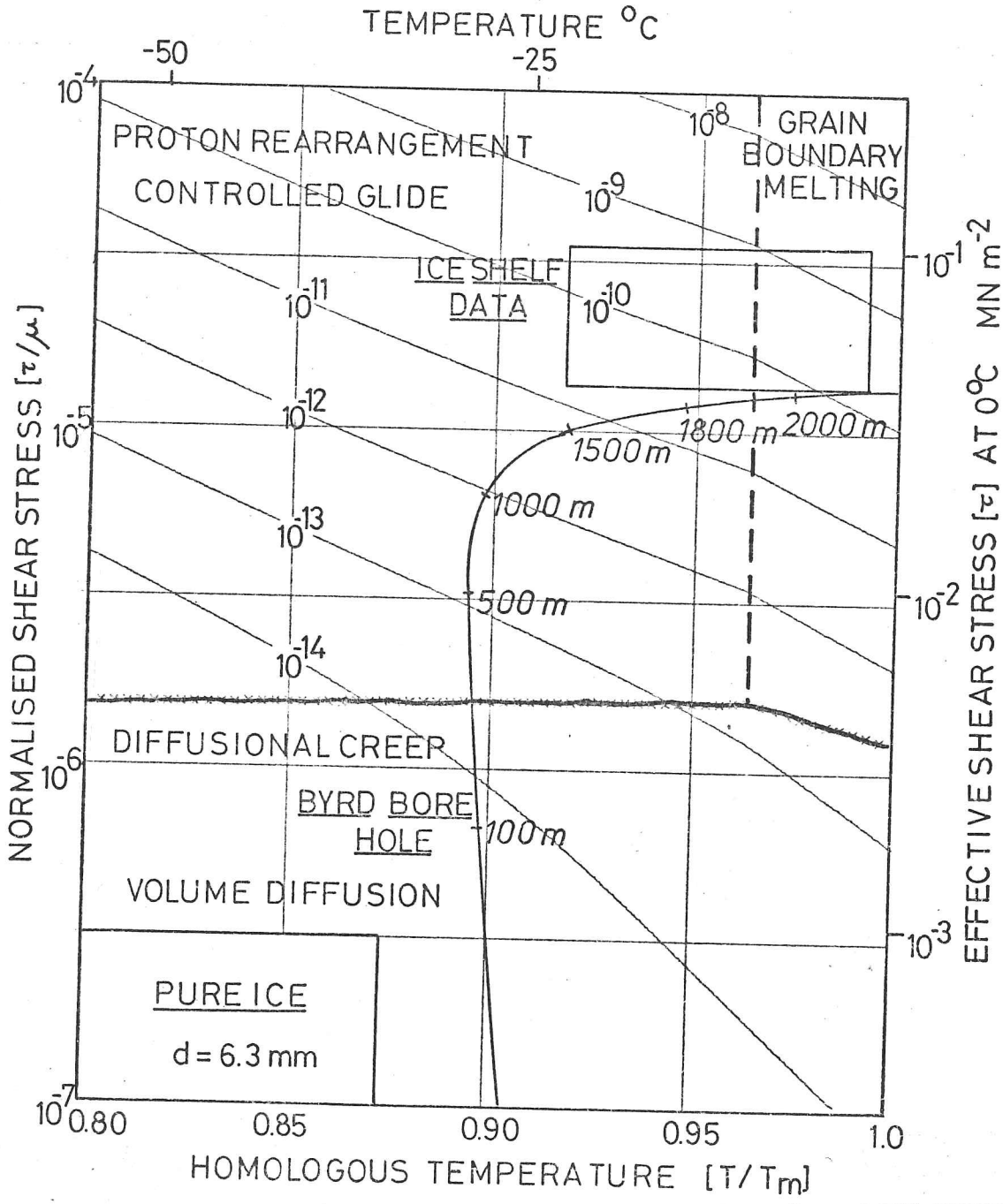

Figure 2.13 Part of the Deformation Map expanded to show the creep mechanisms in the stress/temperature regime of the Byrd borehole and the Ice Shelf data quoted by Thomas (1973). Lines plotted are contours of constant shear strain rate in s^{-1}.

section of the deformation map shown in figure 2.13. The grain size used in the calculations, 6.3 mm, is the average grain size observed by Gow (1970) in the first 1200 m of the borehole. It is clear from the diagram, that for almost the whole depth of the ice sheet, the creep is dominated by proton rearrangement controlled glide. It is

only in the first few hundred metres, that diffusional creep is faster, but then the strain rates are very low (less than 10^{-14} s^{-1}, 1% in 30,000 yrs).

In section 2.5 it was pointed out that evidence for diffusional creep could be obtained from observations of fabric changes because a dislocation mechanism will create a fabric while a diffusional mechanism destroys it. Gow (1970; Gow and Williamson, 1976) found fabric changes at 300m, where a fabric began to develop and 1800 m, where the strong single pole fabric changed to a multi-pole diagram. From the deformation map in figure 2.13, 300 m corresponds to the field boundary between diffusional and dislocation creep, and 1800 m corresponds roughly to the onset of grain boundary melting, where grains would begin to roll over each other. However it should be emphasised that the absence of fabric in the upper 300 m may be simply because the total strain, perhaps less than 1 %, is too small.

When the strain rates are integrated over the ice depth, the velocity of Byrd station, due to the creep in the ice, is found to be a few metres a year. Morgan (1970) attempted to measure this velocity by a trigometric survey, and found values of this order, but thought that the errors in his observations were too large to attach any significance to the values. It soon should be possible to obtain reliable values for the velocity from satellite observations or fading patterns from radio-echo sounding.

4.2 Ice Shelves.

An ice shelf is a floating ice mass, which creeps outwards from forces due to its own weight. Ice shelves range in thickness from 50 to 300 m, and are fed from surrounding land based glaciers or ice sheets. Weertman (1957) first gave the solution for the stress field within an ice shelf. Thomas (1973a, 1973b) extended this analysis and collected together data from a number of ice shelves. He showed that the observed strain rates agreed with an extrapolation of Walker's (1970) laboratory creep data; the strain rate was proportional to the third power of the stress. The data quoted by Thomas has been used to plot on figure 2.13

a box which represents the stress and temperature regime of most ice shelves. Although the grain size is smaller than that for the Byrd borehole data (it ranges from 3 to 4 mm (Gow, 1970)), the box still lies completely in the proton rearrangement controlled glide field of the deformation map (see figure 2.10b for the location of the diffusional creep field boundary for a grain size of 1 mm). Therefore, as Thomas and Weertman pointed out, ice shelves have a spreading rate which depends on the third power of the stress. (see equation 2.08 for the constitutive equation for proton rearrangement controlled glide). The strain rates predicted are

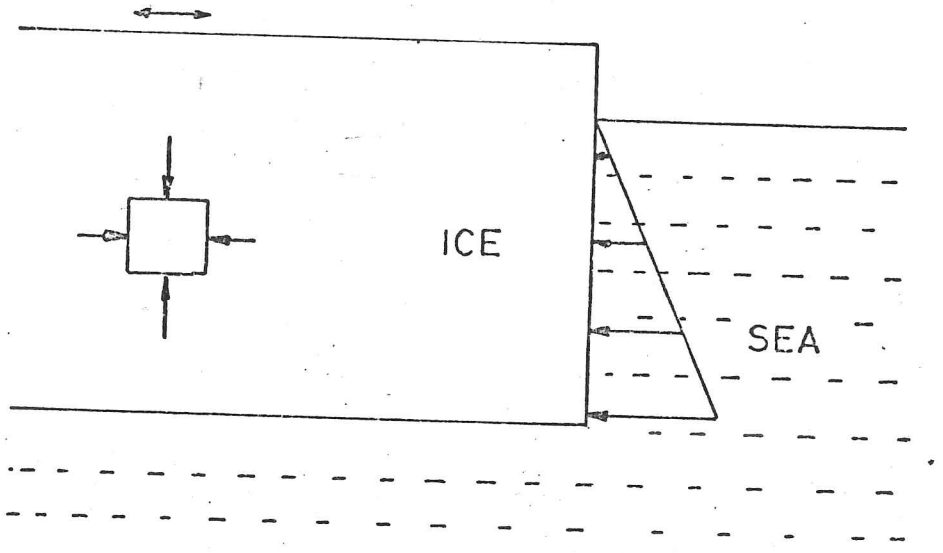

Figure 2.14; A diagrammatic view of an ice shelf. Measurement of the surface strain rate gives the spreading rate which is constant through the thickness of the ice shelf.

of the order of 10^{-10} s^{-1} (3.2×10^{-3} yr^{-1}).

The fabric changes in the Ross ice shelf have been obtained from a borehole drilled in 1958 at Little America V (Gow, 1963; 1970). The fabric is not strongly developed until below 60 m (approximately the depth at which densification ends), and then a distinct multipole fabric is seen. Rapid grain growth occurs towards the bottom of the shelf, as the temperature approaches the melting point. Surprisingly at Maudheim, although the stresses and temperatures lie within the box shown in figure 2.13, Schytt (1958) did not observe any significant trend in the c-axis orientation. This may again be because the total strain is too small, and suggests that fabric

development is not a reliable guide to the creep mechanism unless the total strains are large.

5. SUMMARY AND CONCLUSIONS.

In this chapter, the available creep data, and possible microscopic creep mechanisms for polycrystalline ice have been discussed. Four constitutive equations, which relate the shear strain rate to the shear stress, temperature, and grain size have been presented. It was suggested that Glen's picture of proton rearrangement controlled dislocation glide is correct but, because a satisfactory quantitive picture does not yet exist, the constitutive equation used was deduced on a semi-empirical basis from the creep data of Barnes et al (1971), and the properties of L and D defects determined by electrical measurements. It was found that when this equation was extrapolated to temperatures between -50 and -100°C, it could not predict the hardness data obtained by Schultz and Knappwost (1968); this suggested that another mechanism, lattice resistance or Peierls barrier controlled glide should be introduced, and a suitable constitutive equation was given. On a purely empirical basis, the observations of Barnes et al (1971) that grain boundary melting and other effects become important above -10°C was introduced by the introduction of a similar equation to that for proton rearrangement controlled glide but with the activation energy doubled. From observations made in other materials, it was also suggested that diffusional creep is a feasible mechanism for the creep of ice, and a suitable constitutive equation was given.

The constitutive equations have been combined to construct, on axes of homologous temperature and normalised stress, diagrams or deformation mechanism maps which illustrate how the different mechanisms dominate in different regimes or fields of stress and temperature, and how these fields change for different grain sizes. When the maps were compared with the map for Nickel, ice was found, with the normalisations used to construct the map, to be surprisingly creep resistant.

Two applications of the maps to creep in the Antarctic ice sheet at Byrd station, and to creep in ice shelves were presented.

6. APPENDIX.

6.1 The Temperature Dependence of the Modulus.

Throughout the discussion, the constitutive equations are quoted in terms of the normalised stress, $\hat{\tau}$, which is the shear stress, τ, divided by the modulus, μ. The modulus has a slight temperature dependence, which must be taken into account because the stress often appears in an exponential. Failure to include this effect would give an incorrect activation energy. Gold (1973) has discussed this effect.

The elastic modulus for a hexagonal material such as ice is defined by six independent quantities c_{11}, c_{22}, c_{33}, c_{12}, c_{13}, and c_{44}. The c's or compliances relate the stress, σ_i, to the strain, ϵ_j, by the relation;

$$\sigma_i = c_{ij}\ \epsilon_j \qquad 2.29$$

where σ_i is given by

$$\sigma_i = \begin{bmatrix} \sigma_1 & \sigma_6 & \sigma_5 \\ \sigma_6 & \sigma_2 & \sigma_4 \\ \sigma_5 & \sigma_4 & \sigma_3 \end{bmatrix} = \begin{bmatrix} \sigma_{11} & \sigma_{12} & \sigma_{13} \\ \sigma_{21} & \sigma_{22} & \sigma_{23} \\ \sigma_{31} & \sigma_{32} & \sigma_{33} \end{bmatrix} \qquad 2.30$$

and ϵ_j is given by

$$\epsilon_j = \begin{bmatrix} \epsilon_1 & \frac{1}{2}\epsilon_6 & \frac{1}{2}\epsilon_5 \\ \frac{1}{2}\epsilon_6 & \epsilon_2 & \frac{1}{2}\epsilon_4 \\ \frac{1}{2}\epsilon_5 & \frac{1}{2}\epsilon_4 & \epsilon_3 \end{bmatrix} = \begin{bmatrix} \epsilon_{11} & \epsilon_{12} & \epsilon_{13} \\ \epsilon_{21} & \epsilon_{22} & \epsilon_{23} \\ \epsilon_{31} & \epsilon_{32} & \epsilon_{33} \end{bmatrix} \qquad 2.31$$

and for a hexagonal material (Nye, 1957)

$$c_{ij} = \begin{bmatrix} c_{11} & c_{12} & c_{13} & \cdot & \cdot & \cdot \\ c_{12} & c_{22} & c_{13} & \cdot & \cdot & \cdot \\ c_{13} & c_{13} & c_{33} & \cdot & \cdot & \cdot \\ \cdot & \cdot & \cdot & c_{44} & \cdot & \cdot \\ \cdot & \cdot & \cdot & \cdot & c_{44} & \cdot \\ \cdot & \cdot & \cdot & \cdot & \cdot & \frac{1}{2}(c_{11}-c_{12}) \end{bmatrix} \qquad 2.32$$

The convention for the stresses σ_{ij} $(i,j=1,3)$ is shown in figure 2.15. The relation for c_{ij} assumes that the c-axis is along the x_3 direction.

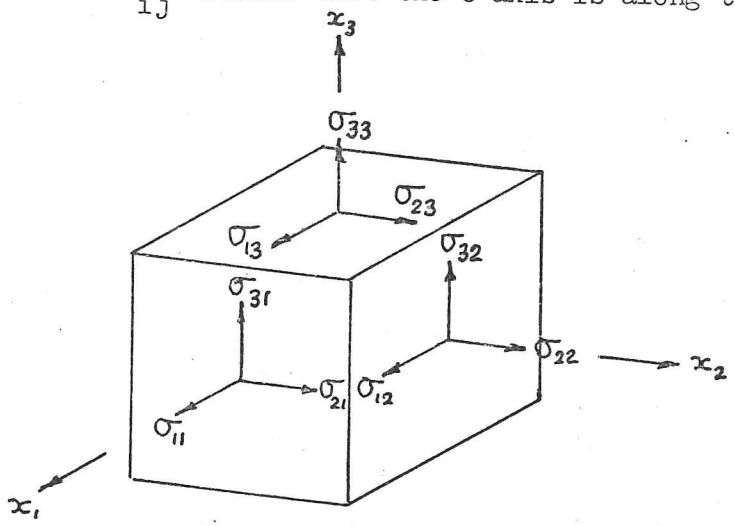

Figure 2.15; The convention for the stresses σ_{ij}.

Dantl (1968) has determined the independent c_{ij}'s for ice, and their temperature dependence by an ultrasonic technique. For the purpose of normalising the shear stress, the shear stress on the slip planes is appropriate. The shear modulus on the basal plane is c_{44}, and on the prismatic planes is $\frac{1}{2}(c_{11}-c_{12})$. To construct the deformation maps the shear modulus, $\mu(T)$, has been set equal to the geometric mean of these two values; thus

$$\mu(T) = \left[\frac{c_{44}(c_{11}-c_{12})}{2}\right]^{\frac{1}{2}} \qquad 2.33$$

When Dantl's results are put into this formula, it is found to the first order in the temperature that

$$\mu(T) = 2.906(\,1 - 1.29 \times 10^{-3}(T - 300)) \quad \text{GN m}^{-2} \qquad 2.34$$

where T is the temperature in ^{o}K.

6.2 Equivalent Shear Stress, and Equivalent Shear Strain Rate.

Rigsby (1958) and Haefeli et al (1968) have shown that the creep of ice is independent of hydrostatic pressure. The creep rate is then only a function of the deviatoric part of the stress tensor, σ'_{ij}, which is defined by the expression

$$\sigma'_{ij} = \sigma_{ij} - \frac{1}{3}\sigma_{kk}\,\delta_{ij}$$

where σ_{ij} is the stress tensor illustrated in figure 2.15, and δ_{ij} is zero when i does not equal j, and 1 otherwise. We have adopted the usual Von Mises criteria, that the creep rate is a function of only the second invariant of the deviatoric stress tensor, so that in the equations an equivalent shear stress, τ, defined by

$$\tau = \left[\frac{1}{2}\sigma'_{ij}\sigma'_{ij}\right]^{\frac{1}{2}}$$

is used. In terms of the principal stresses of σ_{ij}, σ_1, σ_2, and σ_3 this equals

$$\tau = \left[\frac{1}{6}(\sigma_1-\sigma_2)^2+(\sigma_1-\sigma_3)^2+(\sigma_2-\sigma_3)^2\right]^{\frac{1}{2}}$$

These are related to the stress, σ_{11}, in a uniaxial test by the relation

$$\tau = \frac{1}{\sqrt{3}}\sigma_{11}$$

The relations between the octahedral shear stress, τ_{oct}, uniaxial stress, and equivalent shear stress are combined into Table 2.03.

Table 2.03

	τ	σ_{11}	σ_{oct}
τ	1	$1/\sqrt{3}$	$\sqrt{3/2}$
σ_{11}	$\sqrt{3}$	1	$3/\sqrt{2}$
σ_{oct}	$\sqrt{2/3}$	$\sqrt{2}/3$	1

To convert from the stress state in the left hand column to those in the vertical columns multiply by the factor given.

The shear strain rate used in the equations is the equivalent engineering shear strain rate defined by

$$\dot{\gamma} = \left[2\dot{\epsilon}_{ij}\dot{\epsilon}_{ij}\right]^{\frac{1}{2}}$$

where $\dot{\epsilon}_{ij}$ is the shear strain rate tensor. Creep data is also quoted in terms of an effective strain rate defined by $\dot{e} = (\frac{1}{2}\dot{\epsilon}_{ij}\dot{\epsilon}_{ij})^{\frac{1}{2}}$, and

the octahedral shear strain rate, $\dot{\epsilon}_{oct}$, and the uniaxial strain rate, $\dot{\epsilon}_{11}$. The creep rate in a uniaxial test is related to the equivalent shear strain rate by

$$\dot{\gamma} = \sqrt{3}\,\dot{\epsilon}_{11}$$

The conversion factors for all the strain states are given in Table 2.04.

Table 2.04

	γ	$\dot{\epsilon}_{11}$	$\dot{\epsilon}_{oct}$	$\dot{e}$
γ	1	$\sqrt{3}$	$\sqrt{6}$	2
$\dot{\epsilon}_{11}$	$1/\sqrt{3}$	1	$\sqrt{2}$	$2/\sqrt{3}$
$\dot{\epsilon}_{oct}$	$1/\sqrt{6}$	$1/\sqrt{2}$	1	$\sqrt{2/3}$
$\dot{e}$	1/2	$\sqrt{3}/2$	$\sqrt{3/2}$	1

As before, to obtain the conversion factor from a strain rate in the left-hand column to another in the vertical column, multiply by the factor shown.

CHAPTER THREE

DISLOCATION KINK VELOCITIES IN ICE

DISLOCATION KINK VELOCITIES IN ICE.*

1. INTRODUCTION.

In chapter 2 the possible creep mechanisms in polycrystalline ice were reviewed. It was pointed out there that Glen (1968a,b) has shown that the motion of dislocations is opposed by a mechanism peculiar to the hydrogen bonded structure of ice. If the protons cannot rearrange ahead of a dislocation, its motion creates defects of such energy that slip is possible only at stresses of order 0.1μ, where μ is the shear modulus. Slip is only possible at any lower stress if the protons are mobile, and can rearrange by a process resembling diffusion, controlled by the concentration and mobility of Bjerrum and Ionic defects. The rate at which these permit proton rearrangement is known because similar rearrangements are responsible for dielectric losses in ice (Fletcher, 1970; Hobbs, 1974 review the electrical properties of ice).

If proton rearrangement is occurring, an initially straight dislocation in a crystal of ice will advance (when a stress is applied) by the nucleation of pairs of kinks (see figure 2.04). These appear at places where the proton arrangement just ahead of the dislocation is favourable; their position is such that no defect is created when the dislocation advances (see figure 2.02). They then drift apart, advancing the dislocation, and ultimately disappear when they meet kinks of opposite sign.

In this chapter, we concentrate on deriving the average velocity of an isolated kink, and use this to calculate a dislocation velocity. Whitworth, Paren and Glen (1976) present calculations, which like this chapter, quantify the original Glen model, and from them deduce dislocation velocities. The calculation presented arrives at the same result as Whitworth et al but by a quite different route, and reinforces the surprising fact that the kink velocity calculated by assuming the switching rate of proton arrangements close to the dislocation is the same as in the bulk does not agree with the measured kink velocities. This implies that the proton rearrangement rate close to the dislocation is faster, or that some process, at present unknown, is involved in the plastic flow of ice. Such conclusions are in conflict with those

* A substantial part of this chapter appeared in Frost, Goodman, and Ashby (1976)

of Perez, Tatibouët, Vassoille and Gobin (1975).

The method used differs from that of Whitworth et al in the way chosen to describe the position of the kink. They calculate the forward drift of the kink by focussing on its average position between two unfavourable bonds: bonds on which the proton arrangement is such that shear would create a defect. When a stress is applied to the slip plane, the average position of the kink can be found from the spatial dependence of its free energy. Whitworth et al calculate how this position changes when any of the bonds on the dislocation line suffers a proton rearrangement or 'switch'.

By contrast, only the location of the unfavourable bonds is used to define the kink position in our calculation. The probability distribution, which follows from the distribution of free energy, is employed to calculate the probability that a kink lies to one side or the other of a bond which is about to switch.

In the calculation of Whitworth et al, only events which extend the range lead, for an average over the whole ensemble of kinks, to forward motion of the kink. Here the reverse is true; range closing events make all the difference. At first sight it appears that the two models are completely incompatible but it is merely the different definitions of the kink position which lead to the paradox. The two models are completely equivalent and, although the statistical sums differ, the results are identical. The calculation is extended to the physically interesting limiting behaviour at high and low stresses.

2. A MODEL FOR KINK VELOCITY.

2.1 The Statistics of Kink Motion.

Figure 3.01 represents an isolated kink on a dislocation line in the ice lattice (we are not interested, at this stage, in the precise geometry). We assume that the secondary Peierls barrier is small so that the kink moves easily in the range limited by the two unfavourable bonds, between which it is trapped, sampling all positions

in between. The kink visits the limits of its range with a frequency much greater than that with which the bonds switch. We further assume that the kink cannot pass an unfavourable bond; the range of its motion changes only if a bond switches. We shall assume that the strain field of the dislocation has no effect on the switching frequency (which is determined only by the passing and creation of Bjerrum, ionic and lattice defects) although the conclusion we ultimately reach is that this is probably untrue.

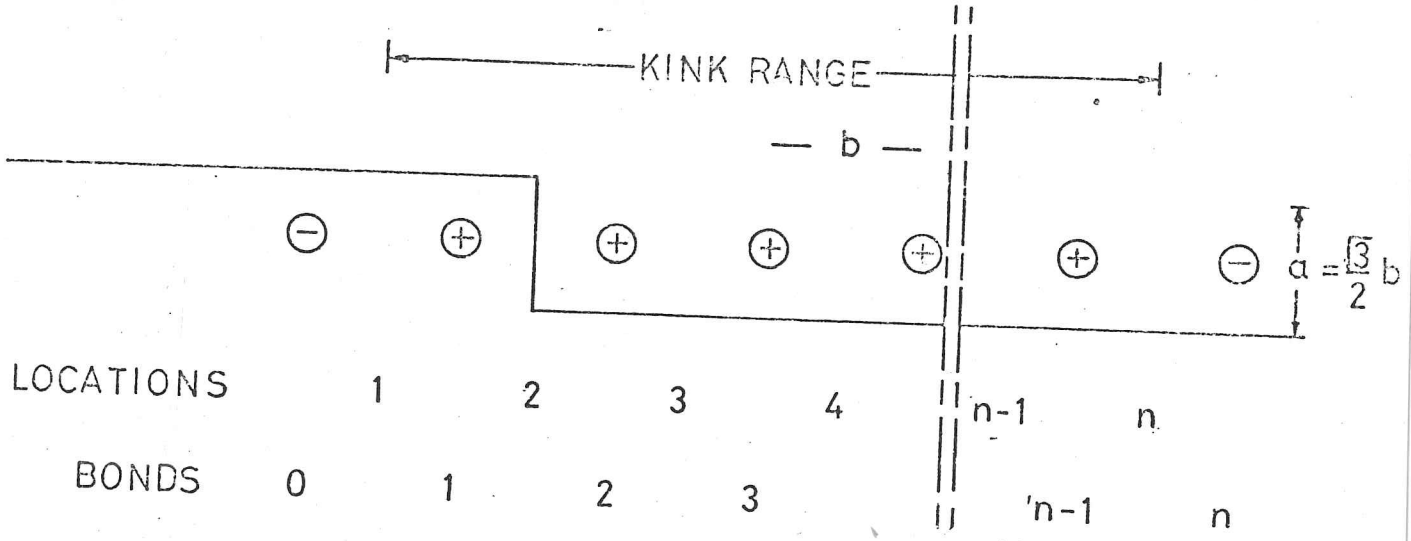

Figure 3.01; A kink on a dislocation line. ⊕ signs represent favourable bonds (bonds which have a proton arrangement so that if a kink passes, Bjerrum or ionic defects are not formed). ⊖ signs represent unfavourable bonds.

In the absence of stress, a kink is located with equal probability at any position within its range. A stress changes this; it increases the probability that the kink will be found near the end of its range (in the direction that allows the stress to do work). If bonds now switch randomly, reducing or extending the range of the kink, there will be a net drift of kinks in a direction that advances the dislocation. To analyse this drift, the location must be specified. We choose the centre of the kink's free range to specify its position; it is here that the model differs from that of Whitworth et al.

Let the length of the range defined by the integer, n, giving

the number of available kink locations. All values of n, the range, are possible, but large n are less likely; it is readily shown that the probability of finding two kinks in the same range is negligible. An ensemble of kinks, which is in thermal equilibrium with the lattice and obeys Boltzmann statistics is considered, with attention concentrated first on kinks with an initial range n and then summed over all n to find a mean kink velocity, $\bar{v}_k$.

The location of a kink can be changed by two sorts of events; range-opening events in which either of the two unfavourable bonds switches, and range-closing events in which a bond within the range switches - the kink is caught on one or other side of the switched bond. Because of the way we define the kink location, range opening events, averaged over all kinks of range n, do not contribute to forward motion of the kink. This is because, if switching is uninfluenced by stress, it is equally likely that the range will be extended in either direction by the same number of locations. Since the position of the kink is fixed only by the unfavourable bonds, averaging over all such range extensions gives no forward drift.

Within the range n the probability that the kink is at a given location, at a given instant in time, depends on its free energy as a function of position. If a range-closing event occurs, the free energy distribution defines the probability that the kink is to one side or the other of the switched bond - which can lie at any of the n-1 positions within the range. This allows us to calculate the velocity, $v_{k,n}$, for kinks of range n. It is the product of L_n, the average distance moved forward (measured from the centre of the free range), ν_n, the frequency, given a range n, that a range-closing event will occur, and P_n, the probability that a range n exists - so that;

$$v_{k,n} = P_n L_n \nu_n \qquad 3.01$$

By summing over n the average kink velocity is obtained;

$$\bar{v}_k = \sum_{n=1}^{\infty} P_n L_n \nu_n \qquad 3.02$$

2.2 Calculation of ν_n, P_n and L_n.

Consider first the frequency of random range-closing events (we note again that range-opening events do not contribute to the drift of the kink). The range contains n-1 locations any of which may switch with equal frequency ν_o. Thus

$$\nu_n = (n-1)\nu_o \qquad 3.03$$

ν_o is the frequency with which locations switch from favourable to unfavourable; it is related to the dielectric relaxation time (Whitworth et al show that this relation is different for 60° and screw dislocations, and whether proton rearrangement is controlled by Bjerrum or ionic defects).

Next, consider the probability of a range n. If the proton can be found with equal probability at either end of its bond, the probability of finding n bonds with a given configuration is $(1/2)^n$. The probability, $p'_{n,m}$, that a potential kink location is the mth location, in a range n, is the product of the probabilities $(1/2)^m$, that there are m-1 favourable, followed by 1 unfavourable, bonds to the left of it, and $(1/2)^{n-m+1}$, that there are n-m favourable, followed by 1 unfavourable, bonds to the right. Thus $p'_{n,m}$ is given by;

$$p'_{n,m} = \left(\frac{1}{2}\right)^{n+1} \qquad 3.04$$

which is independent of m. Then the probability that a given potential kink location is at some location in a range of n is;

$$P'_n = n\left(\frac{1}{2}\right)^{n+1} \qquad 3.05$$

It is assumed that, at zero stress, potential kink sites are randomly occupied by actual kinks, and that application of a stress, while changing $p_{n,m}$ (a distribution function for actual kinks, corresponding to $p'_{n,m}$ for potential kink sites) leaves the corresponding function P_n for actual kinks unchanged. We have taken no account of the difference in entropy between kinks with long ranges and kinks with short ranges.

The most difficult quantity to calculate is L_n, the average

distance moved by a kink when a range-closing event occurs. To do this, we consider the consequences of a particular bond, the ith, switching, and then sum for all values of i. The kink can be caught either ahead of, or behind, the ith bond. If we suppose the secondary Peierls valley is small, the discrete description of the kink position can be replaced by a continuous one, described by the probability $p(x)dx$ that the kink lies between x and x+dx, where x is measured from one end of the range.

As we have assumed the kink is in thermal equilibrium, Boltzmann statistics can be used to calculate $p(x)$. Since the kink must lie within the range 0 to nb (where b is the Burger's vector) we have that;

$$p(x) = \frac{\exp\left(- \frac{F}{kT} + \frac{xab\tau}{kT} \right)}{\int_0^{nb} \exp\left(- \frac{F}{kt} + \frac{xab\tau}{kT} \right)} \qquad 3.06$$

where τ is the stress on the slip plane, F the free energy of the kink when no stress is applied, and a is $\sqrt{3}b/2$ from the geometry of the lattice. From this the probability that a kink lies on a given side of the ith bond can be calculated. If we let $A = \frac{ab^2\tau}{kT}$, the probability, p_f, that the kink is ahead of the ith bond, and so between ib and nb is;

$$p_f = \int_{ib}^{nb} p(x)\, dx \qquad 3.07$$

which when integrated gives;

$$p_f = \frac{\exp(nA) - \exp(iA)}{\exp(nA) - 1} \qquad 3.08$$

Similarly p_b, the probability that the kink is behind the ith bond is;

$$p_b = \int_0^{ib} p(x)\, dx \qquad 3.09$$

which gives

$$p_b = \frac{\exp(iA) - 1}{\exp(nA) - 1} \qquad 3.10$$

If the kink is caught behind the switched bond, its mean

position will change by an amount $b(n-i)/2$; if caught forward, it will change by an amount $bi/2$. Thus if the ith bond switches, the average distance moved by the kink is;

$$L_{n,i} = p_f \frac{bi}{2} - p_b \frac{b(n-i)}{2} \qquad 3.11$$

The probability that a range-closing event switches the ith favourable bond is $\frac{1}{n-1}$. This means that, for the range n, the average distance moved forward by a kink acted on by a stress τ is given by, where Z has been set equal to exp(A);

$$L_n = \frac{1}{n-1} \sum_{i=1}^{n-1} \left[\frac{bi(Z^n - Z)}{2(Z^n - 1)} - \frac{b(n-i)(Z-1)}{2(Z^n - 1)} \right] \qquad 3.12$$

which, when the sum is carried out equals;

$$L_n = \frac{b}{2(n-1)(Z^n - 1)} \left[n(n-1)(Z^n + 1) - n \frac{(Z-Z^n)}{(1-Z)} \right] \qquad 3.13$$

When this expression is put into equation 3.02 together with the relations for ν_n and P_n from equations 3.03 and 3.05, an expression for the average kink velocity is obtained;

$$\boxed{\bar{v}_k = \frac{\nu_o b}{8} \sum_{n=1}^{\infty} \left(\frac{1}{2}\right)^n \left[n^2 \frac{(n-1)(Z^n + 1)}{(Z^n - 1)} - 2\frac{(Z-Z^n)}{(1-Z)(Z^n - 1)} \right]} \qquad 3.14$$

This expression is plotted in figure 3.02 as the curve labelled 'no correlation'. The axes are dimensionless kink velocity $\bar{v}_k/\nu_o b$ and the dimensionless stress $A = \frac{ab^2\tau}{kT}$. At low stresses, and high temperatures, the kink velocity is <u>proportional to the stress</u>; but as the stress increases the velocity reaches a <u>terminal, or saturation</u> value. At either limits, the rather complicated equation 3.14 reduces to simpler expressions. At low stresses, the exponentials can be expanded as series; then, retaining second order terms;

$$\frac{\bar{v}_k}{\nu_o b} = \frac{1}{48} \frac{ab^2\tau}{kT} \sum_{n=1}^{\infty} \left(\frac{1}{2}\right)^n n^2 (n^2-1) \qquad 3.15$$

which, when the sum is evaluated, gives;

$$\frac{\bar{v}_k}{\nu_o b} = 3 \frac{ab^2}{kT} \tau \qquad 3.16$$

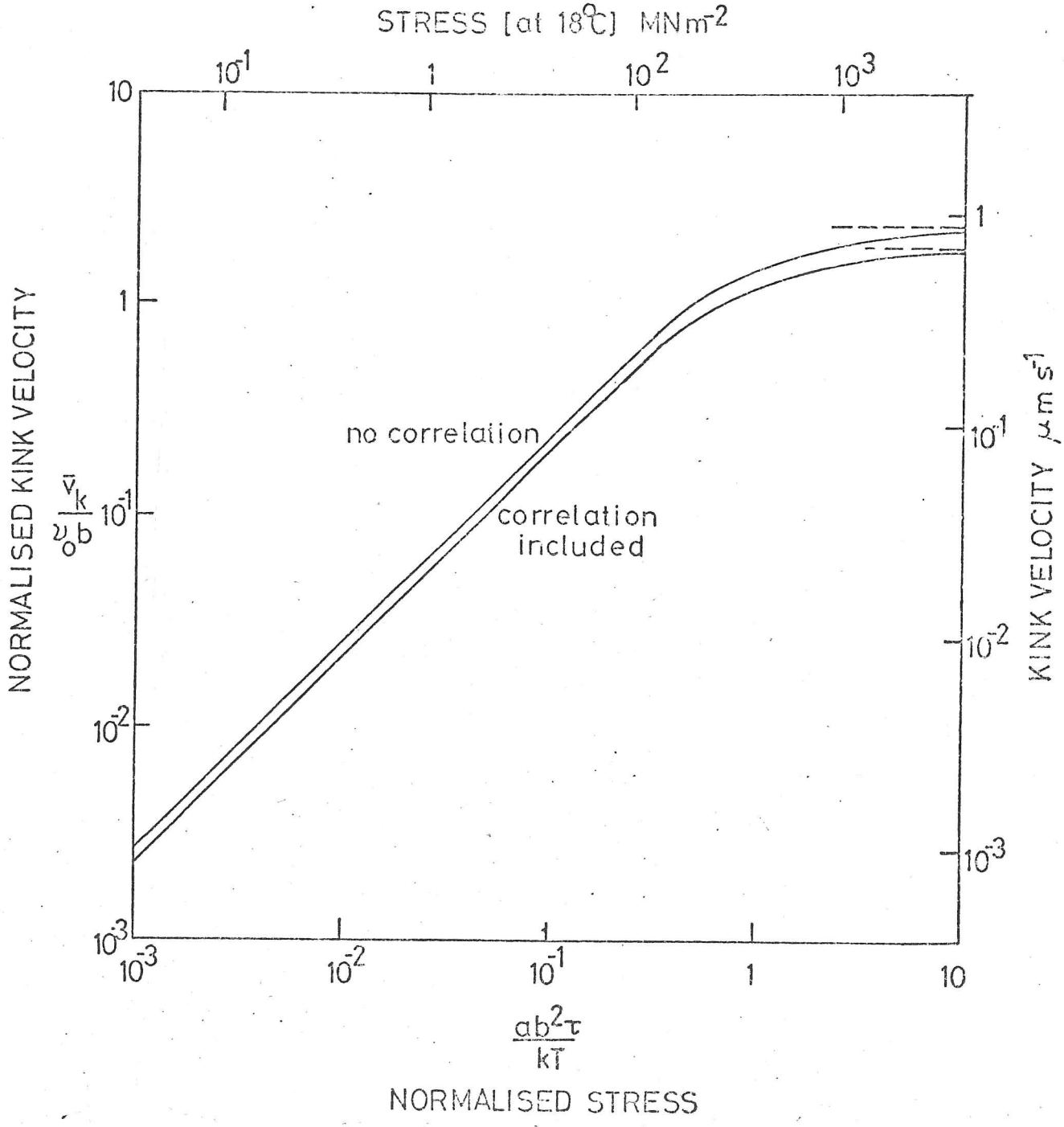

Figure 3.02; A plot of dimensionless stress $\frac{ab^2\tau}{kT}$ against the dimensionless kink velocity $\frac{\bar{v}_k}{\nu_o b}$ showing the effects of including correlation. The Burger's vector has been taken as 4.5×10^{-10} m, and ν_o as 8.3 kBq in the calculation.

At high stresses, exp(nA) is much greater than exp((n-1)A), and the equation becomes;

$$\frac{\bar{v}_k}{\nu_o b} = \frac{1}{8}\sum_{n=1}^{\infty}\left(\frac{1}{2}\right)^n n^2(n-1) \qquad 3.17$$

which, on evaluating the sum, gives;

$$\frac{\bar{v}_k}{\nu_o b} = 2.5 \qquad 3.18$$

2.3 Correlation Effects.

The analysis thus far assumes that when a switching event extends the range, the orientation of bonds outside the original range had no correlation with those inside; they are random. This is not strictly true because, after an interior switching event, some knowledge of the bond arrangement outside the range is retained. The argument that follows shows that this can be important. When the stress is large, the kink will always be very close to one end of its range. There is an obvious upper limit to the velocity, when the kink always moves forward when a switching event occurs on the unfavourable bond next to it. Since the average distance moved to the next unfavourable bond is 2b, the upper limit for $\bar{v}_k$ is;

$$\bar{v}_k = 2\nu_o b \qquad 3.19$$

This differs by a factor of 5/4 from the result obtained in the last section because correlation effects were not included in the derivation of equation 3.14.

It would be very difficult to keep track of proton positions after more than one switch had occurred; but it is possible, in a very simple way, to arrive at a correlation factor which predicts the last result correctly. Consider the case in which a bond switches, reducing the range, and then switches back again without any other bonds switching. The two switches together produce no net result, and in this case should be excluded from the sum in equation 3.14. Similarly the case in which two or more bonds switch and then switch back without further switches should also be excluded from the sum. The chance of returning to the original arrangement after one

switch is $\frac{1}{(n+1)}$. The chance of returning after two switches is $\frac{1}{(n+1)}2$, and so on. Therefore the total chance of the proton configuration returning to exactly the previous arrangement is;

$$\sum_{i=1}^{\infty} \frac{1}{(n+1)^i} = \frac{1}{n} \qquad 3.20$$

If it is assumed cases, other than the above, return the configuration to the random ensemble (with a probability equal to $1 - \frac{1}{n}$), the expression for the drift velocity becomes;

$$\bar{v}_k = \sum_{n=1}^{\infty} \frac{n-1}{n} L_n P_n \upsilon_n \qquad 3.21$$

which leads to the modified expression for the kink velocity allowing for correlations;

$$\bar{v}_k = \frac{\upsilon_o b}{8} \sum_{n=1}^{\infty} \left(\frac{1}{2}\right)^n n(n-1)\left[\frac{(n-1)(Z^n+1)}{Z^n-1} - 2\frac{(Z-Z^n)}{(Z^n-1)(1-Z)}\right] \qquad 3.22$$

This expression has been plotted onto figure 3.02 as the curve labelled 'correlation included'. It has the same shape as the 'no correlation' curve, but predicts slightly slower velocities because, although a single range-closing event allows a kink to move, a range-closing event followed by a correlated range extending event does not.

Again the high and low stress behaviour can be examined. The limit of equation 3.22 at low stresses is;

$$\frac{\bar{v}_k}{\upsilon_o b} = \frac{1}{48}\frac{ab^2\tau}{kT} \sum_{n=1}^{\infty} \left(\frac{1}{2}\right)^n (n-1)n(n^2-1) \qquad 3.23$$

which, when the sum is evaluated, equals;

$$\frac{\bar{v}_k}{\upsilon_o b} = 2.5 \frac{ab^2}{kT}\tau \qquad 3.24$$

The velocity is still proportional to the stress, but is slower by a factor of 5/6 compared to equation 3.16.

The limit at high stresses is;

$$\frac{\bar{v}_k}{\nu_o b} = \frac{1}{8} \sum_{n=1}^{\infty} \left(\frac{1}{2}\right)^n (n-1)^2 \, n \qquad 3.25$$

which, when the sum is evaluated, gives;

$$\frac{\bar{v}_k}{\nu_o b} = 2 \qquad 3.26$$

This agrees with the upper limit velocity calculated earlier, and is less by the factor 5/4 than that of the uncorrelated calculation.

The above effect is one of many correlations. It is included here to illustrate that there is a high stress limit, which does not agree with the analysis of section 2.2 but can be derived if correlation effects are included.

To summarise the model predicts a kink velocity which depends linearly on the stress when $\frac{ab^2}{kT}\tau$ is less than 1, but tends to an upper bound of $2\nu_o b$ when $\frac{ab^2}{kT}\tau$ is greater than 1.

3. THE DISLOCATION VELOCITY.

When a dislocation advances at a steady velocity, v_{dis}, the rate at which kinks are nucleated equals the rate at which they are annihilated. Figure 3.03 shows a number of kinks drifting along a dislocation line.

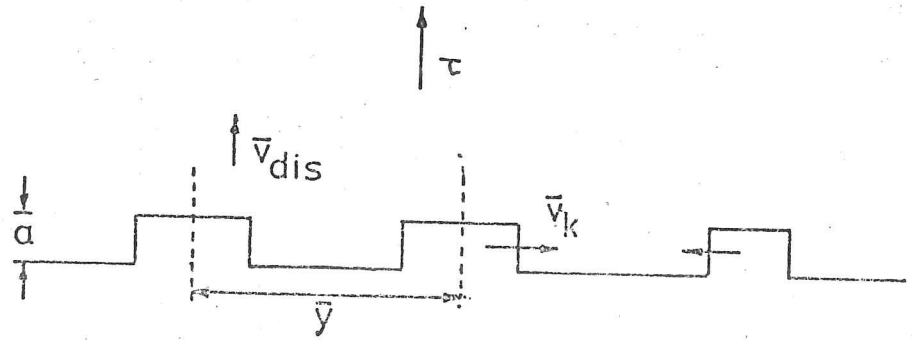

Figure 3.03; A collection of double kink pairs on a dislocation line. $\bar{y}$ is the mean distance between pairs and $\dot{n}_k$ the rate of double kink pair nucleation per unit length of the dislocation line.

If $\dot{n}_k$ is the rate at which pairs of kinks are nucleated per unit length of the dislocation line, and $\frac{\bar{y}}{2}$ is the mean distance a kink travels before annihilating with a kink of opposite sign, for a steady-state;

$$\dot{n}_k \bar{y} = \frac{2\bar{v}_k}{\bar{y}} \qquad 3.27$$

If a kink sweeps along a segment of dislocation, the segment advances by a distance a (equal to $\sqrt{3}b/2$ on the basal plane for screw dislocations) and the dislocation velocity is;

$$v_{dis} = \frac{a\bar{v}_k}{\bar{y}} \qquad 3.28$$

which when combined with equation 3.27 gives an expression for v_{dis} in terms of $\bar{v}_k$ and $\dot{n}_k$;

$$v_{dis} = a\left[\frac{\bar{v}_k \dot{n}_k}{2}\right]^{\frac{1}{2}} \qquad 3.29$$

It is difficult to calculate $\dot{n}_k$ because it depends on the free energy of formation of the kink, the calculation of which involves a detailed model for the dislocation core, and for the way the kink energy changes with position (Hirth and Lothe, 1968). However we can, without finding $\dot{n}_k$, assign certain limits to v_{dis}.

First, the assumption that kinks are isolated, imposes a limit to the range of validity of the model. We would expect $\bar{y}$ to be no less than about 20b, so that

$$v_{dis} \leqslant \frac{a\bar{v}_k}{20b} \qquad 3.30$$

Second, it is clear that an absolute upper limit for the dislocation velocity is given by

$$v_{dis} \leqslant \bar{v}_k \qquad 3.31$$

where $\bar{v}_k$ is given by equation 3.14 or 3.22. These limits will be used in the next section when the model is compared with experimental measurements of the dislocation velocity.

4. COMPARISON WITH EXPERIMENT, AND DISCUSSION.

4.1 Measurements at low stresses.

Dislocation velocities, as a function of stress, have been measured by X-Ray topography (Fukuda and Higashi, 1969, 1973; Jones and Gilra, 1973a, b) by optical studies of small angle grain boundaries (Higashi and Sakai, 1961). Although in such experiments the shear stress on the slip plane is not precisely known, Fukuda and Higashi are able to deduce the dislocation velocity as a function of stress at a temperature of $-18^{\circ}C$. The experiments covered a range of stress from 0 to 0.3 MN m^{-2} (where $\frac{ab^2\tau}{kT}$ is much less than 1) and showed that the velocity depended linearly on the stress. Maï (1976) has recently reported a further study by X-Ray topograpy. His results agree with those of Higashi and Sakai at low stresses (τ less than 0.1 MN m^{-2}) but show some deviation away from linear behaviour for larger stresses for temperatures greater than $-9^{\circ}C$. His results are shown in figure 3.04.

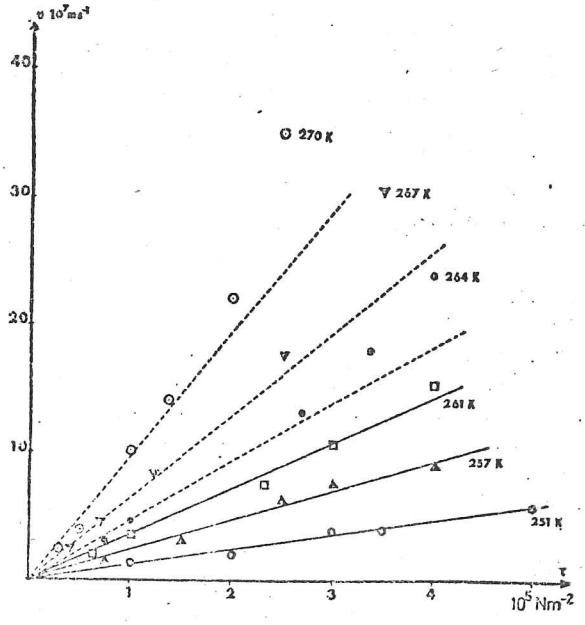

Figure 3.04; Experimental results of Maï (1976) which show how the dislocation velocity varies as a function of stress and temperature.

For the linear parts of the curves, he finds an activation energy of 0.55 ± 0.05 eV (52.3 kJ mol^{-1}).

These results are in qualitative agreement with the

predictions of the model presented, and that of Whitworth et al. If we can assume that the nucleation rate, $\dot{n}_k$, has the same stress dependence as $\bar{v}_k$ (it seems inevitable that both are controlled by the same microscopic process - bond switching), then v_{dis} will be proportional to $\bar{v}_k$. Figure 3.02 then shows that when the stress is 0.1 MN m^{-2}, as it is in these experiments, v_{dis} is proportional to the stress.

Onsager and Runnels (1969) show that a model, which assumes the average time between molecular reorientations equals the dielectric relaxation time, can satisfactorily account for the diffusion and relaxation phenomena in ice. Whitworth et al point out that the molecular reorientation time does not always equal the proton rearrangement time because firstly a proton on a dangling bond (for instance in a 60° dislocation) can only be rearranged by a Bjerrum defect, and secondly each time a molecule is reorientated only two of the four bonds to which it is attached have the position of their protons changed. So for any bond the mean time between proton rearrangements will be twice the dielectric relaxation time, τ_{diel}, but, in the special case of 60° dislocations where either of two bonds (the dangling bond or the bond about to be broken) can suffer a proton rearrangement to produce a switch from 'favourable' to 'unfavourable', the mean time between switches equals $\frac{1}{2} \times 2\tau_{diel}$ or just τ_{diel}. Hence in this case ν_o equals $1/\tau_{diel}$, and the switching is controlled by the diffusion of Bjerrum defects. We would therefore expect

$$\nu_o \propto \exp\left(-\frac{F_m+F_f}{kT}\right) \qquad 3.32$$

from the temperature dependence of τ_{diel}, where F_m and F_f are the activation energies for Bjerrum defect migration and formation respectively. Fletcher (1970) gives the value of F_m+F_f as 0.571 eV (54.3 kJ mol^{-1}). Examination of the expressions for v_{dis} shows that the temperature dependence must come from ν_o, and so we would expect

$$v_{dis} \propto \exp\left(-\frac{F_m+F_f}{kT}\right) \qquad 3.33$$

Further, if there is an extrinsic concentration of Bjerrum defects through the introduction of hydrogen fluoride, for instance, v_{dis} will no longer depend on F_f, and so the activation energy will fall

to F_m (0.235 ev, 22.4 kJ mol^{-1}). This agrees with the value of Maï for the activation energy, and the observations of dislocation motion in HF doped ice by Jones and Gilra (1973a,b) and single crystal deformation studies of Jones and Glen (1969a,b) of HF doped ice. Jones and Gilra do point out that the HF also causes a sharp rise in the dislocation density and this could account for the softening observed.

However when the model is used to predict the numerical value of the dislocation velocity, it is found to be at least an order of magnitude too low. From figure 3.02 a value for $\bar{v}_k$ can be determined for a stress of 0.1 MN m^{-2} and a temperature of -18°C, then an upper bound to v_{dis} from equation 3.02 is

$$v_{dis} \leq 2.1 \times 10^{-8} \text{ m s}^{-1} \qquad 3.34$$

where ν_o has been set equal to $1/\tau_{diel}$, and the value of τ_{diel} quoted by Hobbs (1974) at -18°C of 1.2×10^{-4} s (ν_o = 8.3 kBq) has been used. This is at least an order of magnitude less than either Fukuda and Higashi (3×10^{-7} m s^{-1}) or Maï observed. Hence, since equation 3.31 is an absolute upper bound, we are forced to conclude that an essential physical process is missing from our model and that of Whitworth et al. Because our results independently agree with those of Whitworth et al, we believe that they correctly analyse the statistics. Then, if the basis of the model is taken as correct, the only variable which could be in error is ν_o, and we must conclude that the choice of ν_o equals $1/\tau_{diel}$ is too small, and thus that stress influences the rate of bond switching, or that the electric or displacement field of the dislocation itself increases ν_o.

4.2 Measurements at High Stresses.

The model predicts that, when $\frac{ab^2\tau}{kT}$ exceeds 1, $\bar{v}_k$ approaches the constant value of $2\nu_o b$. At -18°C, this corresponds to a stress of roughly 200 MN m^{-2} (τ/μ equals 0.07). No dislocation velocity measurements are available at such high stresses, but there have been some creep experiments (extrusion data of Kuon and Jonas, 1973; hardness data of Schultz and Knappwost, 1968).

The creep rate, $\dot{\gamma}$, is related to the dislocation velocity by Orowan's equation;

$$\dot{\gamma} = \rho b v_{dis} \qquad 3.35$$

where ρ is the mobile dislocation density. There are a variety of arguments to show that ρ is proportional to the stress squared (see for example Kocks, Argon, and Ashby, 1973); so that if v_{dis} has its maximum value, this would imply that

$$\dot{\gamma} \propto \tau^2 \qquad 3.36$$

The creep tests at high stresses do not support this. In fact most experiments indicate (see figure 2.05 for instance), that as the stress is increased, the strain rate depends on an ever increasing power of the stress - 3 and upwards. These experiments, too, suggest that ν_o must be stress dependent, since it is the only parameter in the theory which is not known precisely.

5. CONCLUSIONS.

An alternative method for calculating the drift velocity of a kink on the dislocation line to that given by Whitworth et al has been presented. The solution agrees with theirs. It is in complete agreement that such a model cannot account for the observed dislocation velocities unless the switching rate for proton rearrangement is considerably faster in the neighbourhood of a moving dislocation. Since the model also predicts that at high stresses, when $\frac{ab^2\tau}{kT}$ is greater than 1, the kink velocity will tend to a limiting value, this suggests that a stress controlled switching mechanism must operate to agree with the observation that the strain rate, in a polycrystalline test, in secondary creep depends increasingly on the stress as the stress is raised.

CHAPTER FOUR

PRELIMINARY RESULTS FROM AN EXPERIMENT TO MEASURE THE FRACTURE TOUGHNESS OF ICE

Chapter 4.

PRELIMINARY RESULTS FROM AN EXPERIMENT TO MEASURE THE FRACTURE TOUGHNESS OF ICE.

1. INTRODUCTION.

In chapter 2 it was assumed that there was a superimposed hydrostatic pressure which suppressed the initiation and propagation of cracks. Here this assumption is relaxed. The ultimate goal, which is not reached, is to draw on the deformation maps given in figure 2.10 fields which show where fracture mechanisms dominate over creep. In this chapter experimental data, which are the preliminary results of an experiment to be concluded after this thesis has been completed, are presented which predict the applied stress necessary for a crack of known geometry to propagate. This is embodied in one parameter, the fracture toughness, K_c, which is explained in the next section (for a review see Lawn and Wilshaw, 1975).

Fracture mechanisms are more difficult to characterise than creep mechanisms because they depend on two or more of the principal stresses (creep depends only on one), and little data for ice exist. The switch from ductile to brittle failure (creep rupture to failure by crack propagation) is controlled by the time constant of stress relaxation at a crack tip. At high stresses and low temperatures or high strain rates, the time constant is too long to prevent cracks reaching a critical size beyond which they are unstable, and propagate catastrophically through the lattice. In the experiments to measure the 'strength' of polycrystalline ice by Hawkes and Mellor (1972), and Wu, Chang and Schwarz (1976) in uniaxial compression and tension, a transition from ductile to brittle behaviour was observed at a strain rate of about 10^{-5} to 10^{-3} (the temperature was between -1 and -10°C in Wu et al's experiment, and -7°C in Hawkes and Mellor's experiment).

Hawkes and Mellor also observed different strengths for tensile and compressive failure in the brittle region. This is to be expected because in a tensile test a single crack can lead to the eventual failure (unless failure is by void growth when many

voids join up), but in a compression test many cracks nucleate, change the local stress field and link up in the final catastrophic failure (often called cataclastic failure, especially with reference to rocks). If it is assumed that a suitable condition for crack growth is a critical tensile stress (McClintock and Argon, 1966, p491), then a single crack in a compression test propagates at a stress eight times the stress for the same crack in a tensile test. Hawkes and Mellor found the ratio of compressive to tensile strength to be of the order of five, which indicates the effect of multiple crack interactions.

Gold in a series of papers (1960, 1965, 1966, 1967, 1969, 1972a, 1972b) and Wakahama (1965) have investigated the nucleation of cracks in columnar grained ice loaded perpendicular to the long axis of the grains. They observe cracks which nucleate at the triple junctions of grains, transgranular cracks, cleavage cracks along the basal plane, and void growth at grain boundaries. In metals it is possible to separate the stresses, temperatures, and strain rates where these different modes of crack nucleation occur (Ashby, personal communication) but as yet it is not possible to do this for ice. However Gold (1967) has made substantial progress in the understanding of crack nucleation in ice by successfully applying the dislocation theories of Stroh (1954) and Bullough (1964) to explain the observed increase of crack density with time.

Only two previous estimates of the fracture toughness have been found. Gold (1963) formed thermal cracks by bringing two blocks of ice at different temperatures together. He measured the depth to which cracks propagated, and the time after the blocks were brought together for the cracks to run. Then, using an analysis of the diffusion of a thermal wave in the block, and the stresses produced by the temperature, he deduced a value for the fracture toughness. Liu and Loop (personal communication, unpublished data) have used a simple compact specimen (a single cracked block pulled apart by fixtures through holes above and below the crack), a common technique for fracture toughness measurements, to measure K_c over a range of temperatures.

After the concept of fracture toughness has been introduced in the next section, a variety of techniques for measuring the fracture toughness will be described and the results obtained discussed.

We would expect the fracture toughness to depend on the applied stress, the strain rate at the crack tip, the temperature, the hydrostatic pressure, and the grain size. We shall see below how the fracture toughness dependence on temperature is a reflection of the size of the plastic zone at the crack tip. The experiments described here were designed to find the most convenient method for determining K_c, but did not explore variations in strain rate or grain size.

2. THE CONCEPT OF FRACTURE TOUGHNESS.

In the introduction it was noted that, although data exist on the nucleation of cracks, and multiple crack interactions in strength tests in ice, little information exists on the critical stress required to make a crack of known geometry propagate. The concept of fracture toughness is widely used in the metals literature, but has not yet gained acceptance in the ice literature and so a short outline will be given here.

Comprehensive reviews of fracture toughness can be found in Lawn and Wilshaw (1975), Knott (1973), Kenny and Campbell (1967), Liebowitz (Ed, 1968, 1971, 1972), Turner(1975). In a brittle solid, there is a critical stress at which a crack becomes unstable, and propagates. Griffith (1920) first showed, by a simple energy argument, which avoids the need to know the stresses at the crack tip, that the critical stress for a crack of length 2c in an infinite body, with a stress σ, at right angles to the crack plane is obtained by

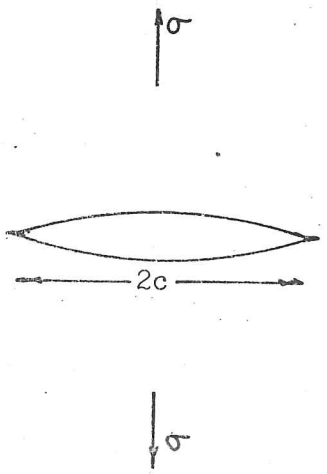

Figure 4.01; The crack geometry for Griffith's calculation.

equating the rate of strain energy release to the incremental work done to create new surface. This gives;

$$\sigma_c = \left[\frac{2E\Gamma}{\pi c}\right]^{\frac{1}{2}} \qquad 4.01$$

where Γ is the surface energy, c the half crack length, and E Young's modulus if the crack is in plane stress (in plane strain E would be replaced by $E/(1-\nu^2)$, where ν is Poisson's ratio). The crack geometry is given in figure 4.01. This expression was successfully used to explain the brittle fracture of glass.

In most solids some energy is lost irreversibly in doing plastic work at the crack tip as it advances; this makes equation 4.01 a lower bound to the critical stress, and led to the introduction of an argument which calculated the stress field at the crack tip (assuming linear elastic behaviour) which was then modified to take an approximate account of the plastic zone at the crack tip.

A crack can open in three ways; faces can be pulled apart by a stress normal to the crack plane (mode I), the faces can be sheared over each other perpendicular to the crack front (mode II), or the faces can be sheared parallel to the crack front (mode III). We are concerned here only with the mode I case, in which case the stresses at the tip of a sharp crack in the linear elastic approximation are given by;

$$\sigma_{xx} = \frac{K_1}{\sqrt{2\pi r}} \cos(\theta/2)\left[1 - \sin(\theta/2)\sin(3\theta/2)\right]$$

$$\sigma_{yy} = \frac{K_1}{\sqrt{2\pi r}} \cos(\theta/2)\left[1 + \sin(\theta/2)\sin(3\theta/2)\right]$$

$$\sigma_{xy} = \frac{K_1}{\sqrt{2\pi r}} \sin(\theta/2)\cos(\theta/2)\cos(3\theta/2) \qquad 4.02$$

and in plane strain

$$\sigma_{zz} = \nu(\sigma_{xx} + \sigma_{yy})$$

and

$$\sigma_{xz} = \sigma_{yz} = 0$$

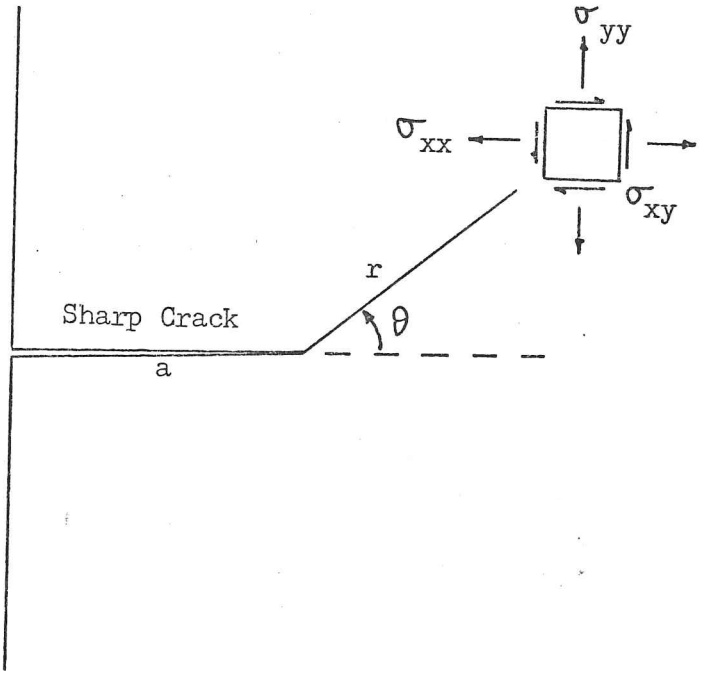

Figure 4.02; Co-ordinate definitions for equation 4.02.

K_1, the stress intensity factor, is a material constant which scales the local stresses close to the crack, but also depends on the positions of the free surfaces (the subscript $_1$ implies mode I opening). By dimensional arguments alone we would expect K_1 to depend on the square root of the crack length, and the applied stress, σ_o. Note that sometimes the factor $\sqrt{\pi}$ is omitted from the denominator of the expressions in equation 4.02.

The stress intensity factor has been calculated for a variety of crack geometries (Paris and Sih, 1965; McClintock and Argon p406, 1966; Sih, 1973). For the cylindrical crack in figure 4.02 K_1 is $\sigma_o\sqrt{\pi c}$, for a semi-circular crack in a semi-infinite solid, or a three or four point bend specimen (used in the experiments below) see table 4.01. We would expect, because K_1 characterises the stresses at the crack tip, that there is a limiting value of K_1, denoted by K_{1c}, at which fracture occurs. We shall see below that this will only be true if certain provisos are met.

An equally useful parameter, and perhaps intuitively more reasonable, to describe the singularity at the crack tip is G, the crack extension force (the rate of change of internal energy as the crack advances). In the perfectly brittle case G can

Table 4.01

Stress Intensity Factors for the specimen geometries used.

Three-point bending; (BSI, 1971)

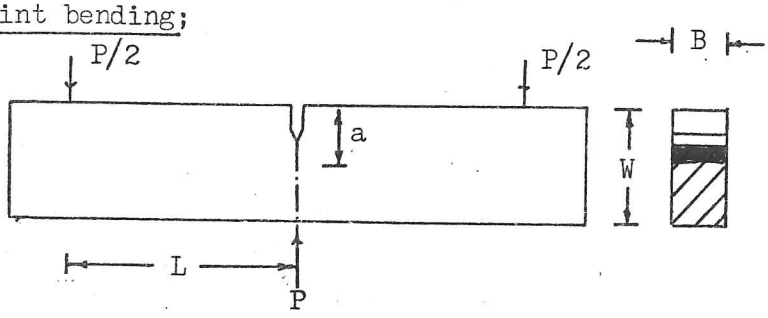

$$K_1 = \frac{PL}{BW^{\frac{3}{2}}} Y \qquad Y = 3\left[1.93\left(\frac{a}{W}\right)^{\frac{1}{2}} - 3.07\left(\frac{a}{W}\right)^{\frac{3}{2}} + 14.53\left(\frac{a}{W}\right)^{\frac{5}{2}} - 25.11\left(\frac{a}{W}\right)^{\frac{7}{2}} + 25.8\left(\frac{a}{W}\right)^{\frac{9}{2}}\right]$$

$\frac{a}{W}$	Y	$\frac{a}{W}$	Y
0.20	2.33	0.45	4.55
0.21	2.40	0.46	4.69
0.22	2.46	0.47	4.83
0.23	2.53	0.48	4.98
0.24	2.60	0.49	5.14
0.25	2.67	0.50	5.31
0.26	2.74	0.51	5.48
0.27	2.81	0.52	5.66
0.28	2.88	0.53	5.86
0.29	2.96	0.54	6.06
0.30	3.04	0.55	6.27
0.31	3.11	0.56	6.50
0.32	3.20	0.57	6.74
0.33	3.28	0.58	6.99
0.34	3.37	0.59	7.25
0.35	3.45	0.60	7.53
0.36	3.55	0.61	7.82
0.37	3.64	0.62	8.13
0.38	3.74	0.63	8.45
0.39	3.84	0.64	8.79
0.40	3.95	0.65	9.15
0.41	4.06	0.66	9.53
0.42	4.17	0.67	9.93
0.43	4.29	0.68	10.35
0.44	4.42	0.69	10.79

In the BSI draft standard $L = 2W + 5$ mm, $B = \frac{W}{2}$, $0.45 \leq \frac{a}{W} \leq 0.55$.

Semi-circular Crack in Semi-infinite Solid. (Paris and Sih, 1965)

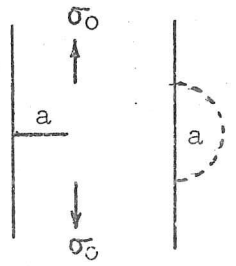

$$K_1 = 1.12\sigma_o\sqrt{\pi a}\,\frac{2}{\pi}$$

be identified with 2Γ (where Γ is the surface energy) from the Griffith's argument, but if irreversible work is done at the crack tip, G is the sum of the plastic work and the surface energy. Thus the difference $G - 2\Gamma$ is a measure of the plastic work involved in crack propagation (for a steel 2Γ is about 10 J m^{-2} while G is 2000 J m^{-2}). G can be measured by observing the change of compliance as the crack extends.

By allowing a crack to undergo a hypothetical extension, and then applying tractions to restore it to its orginal length G can be related to K, if the stresses are given by equation 4.02 and are linearly proportional to the strains. In plane stress

$$G = \frac{K^2}{E} \qquad 4.03$$

and in plane strain

$$G = K^2 \frac{(1-\nu^2)}{E} \qquad 4.04$$

where E is Young's modulus and ν is Poisson's ratio.

In the discussion so far it has been assumed that the solid is everywhere linearly elastic - this is clearly unlikely and plasticity must be incorporated into the fracture criteria. A complete solution to the elastic plastic problem of crack propagation (where plastic is taken to mean perfect plasticity - infinite strain rate above a given stress σ_y) only exists for the mode III crack opening problem. To find approximately the stress distribution in the mode I case both energetic (Irwin-Orowan model), and mechanistic (Barenblatt-Dugdale model) approaches have been used.

In the Barenblatt-Dugdale model a small non-linear region, size r_{BD}, close to the crack tip is introduced which produces stresses that exactly cancel the stresses predicted from a linear elastic model which uses a crack length of $a + r_{BD}$ (thereby removing the infinite stress at the crack tip but retaining the $1/\sqrt{r}$ of the stresses in equation 4.02). The non-linear relation used is either a cut off at the theoretical strength above which the stress is zero or

a rise to a constant yield stress (this is illustrated in figure 4.03).

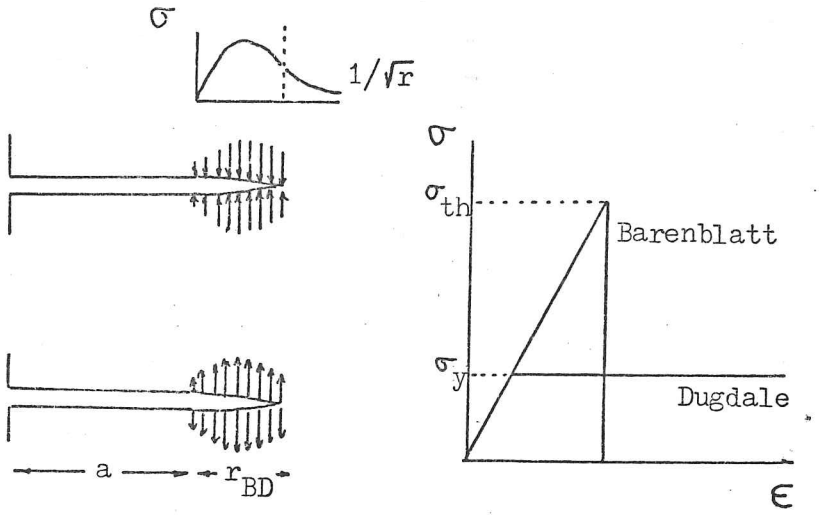

Figure 4.03; The Barenblatt-Dugdale model of the stresses at the crack tip.

The two cases predict that G is Eb/50 (b is a suitable lattice parameter) or $6\sigma_y u_c$ (where u_c is the crack opening displacement which will be referred to later). The non-linear zone size is given by

$$r_{BD} = \frac{\pi K^2}{8\sigma_y^2} \qquad 4.05$$

The Irwin-Orowan model assumes that plasticity is confined to a small cylindrical region close to the crack tip of radius r_p. The value of r_p is chosen so that the crack system with plastic and elastic regions is replaced by a perfectly elastic system with crack length $a + r_p$ with the same stored elastic strain energy (see figure 4.04).

In plane strain the radius of the plastic zone size is found to be

$$r_p = \frac{1}{3}\frac{1}{2\pi}\left(\frac{K^2}{\sigma_y^2}\right) \qquad 4.06$$

where σ_y is again the perfect plastic yield stress. In chapter 2 it was emphasised that a material at a high homologous temperature does not have a well defined yield stress.

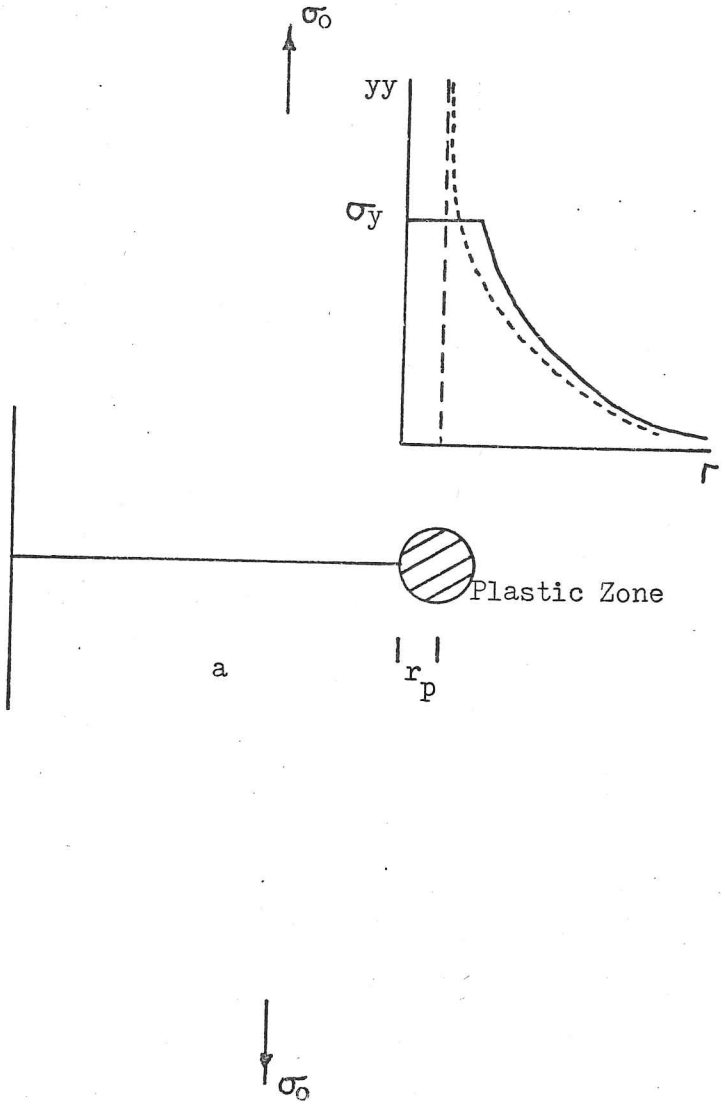

Figure 4.04; The Irwin-Orowan model.

However all the tests to be described were carried out at a high loading rate (the loading time was always less than 10 s), so that the strain rate was greater than 10^{-4} s^{-1}. From the deformation map in figure 2.10, the stress is from 3 to 4 MN m^{-2} (at -20°C). In the tests it was found that K_{1c} is about 100 kN $m^{-3/2}$, and consequently for either model the plastic zone is no greater than 0.04 mm. Except for the observations made on cracks beneath a Vickers hardness indenter, the crack lengths and specimen dimensions were always 50 times greater than this (the recommended standard - see BSI DD3, 1971). Therefore it is likely that the stresses at the crack tip are given by equation 4.02, and the critical value of K_1 can be deduced from the formula for stress intensity factors in table 4.01. But it is very necessary to carry out further experiments to verify that it is possible

to assume that the creep is confined to a small region close to the crack tip. The assumption will break down when the strain rates are low (this is unlikely because of the effect of strain concentration at the crack tip), and at temperatures very close to the melting point. It is then necessary to resort to the concepts of yielding fracture mechanics (Turner, 1975), in particular the path independent integral, J, first introduced by Rice (for a review see Rice, 1968), and crack opening displacement (COD)(Wells, 1961) (which is a direct measure of the plasticity at the crack tip). It is important to note that if creep is extensive, then the relation between the applied stress and the stresses at the crack tip will no longer be related by a single parameter, and that critical values of K, J or COD will not be suitable fracture criteria.

Rice's integral, J, is defined by the line integral;

$$J = \int_{\Gamma} \left[W dy - T_i \frac{du_i}{dx} \right] ds \qquad 4.07$$

where Γ is a contour around a crack aligned in the x direction, W is the stored elastic energy, and T_i and u_i (i=1,2,3) are the tractions and displacements on the contour due to the introduction of the crack. Provided the crack surfaces are stress free, J is independent of the contour; it has the same value independent of whether the contour passes through linear or non-linear regions of the material. It is a measure of the change in internal energy when the crack advances, and is numerically equal to G (G is only defined for linear elastic fracture mechanics). In metals, where the ratio of K_{1c} to σ_y is much larger than that for ice, it is often difficult to make specimens in which the plastic zone size is small compared to the specimen dimensions. J has been successfully used in such cases as a fracture parameter. It can be deduced from load-displacement curves for specimens of different crack length (see figure 4.05). Because J sums irreversible work, it is only a useful parameter if there is no unloading.

It has been found that the relative displacement of the crack faces or crack opening displacement (COD) has a critical value at fracture, although the results are be no means conclusive (probably because of the effects of slow crack growth) (Burdekin

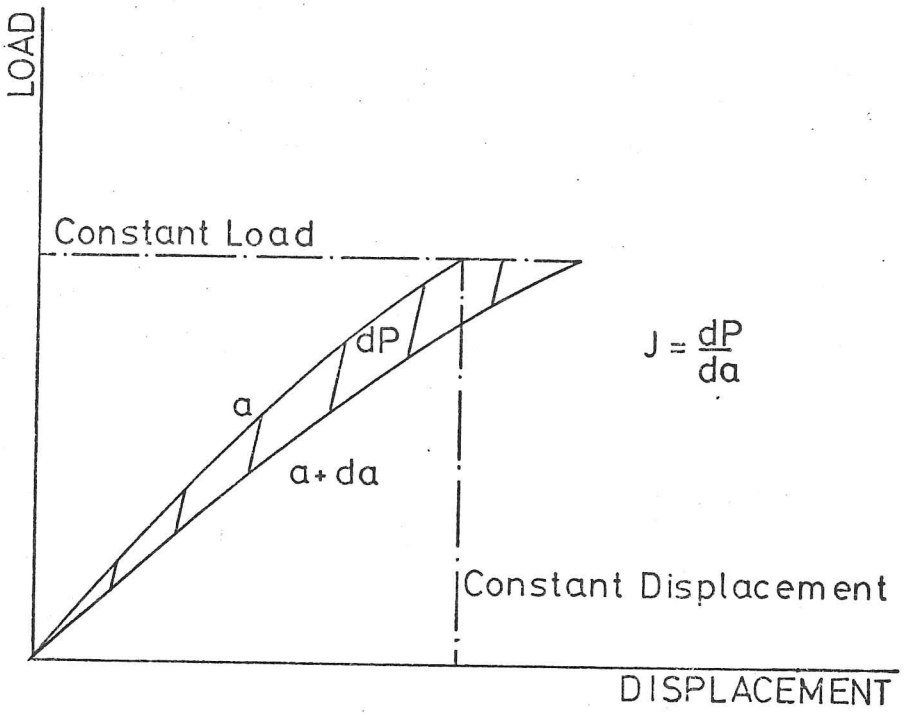

Figure 4.05; Evaluation of J from load-displacement curve.

and Stone, 1966). The crack opening displacement can be related to G by the Dugdale model, and for plane strain it is found that;

$$G = \alpha \sigma_y \delta \qquad 4.08$$

where α is a constant between 1 and 2, and δ is the COD. Therefore, the ratio of G to σ_y could be found for ice for different loading rates and temperatures by measuring the COD. This would give some indication of the role of creep in the fracture process. Measurement of COD was attempted in the experiments to be described but so far reliable data have not been obtained.

Hence for the purposes of the experiments to be described, it is thought reasonable to apply linear elastic fracture mechanics concepts, although it is recognised that further experiments are required to confirm that the creep or plasticity is restricted to a zone which is small in size compared to the crack lengths used.

To obtain reproducible values of K_{1c} two further conditions must be met. First the specimen width must be large enough so that the majority of the crack is in plane strain

conditions (this is usually met if the width is greater than about 50 r_p (Knott, 1973)). Secondly the crack tip radius must be small enough so that the stress field is given to a good approximation by equation 4.02. In metals the value of K_{1c} has been found to fall to a limiting value as the root radius is reduced, and it is usual, in a fracture test, to introduce a small sharp crack by fatigue. It is not possible to introduce a fatigue crack into the ice specimens with the present set up, but a very sharp crack was formed by pushing a razor blade into a slot formed by melting. The effect of these two conditions for metals is illustrated in figure 4.06. Because of the smaller plastic zone in the centre of the crack, the crack advances first near the centre, which is detected by a jump in the load-displacement curve or 'pop-in'. The stress at pop-in is used to deduce K_{1c}.

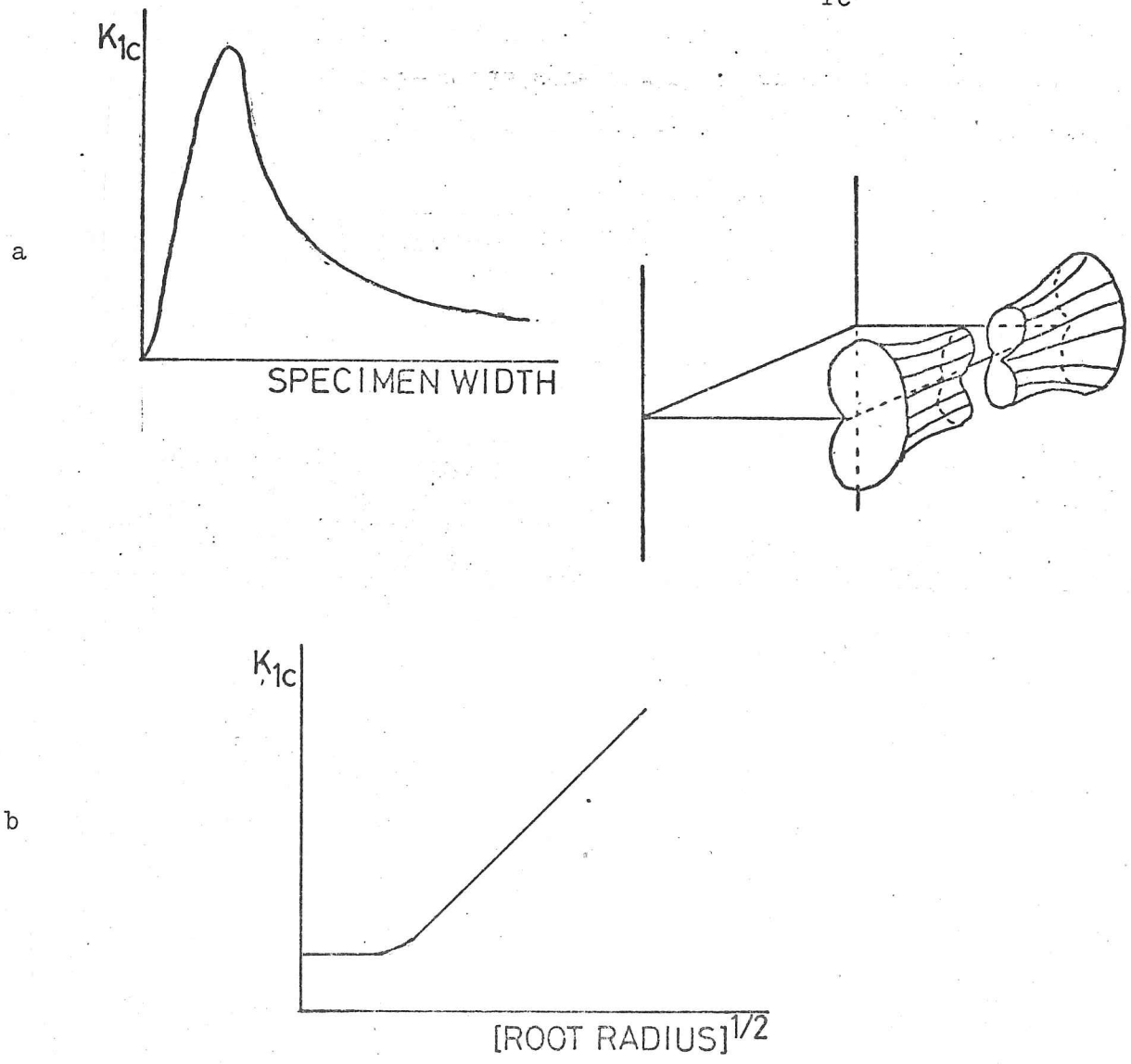

Figure 4.06; The effect of plane strain (a) and root radius (b) on K_{1c} in metals.

Before closing this section, it should be pointed out that it is usually not possible to measure K_{1c} to better than $\pm$ 10 %, and environment often has a profound effect on the processes at the crack tip. Johnston and Parker (1957) report a drastic reduction in strength for ice sprayed with methyl alcohol. It would be interesting to measure K_{1c} for cracks containing salt water.

3. EXPERIMENTS.

3.1 Specimen Preparation.

Specimens were grown in a water filled tank inside a deep freeze (air temperature -10°C). The arrangement is shown in figure 4.07. The water used was once distilled.

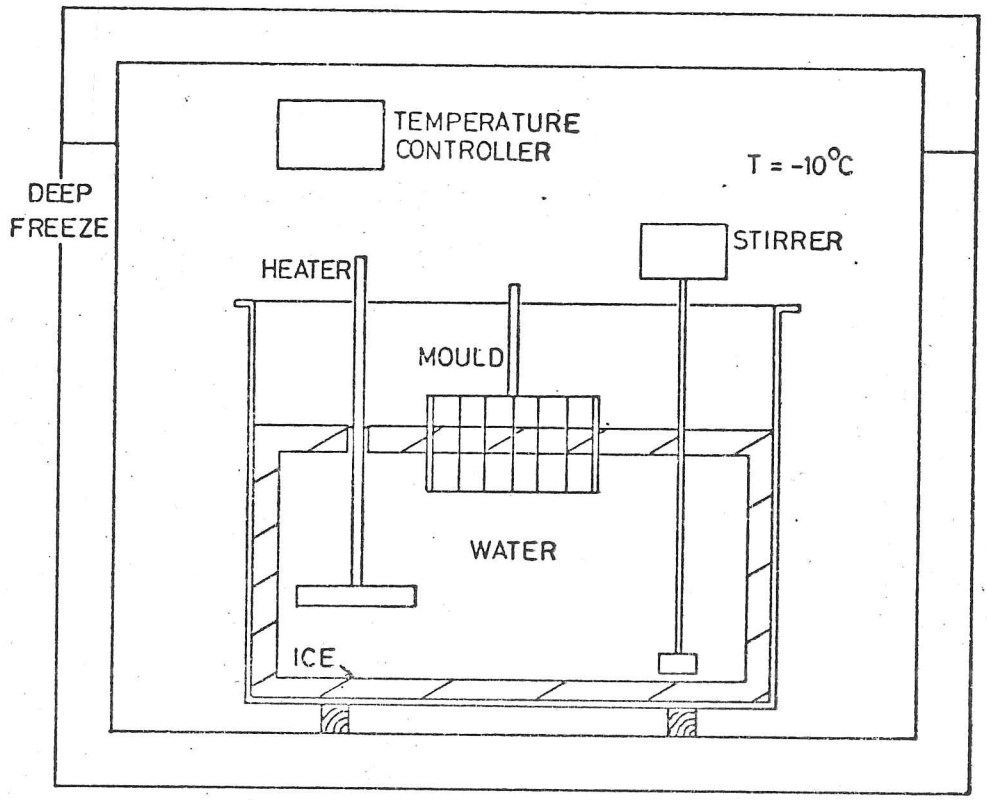

Figure 4.07; The arrangement used to grow the specimens. Ice particles from the deep freeze walls were sprinkled on the surface to nucleate growth. The mould was coated in paraffin wax to ease the removal of the specimens. The temperature of the water was thermostated.

The rate of growth could be varied by changing the setting on the water temperature thermostat. Bubble free specimens roughly 130 mm x 30 mm x 20 mm could be obtained after about a night and a day. The specimens were brought to the desired shape by melting them on an aluminium block at room temperature. They were stored at -10°C, in air, in the deep freeze. They were usually used within two days of manufacture; many were reshaped just before a test. Observations of the grain size (which varied from 1 mm to almost single crystals) were made with a universal stage.

3.2 Loading Arrangement.

The fracture toughness of ice is very low; a bar of cross-section 20 mm x 20 mm can be broken with one's fingers. Therefore it is possible to use a small, inexpensive rig completely contained within a small deep freeze to measure the fracture toughness. The arrangement is shown in figure 4.08.

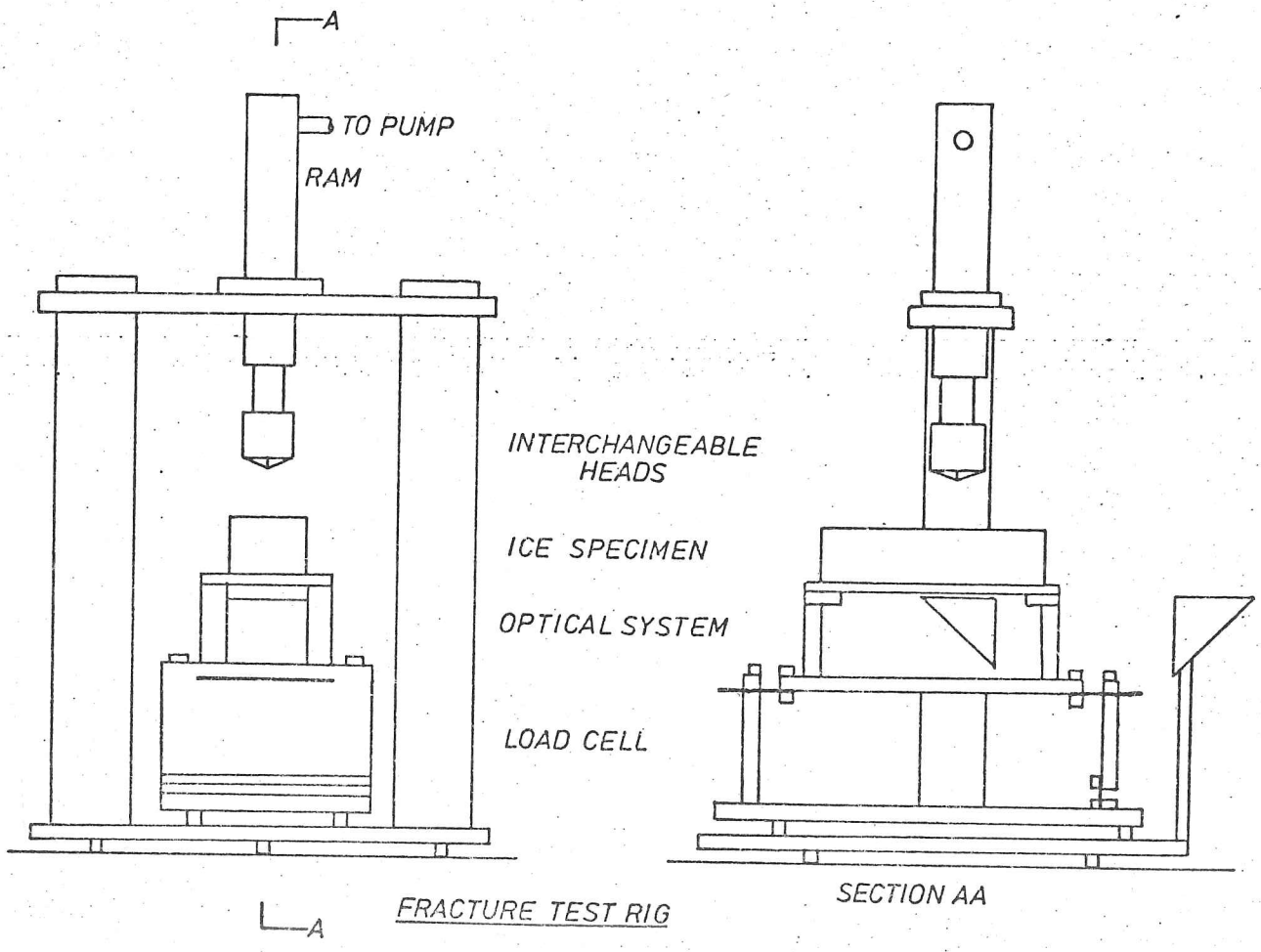

Figure 4.08; The fracture test rig for Vicker's hardness measurements.

Oil from a hand pump (this will later be replaced by a hydraulic pump powered by compressed air), is driven into the ram to force the indenter into the ice block. The ram heads can be interchanged to give various loading arrangements (3 and 4 point bending, Diamond Vickers Hardness, or Hertzian ball). The magnitude of the force is measured with a load cell beneath the ice block (shown in figure 4.09).

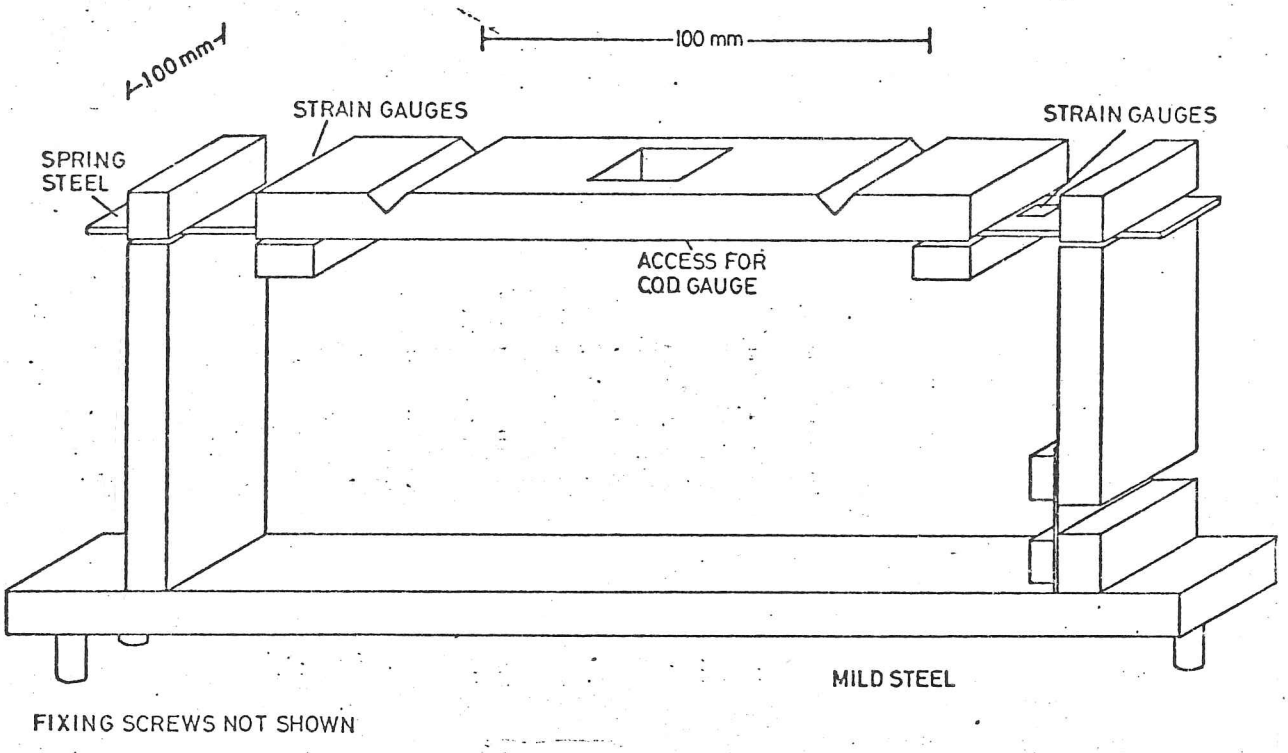

Figure 4.09; The Load Cell.

A thick steel plate is attached by steel springs (75 mm wide) to two supports. The deflection of the springs, which measures the force, is detected by strain gauges glued to the top and bottom of the springs. The gauges are in a four sided bridge to reduce drift from temperature changes. A 1 V, 1.5 kHz wave is fed into the network from a Philips strain gauge bridge, which also detects and amplifies the bridge output. The signal is recorded continously on a Bryans 28000 flat bed chart recorder. Before each test the load cell was calibrated with a weight. It was found to be linear over a range of 10 g to 40 kg (vibrations are

the limiting factor at low stresses), which is more than sufficient to measure the loads expected.

3.3 Three and Four Point Bend Tests.

Specimens, from the tank, were melted down to a bar shape, and then mid-way along one side a slot was melted with a thin copper plate to about half the thickness of the bar. At the end of the slot a very sharp crack was formed by pushing a razor blade into the ice. The dimensions of the bar, and the length of the crack were then measured with a pair of vernier calipers. The ice block was put into the small deep freeze containing the loading rig and allowed to equilibrate. The temperature could be varied between 0 and -40°C, and a block of similar dimensions to those tested was kept permanently in the deep freeze with a thermocouple frozen into its centre to indicate the equilibration time. Other thermocouples surrounded the rig. The signal from the thermocouples was fed into a ten channel Comark digital thermometer (accurate to 1°C).

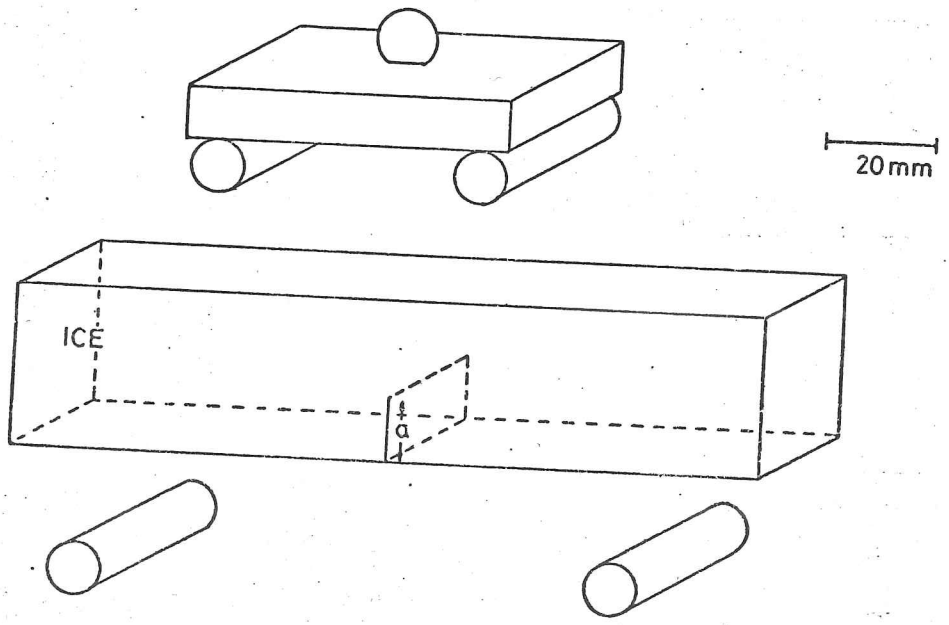

Figure 4.10; The loading arrangement for the four point bend tests.

The ice block was loaded in either three(to satisfy the BSI standard for K_{1c} measurement) or four point bending, and the load at failure recorded. In each case the loading time was less than ten seconds. Four point bending (shown in figure 4.10) is preferable to three point bending because a constant bending moment exists in the central section of the bar between the two upper loading points, and therefore the crack need not be located exactly beneath the ram.

Other tests were carried out in which the starter crack was a median crack formed under a diamond Vickers hardness indenter (see next section). This has been successfully used to measure the fracture toughness of glass (Swain, personal communication).

So far tests have only been carried out at $-20^{\circ}C$, $-15^{\circ}C$, and $-2^{\circ}C$. Experimental work has been concentrated on the median crack formation beneath the hardness indenter to be described next.

3.4 Median Crack Formation Beneath a Diamond Vickers Indenter.

When a diamond Vickers indenter (Tabor, 1971) is forced into the surface of an ice block, as well as the usual hardness indentation, median cracks form with their planes perpendicular to the surface (see figure 4.11). These are thought to form because the indenter behaves like a wedge. When the load is

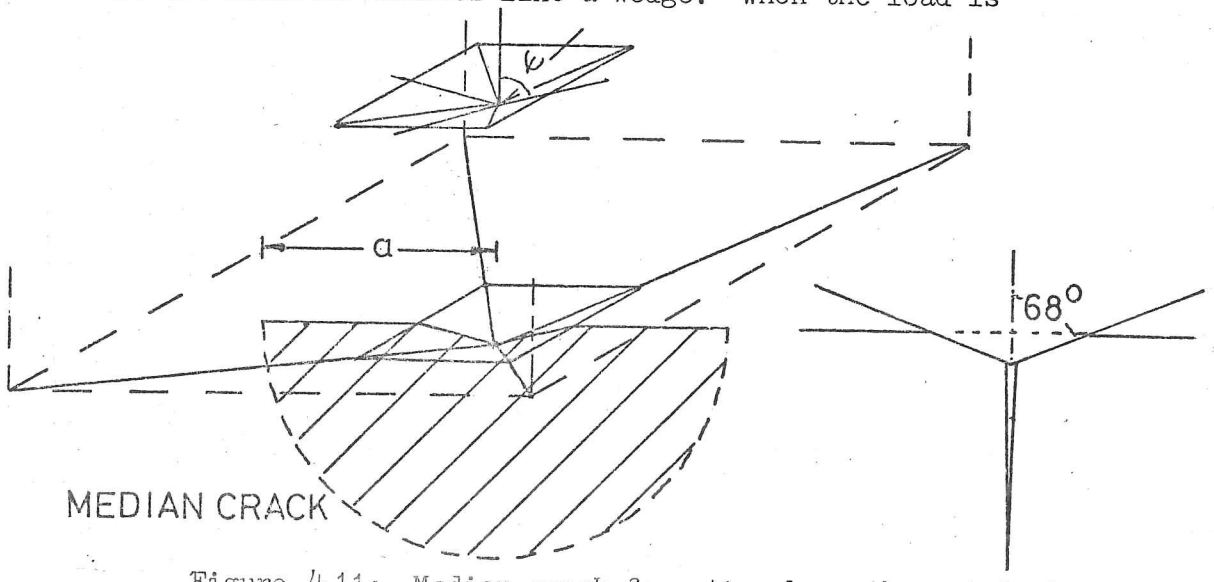

Figure 4.11; Median crack formation beneath an indenter.

removed the subsurface tension component about the deformed zone below the indentation nucleates and propagates another set of laterally extending cracks. The depth of the median crack is a measure of the fracture toughness, and can be deduced from the trace on the surface assuming that it is semi-circular in shape. If ψ is the semi-angle of the Vickers pyramid, the fracture toughness is given by (Swain, and Lawn, 1976);

$$K_{1c} = \frac{1.12\,P}{(a\pi)^{\frac{3}{2}}} \frac{1}{\tan\psi} \qquad 4.09$$

where a is the crack length, and P is the load. If K is constant then P should be proportional to $a^{3/2}$ (see results below). A plot of P versus $a^{3/2}$ was used to deduce K_{1c}.

By attaching a diamond Vickers indenter to the ram, it was possible to form median cracks for different loads. The length of the trace of the crack was measured by comparison with a graticule inside a microscope. The cracks ranged in length from 1 to 10 mm and could be measured with an accuracy of about 2 %. Often three cracks were formed with trigonal symmetry, and changed their direction at a grain boundary. This suggests, as others have observed (Gold, 1961), that ice has specific cleavage planes.

Most of the tests were carried out at -38°C, and median cracks almost always formed, but in the few tests carried out at higher temperatures median cracks were not always seen. The size of the hardness indentation was measured at the same time as the length of the crack trace.

Some time was spent investigating this test because it would be a great advantage to find a technique which enables a large number of K_{1c} values to be determined from a small number of specimens. Naturally the test is only useful if first the surface properties of the ice are not very different from the bulk, and secondly the ice is homogeneous on a scale the size of the crack.

It would be interesting to monitor the growth of the crack as the load is applied. The optical arrangement in figure 4.08

has been used for this, but it is not clear whether the crack begins to propagate as soon as the load is applied or is initiated some time after the indenter meets the surface.

4. RESULTS AND DISCUSSION.

The interior angle of a Vickers pyramid is 68°. If this

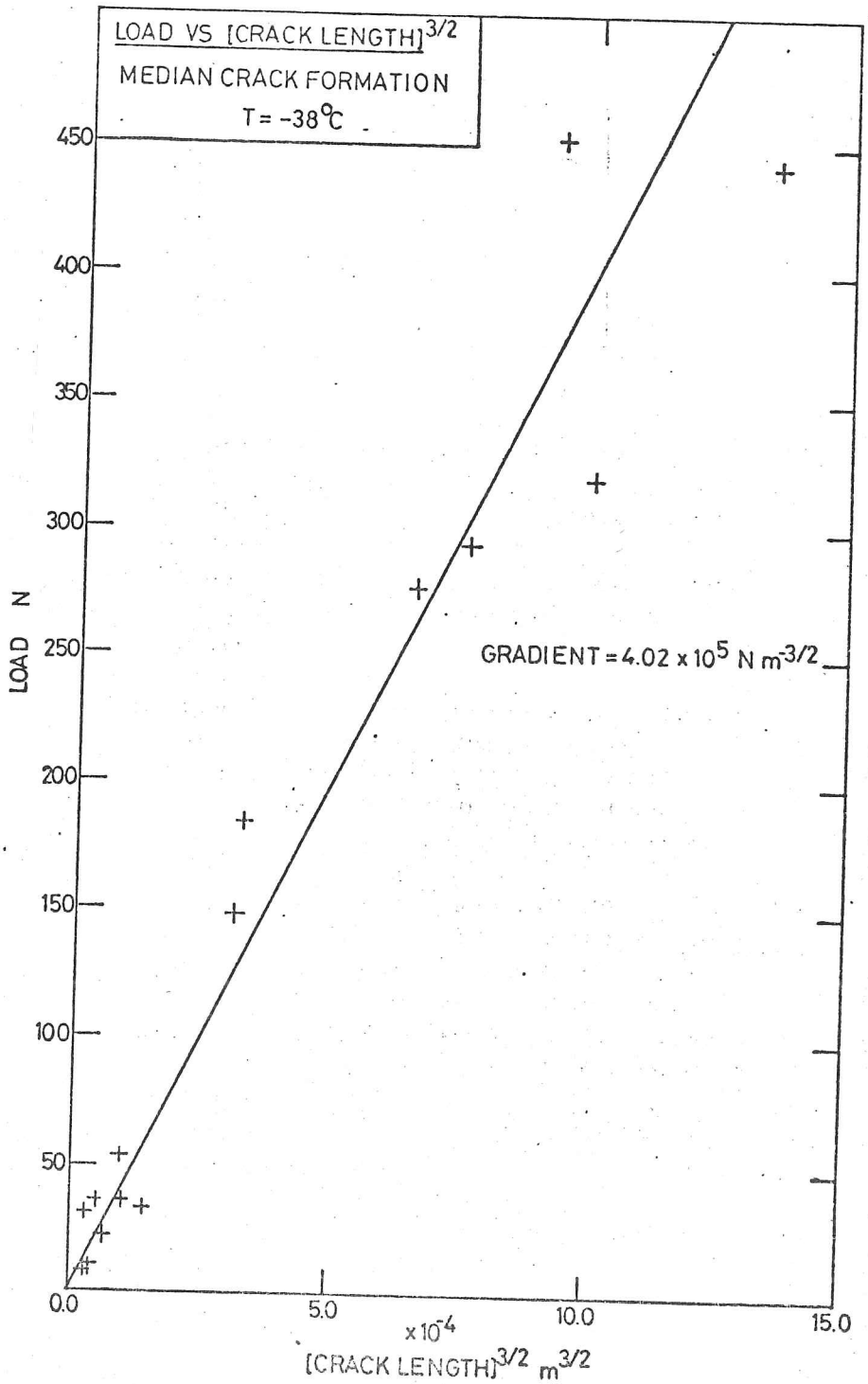

Figure 4.12; Load versus Crack Length to derive value for K_{1c} using equation 4.09.

is inserted into equation 4.09, it can be seen that a plot of load (P) against crack length to a power of three over two will yield a value for the fracture toughness, K_{1c}. This has been plotted in figure 4.12, and gives a value of 103 kN $m^{-3/2}$. By equation 4.04 this can be related to the crack extension force, G. Here we have used a value of E, the Young's modulus, given by;

$$E = 8.716(1 - 0.00125\ T)\ \text{GN m}^{-2} \qquad 4.10$$

where T is the temperature in ^{o}C, and has been computed from the temperature dependence of the shear modulus given in the appendix of chapter 2, and a Poisson's ratio of 0.31 (Hobbs, 1974) in the equation;

$$\mu = \frac{E}{2(1+\nu)} \qquad 4.11$$

This gives a value of G of 1.16 J m^{-2}.

The few three point bend tests gave values of K_{1c} of 116 $\pm$ 13 kN $m^{-3/2}$ (G = 1.5 $\pm$ 0.3) when a starter crack of at least 0.3 of the specimen width was used. When a median crack was used as a starter crack, and the formula for a semi-circular crack in an infinite body used to calculate K_{1c} a value of 69 kN $m^{-3/2}$ (G equals 0.48 J m^{-2}) was obtained (the grain size was only 3 mm, with columnar grains with long axes parallel to the crack face; in the other tests the grain size was about 10 mm).

Some tests were carried out with no starter cracks present. If a value for K_{1c} of 100 kN $m^{-3/2}$ is assumed, then the results suggest a Griffith flaw of 1 μm is required on the surface.

The data obtained have been compared with those of Liu and Loop (1976, unpublished), and Gold (1963) in table 4.02, and figure 4.14. The agreement is satisfactory, although it is clear that many more tests are required before positive comparisons can be made. Liu and Loop's data have been replotted as G against temperature (figure 4.14) to remove the temperature dependence of the modulus inherent in K_{1c}, which they had plotted.

Liu and Loop used two types of specimens - compact tensile

Table 4.02

Fracture Toughness Values.

	T ^{o}C	K_{1c} kN $m^{-3/2}$	G J m^{-2}	Method of Test
Liu and Loop (1976)	-45 to -4	140 to 100	3 to 1	Compact Tension Specimen (Various Loading rates).
	-12 to -4	177 to 222	3.6 to 5.6	Wedge opening of double cantilever.
	-12 to -4	123 to 149	1.7 to 2.5	Crack Arrest (K_{1A})
Gold (1963)	-16.7	53 to 62	0.3 to 0.4	Thermal Shock
Goodman	-38	103	1.16	Median Crack Formation (see figure 4.12).
Goodman	-13	116 ± 13	1.5 ± 0.3	Three point bend test (large initial crack, pop-in load).
Goodman	-20	69	0.48	Three point bend test (Median crack as starter crack, grain size 3 mm, columnar grains perpendicular to crack).
Goodman	-40	-	-	Four point bend test, no starter crack but if K_{1c} is 100 kN $m^{-3/2}$, crack size 1 μm.
Glass	20	490	3.5	
Steel	20	98000	42	

Plane strain assumed, plastic zone size ($\frac{1}{3}\,\frac{1}{2\pi}(\frac{K_{1c}}{\sigma_y})^2$) assumed negligible, Poissons ratio, ν, taken as 0.31 (Hobbs 1974), and Young's modulus, E, as; $E = 8.716(1 - 1.25 \times 10^{-3}T)$ GN m^{-2} T in ^{o}C from appendix to chapter 2 and $\mu = \frac{E}{2(1+\nu)}$. Note that in plane strain $K_{1c}^2 = \frac{GE}{(1-\nu^2)}$.

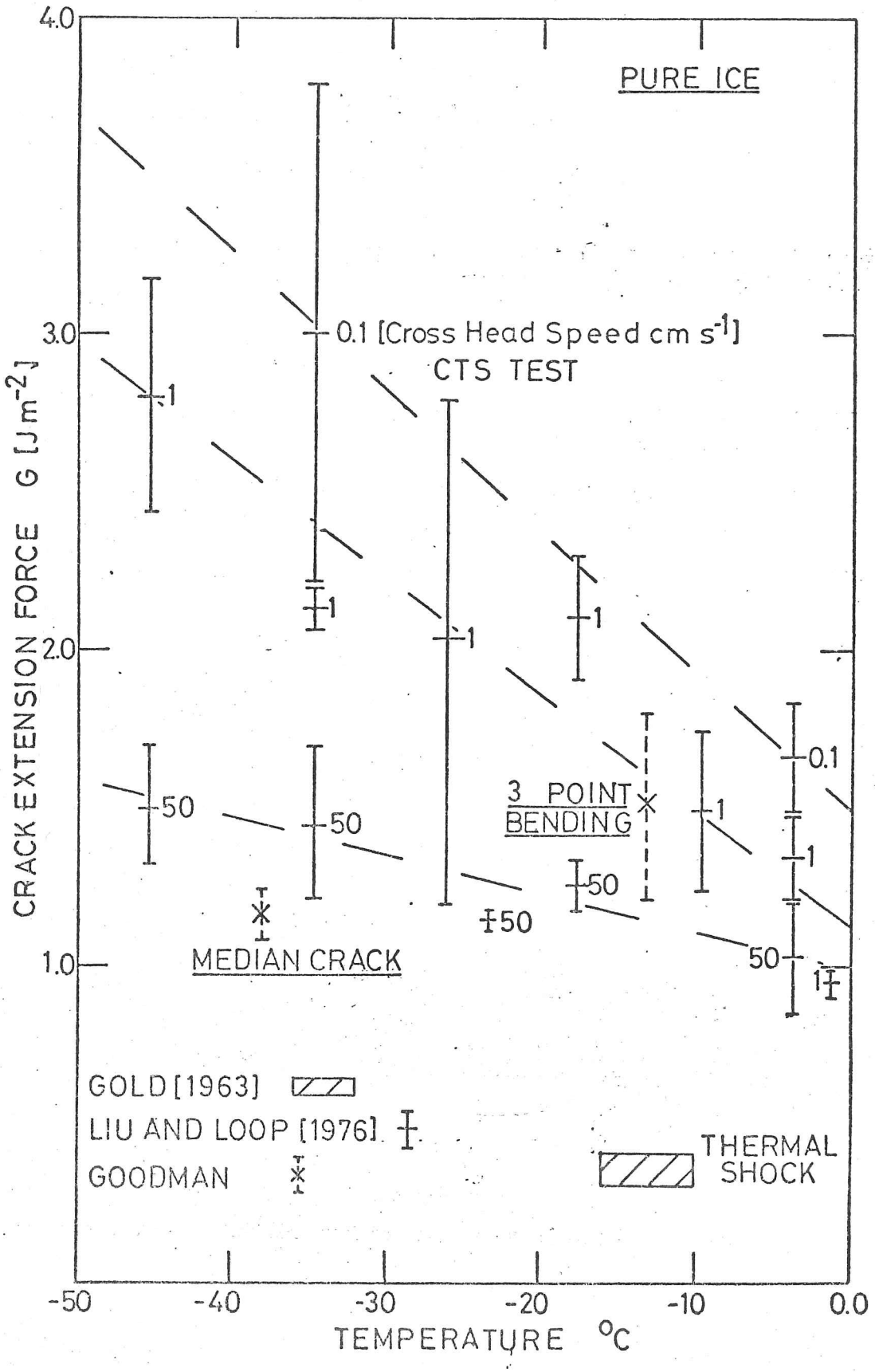

Figure 4.14; Crack Extension Force, G, against Temperature for various test methods.

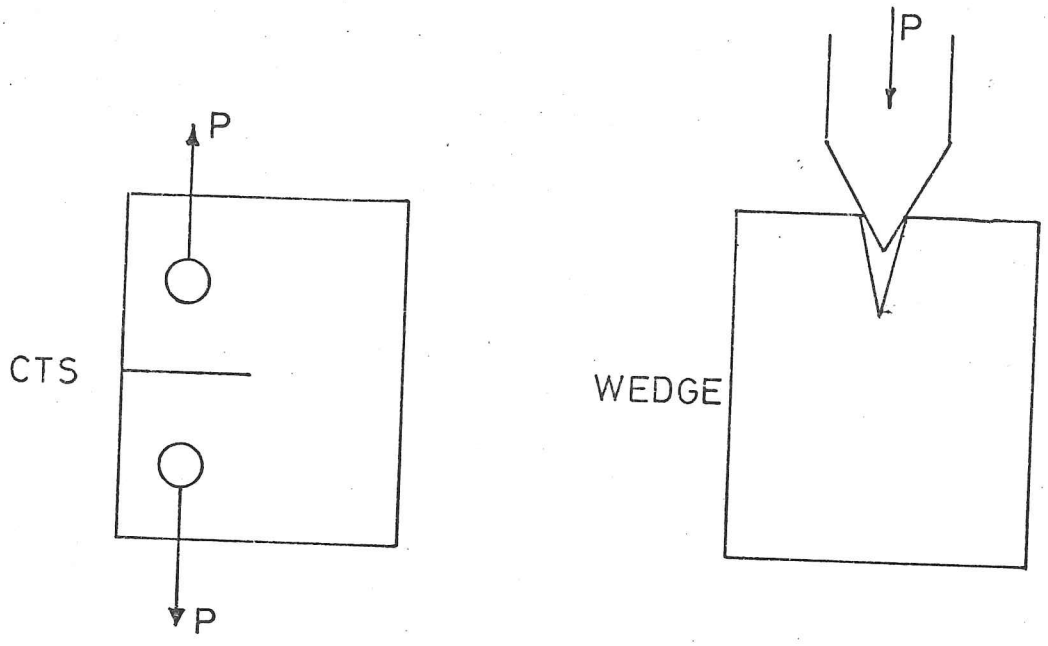

Figure 4.13; The test specimens used by Liu and Loop.

and wedge opening. These are shown in figure 4.13, and are commonly used shapes in tests on metals. It is apparent from their data, that there is a marked strain rate effect; this is due to the difficulty of defining a yield stress for a material at a high homologous temperature. The K_{1c} values they compute from the wedge opening tests, given in table 4.02, are significantly greater than their CTS data. They suggest that this might be due to a grain size effect; the grains were bigger in the wedge opening tests. Our low value in the three point bend tests with the median crack may also be due to a grain size effect.

Gold(1963), who formed cracks by propagating a thermal stress wave into an ice block by bringing two blocks of different temperatures together, also has a lower value (K_{1c} equals 53 to 62 kN $m^{-3/2}$) and had a grain size of only 1 mm. However this is probably because, as in the crack arrest data of Liu and Loop, the 'inertia' of the moving crack gives a lower apparent K_{1c}.

The surface energy for ice has been determined by Ketcham and Hobbs (1969), who measured contact angles from the contours of bubbles on surfaces, and Jones (1973), who looked at the motion of a water-ice interface in a temperature gradient. Jones disagrees with Ketcham and Hobbs's value but offers reasons for the discrepancy.

He gives a value of 46 mJ m^{-2} for the solid-liquid energy, which gives a solid-vapour surface energy of 122 mJ m^{-2} (where the liquid vapour surface energy has been taken from Hobbs, 1974). If the ice were perfectly brittle, from Griffith's argument we would expect G to be twice the solid-vapour surface energy, 0.24 J m^{-2}. We can see from the table that it is considerably more than this, which suggests there is some contribution to G from the work done plastically at the crack tip. However the difference, although it is greater than that for glass, is nowhere near as large as the difference for a typical steel. Thus the assumption of a small plastic zone is probably satisfactory, although Liu and Loop's data at low cross head speeds suggests that strain rate effects cannot be neglected.

There is plenty of scope for fundamental experimental work to investigate the fracture toughness of ice. The experiments seem to suggest that the formation of median cracks can be used to carry out a great many tests to obtain a statistically meaningful result for K_{1c}. However, it is perhaps more important to make simple observations of crack surfaces, perhaps by a replication technique, which can more easily be carried out with a three point or four point bend specimen. The first aspect to tackle must be the temperature dependence of K_{1c}. In metals, the fracture toughness falls as less plastic work is done at the crack tip; we can see from the data of Liu and Loop that it appears to rise when the temperature is reduced (even when the temperature dependence of the modulus is removed by plotting G). We would expect the behaviour of a material at such a high homologous temperature to be different to that of a metal which is used in a regime of low homologous temperature. An understanding of the fracture toughness of ice should provide much insight into the behaviour of all materials at high homologous temperatures, in particular whether recrystallization is important. It is hoped, after this thesis is completed, to return and develop these aspects.

The concepts of fracture toughness have been applied to the load bearing capacity of sea ice (Parmeter, 1975), and to crevass formation (Smith, 1976; Weertman, 1977) but in each

case a value for K_{1c} was guessed. Sea ice often contains cracks, which, clearly, can dramatically reduce the load bearing capacity, and so it is important to obtain better values for K_{1c}, particularly for ice containing brine pockets.

5. SUMMARY AND CONCLUSIONS.

This chapter should be regarded as a progress report on work that will be completed over the next six months. However this chapter has set out to show that fracture toughness concepts can be applied to ice, despite its strain-rate dependent mechanical properties. Values for K_{1c} have been experimentally measured by median crack formation, three and four point bending. These agree with previous observations; further measurements of median cracks should provide a large number of values for K_{1c} for a small number of specimens which should make it possible to deduce an improved value for K_{1c}.

It should be emphasised again that the concepts of a singularity at the crack tip will break down when widespread creep takes place (which occurs for strain rates below about 10^{-4} s^{-1}). This will lead to a confusion of mechanisms, as creep deformation becomes more significant than change of shape by crack propagation. Temperature has a profound effect on creep (see chapter 2) but will only affect fracture mechanisms if they are creep controlled, such as void growth. The most informative experiments which should now be carried out are firstly to measure K_{1c} over as wide a temperature range as possible by the median crack method (where the strain rate is probably high enough to remove the strain rate dependence), and to make observations by a replication technique in the scanning electron microscope of fracture surfaces formed in three point bend tests at various temperatures.

PART II

FIELD WORK

SEA ICE IN BYLOT SOUND, NW GREENLAND 1974

ROSLIN GLACIER, EAST GREENLAND 1974

CHAPTER FIVE

SURFACE STRAIN MEASUREMENTS ON GLACIERS AND SEA ICE

SURFACE STRAIN MEASUREMENTS ON GLACIERS AND SEA ICE.

1. INTRODUCTION.

The last part of this thesis describes the results from a series of field experiments which were designed to evaluate a new technique for the rapid measurement of surface strain rates on glaciers and sea ice. The technique uses a modified geophysical wire strainmeter, which was first developed to measure Earth tides (Sydenham, 1969; Gerard, 1971; Bilham, 1970; Bilham and King, 1970; King and Bilham, 1973, 1976; Evans, 1976), to monitor continuously the distance between two points from two to ten meters apart on the ice surface. In such conditions the strainmeter can resolve strains as small as 10^{-7}, but has a range of 10^{-4} to 10^{-7} strain.

The first experiment, on the sea ice in Bylot Sound, NW Greenland ($76^{\circ}27'$N, $69^{\circ}30'$ W), was motivated by an interest in the way sea waves penetrate pack ice. Wadhams (1973a,1973b) had suggested that creep in the ice led to attenuation of the swell, and Robin (1963, 1966) that the waves may be responsible for the break-up of a large floe or expanse of fast ice. Strain amplitude spectrums were successfully collected, and the experiment was subsequently repeated in Forteau Bay, Labrador by Allan (1975). The spectrums will be used to test a model of the response of sea ice to the action of waves (Squire, 1978). Previously wave amplitude data on ice floes had been collected with gravimeters (Hunkins, 1962; LeSchack and Haubrich, 1964), tiltmeters(Sytinskiy and Tripol'nikov, 1964) and seismometers (Smirnov, and Lin'kov, 1971). It is a non-trivial matter to integrate data so obtained because in general it will contain a systematic error, which appears as a constant multiplied by the time squared when the data was integrated to give a displacement (Wadhams, 1973b) A disadvantage the strainmeter does not suffer from. Also, if three strainmeters are used, it is a simple matter to compute the directions of the principal strain rate axes. If the model of the response of the sea ice to wave impact is successful, it should be possible, from the strain results, to deduce the apparent modulus (which in turn will give information about the average crack, and void density in the ice) if the incident wave amplitude is known. In the section on sea ice, some observations will be made about changes in modulus observed.

Further experiments were carried out to test the viability of the strainmeter for rapid surface strain measurements on a glacier surface. Three instruments were installed first on the Roslin glacier, east Greenland (71°51'N, 24°59'W), where only one gave satisfactory results, and subsequently on the Barnes Ice Cap, Baffin Island (69°45'N, 72°15'W) (Evans, Goodman, and Holdsworth, 1976). On the Roslin glacier some interesting rapid changes in strain, which lasted about an hour, were observed, while on the Barnes Ice Cap large strain rates (about 10^{-6} per day) were observed, which were compatible with the strain rates expected and agreed with measurements made on stake arrays (50 m and 50 km apart) that surrounded the instruments at one site, but disagreed at the other site (probably because of poor resolution of the stake measurements). In the past other devices have been installed to make continuous observations of strain changes in glaciers; these have used the change of resistance of a wire when it is pulled to detect strain changes (Meier et al, 1957; Warner and Cloud, 1974), and suffer from the obvious disadvantage that a changing stress is exerted on the supports in the ice, which (because of the non-linear creep law) will give a non-linear drift. Also arrangements have not always been made to allow for large strain changes so that frequent adjustment was necessary.

Colbeck and Evans (1971) made accurate observations daily over a gauge length of 2m on the Blue Glacier, Washington. Large spatial variations of surface strain were observed, and they concluded that 2m was too short a distance to obtain meaningful average strain data for the glacier. The observations made over 5m on the Barnes Ice Cap to be described, suggest that, in this case, the local strain variations are less than 5m. It is clear that strainmeters should be used in arrays and installed at more than one site to observe the spatial distribution of strains.

Finally the results from a quite different experiment will be included. Three wire strainmeters, which had 10 m gauge lengths, were installed in two rock tunnels that have been cut within ten meters of the ice/rock interface under the glacier d'Argentière in the French Alps (46°00'N, 7°00'E). These were used to detect the elastic strain changes in the rock, as the glacier slid over its bed. Events, which could be due to stick-slip motion of the glacier, were frequently seen on the strain records obtained. For a short period a seismometer was installed alongside the

strainmeters; the records obtained also showed many seismic events which had their origin in the glacier.

The next section gives a description of the wire strainmeter and the modifications made for its use on glaciers and sea ice. The section also contains the design of a new instrument which uses as a length standard a 1 m Invar rod. This has been constructed and tested first by deployment from HMS Sovereign on a visit to the North pole in the autumn of 1976, and is at present in use on the sea ice off the Newfoundland coast.

A short appendix is given which gives the necessary algebra which relates the observation of linear strain to the components of the strain tensor.

2. STRAINMETERS.

2.1 The Wire Strainmeter.

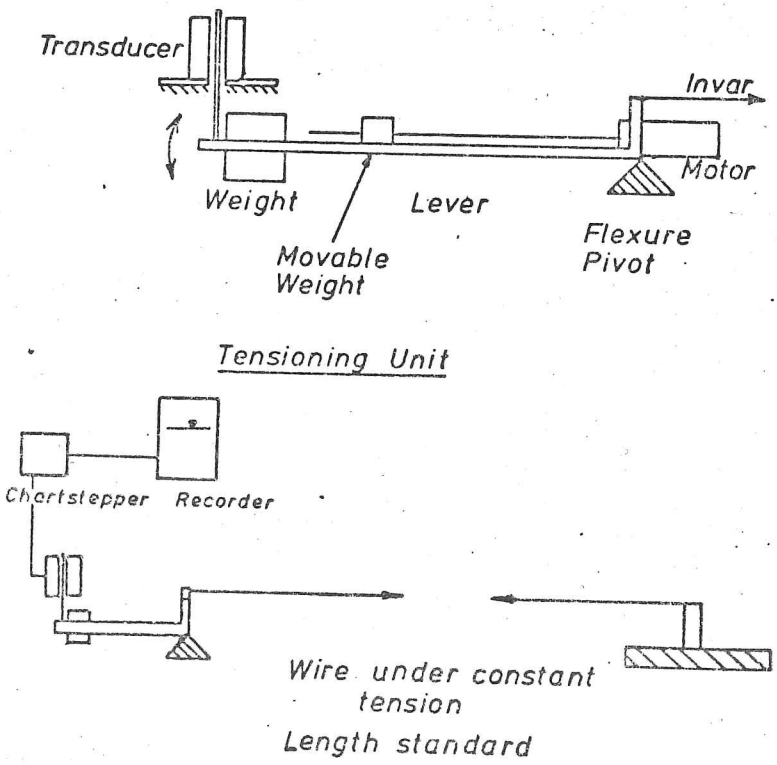

Figure 5.01; The Wire Strainmeter. Strain in the ice appears as rotations of the lever, which is pivoted to the base by two flat strips of Invar. The rotations are detected with an inductive displacement transducer.

The wire strainmeter was developed to measure Earth tides (typically 5×10^{-9} strain) (Bilham, 1970); it is described in detail in King and Bilham (1976). A 0.56 mm Invar wire, which is kept under constant tension by a lever and weight, is used as a length standard. The tension in the wire is about 7 N. Figure 5.01 shows the principle and figure 5.02 is an exploded view of the tensioning unit.

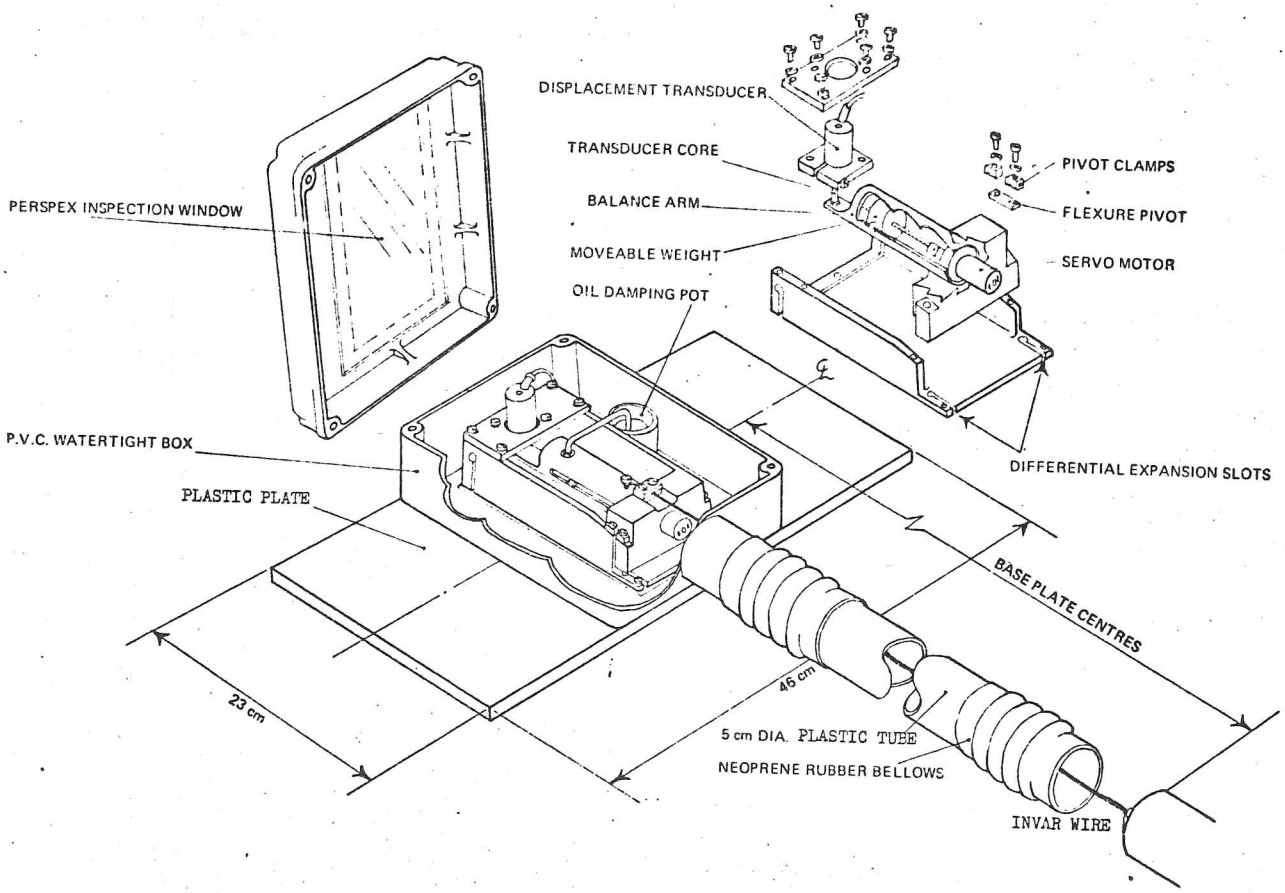

Figure 5.02; An exploded drawing of the tensioning unit of the Cambridge wire strainmeter (from King and Bilham, 1976).

The lever is attached to the base by two flat strips of Invar (60 to 90 μm thick) which remove stick-slip effects. When strain occurs, the lever rotates, and the rotation is detected by the motion of a ferrite core, attached to the lever, in the coils of an inductive displacement transducer fixed to the base. The transducer can easily detect motions as small as a micron, and the lever arm gives a ten to one gain; thus for a 10 m instrument strains of 10^{-8} can be resolved. The instrument has been found to be linear to 0.1 % over a range of 10^{-8} to 10^{-5} strain. The gain of the instrument is affected by bending moments at the wire clamp, which change as the length of the wire is altered; the attenuation is linear and about 2 per cent per meter, for gauge lengths less than 20 m. The frequency response of the instrument is limited by the natural oscillations of the weight, which for 10 m is 3 Hz, 20 m 1.5 Hz, and 2 m is 5 Hz; the bandwidth is fixed by electronic filtering - for the sea ice work this was set at 1 Hz (-6 dB point) and for the glacier experiments at 1/6 Hz. Sometimes mechanical damping from an oil damping vane was used to remove unwanted oscillations during rezeroing. The accuracy of the instrument is determined by the maximum temperature changes in the wire (thermal expansion is apparent strain). At room temperature the Invar has a temperature coefficient of $5 \times 10^{-7}\ ^{o}C^{-1}$, but increases as the temperature is reduced. In all the experiments to be described the strains observed were much larger than any strains expected from thermal effects provided the wire was protected from the sun by a suitable cover, or the instrument buried in a trench. The pressure coefficient is 10^{-9} mbar^{-1} (10^{-11} m^{2}N^{-1}).

A purpose built electronics package (T. Owen, personal communication) supplies a stabilised voltage to the transducer, amplifies the signal, and detects when the output moves beyond preset limits (usually the input range of the recorder). If the signal is outside the limits, the electronics will automatically either add or subtract a DC offset to the output, or activate a mechanical rezeroing device. The current drain of the package is about 40 mA (30 mA for the transducer and 10 mA for the offset electronics). The output was recorded on a chart recorder.

Several mechanical rezeroing methods have been used. The strainmeter is of limited use unless it is fitted with some sort of

device which will return the transducer core to the centre of the transducer when the strainmeter has reached the limit of its range; it can then be left unattended. At Earth tide sensitivites Bilham and King use a small weight, which can be moved along the lever by a motor, to adjust the tension in the wire. In the experiments described here more adjustment was needed; two approaches proved successful. Firstly the tensioning unit was mounted on a table which could be moved by a motor (shown in figure 5.03), and secondly the end clamp, away from the tensioning unit, was servoed (Allan, and Ridings, personal communication). Either of these methods allows strains up to 10^{-2} to be accommodated before the system goes out of range; this is very useful during the initial settling in period. The first method is slightly more convenient

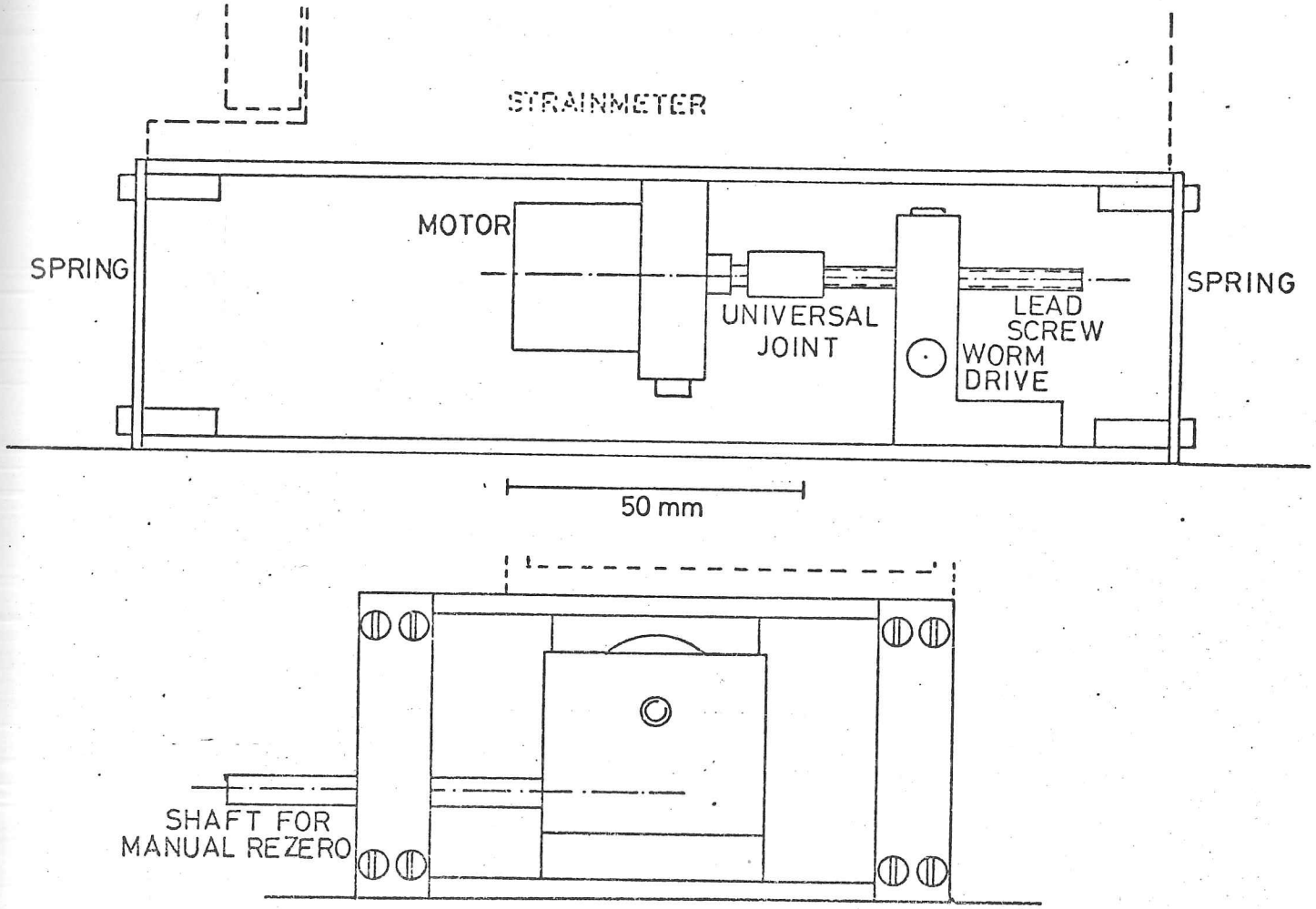

Figure 5.03; The rezeroing unit used in the Barnes Ice Cap experiment. When the motor is energised, the lead screw turns so that the top plate is moved relative to the bottom plate (the two plates are held parallel by four steel springs at the corners). The lead screw drives against a thread in the centre of a cog, which can be rotated manually by a worm drive. A torsion cable is attached to the worm drive shaft and taken to the surface.

because, in general only the tensioning unit is accessible if the instrument is buried in a trench. Some form of manual rezero should always be included to make setting up easier; in figure 5.03 the shaft shown in the end elevation is connected to a worm drive which can move the top plate relative to the bottom. In the field this shaft was connected to a flexible cable which was brought to the surface so that the instrument could be rezeroed without digging down to the tensioning unit.

The wire is protected from air currents by a plastic tube (decoupled from the tensioning unit by rubber bellows). The tensioning unit and the clamp at the other end were mounted on plastic plates (to avoid thermal conduction problems), which were fixed to the ice with ice screws (figure 5.04). A variety of methods were used for fixing the plates but the most reliable, and convenient was found to be four ice screws. All the installations were in areas where the air temperature was well below 0°C, so that regelation problems were not found to be significant.

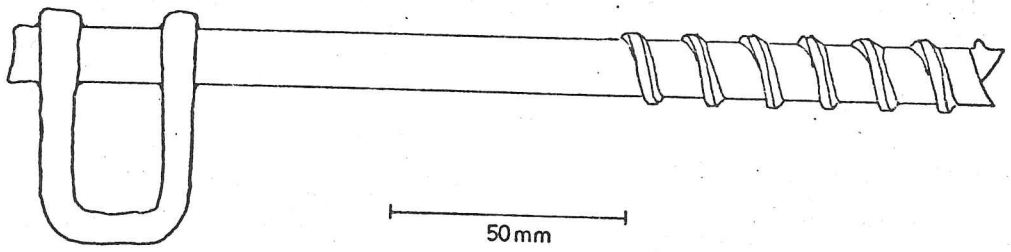

Figure 5.04; A typical ice screw. The shaft is hollow to allow ice to escape when the screw is cutting its way down.

The instrument survived the parachute drop onto the Roslin glacier, and being carried over glaciers and moraines for 50 km in a rucksack, as well as numerous air flights, without apparent damage.

2.2 The 1 m Invar Rod Strainmeter.

The wire strainmeter cannot be quickly installed (installation

because, in general only the tensioning unit is accessible if the instrument is buried in a trench. Some form of manual rezero should always be included to make setting up easier; in figure 5.03 the shaft shown in the end elevation is connected to a worm drive which can move the top plate relative to the bottom. In the field this shaft was connected to a flexible cable which was brought to the surface so that the instrument could be rezeroed without digging down to the tensioning unit.

The wire is protected from air currents by a plastic tube (decoupled from the tensioning unit by rubber bellows). The tensioning unit and the clamp at the other end were mounted on plastic plates (to avoid thermal conduction problems), which were fixed to the ice with ice screws (figure 5.04). A variety of methods were used for fixing the plates but the most reliable, and convenient was found to be four ice screws. All the installations were in areas where the air temperature was well below 0°C, so that regelation problems were not found to be significant.

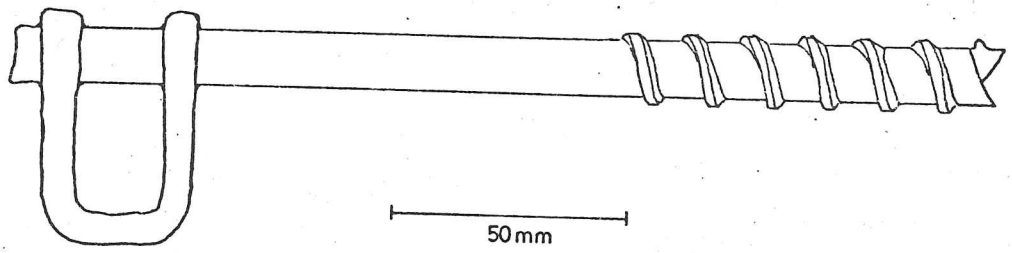

Figure 5.04; A typical ice screw. The shaft is hollow to allow ice to escape when the screw is cutting its way down.

The instrument survived the parachute drop onto the Roslin glacier, and being carried over glaciers and moraines for 50 km in a rucksack, as well as numerous air flights, without apparent damage.

2.2 The 1 m Invar Rod Strainmeter.

The wire strainmeter cannot be quickly installed (installation

takes about 30 mins on sea ice), and it is not easy to explain to someone unfamiliar with the instrument how it should be set up. To study wave amplitudes over a wide area on sea ice, particularly where weather conditions may dictate a rapid retrieval of the equipment, a new instrument of a different design (which could be rapidly set up or removed) was required. In the summer of 1976, an offer was made to take some instruments under the Arctic ice in a nuclear submarine, HMS Sovereign, to the North Pole. This offer provided the incentive to redesign a strainmeter, which instead of a wire under constant tension uses a 1 m Invar rod as a length standard, that had been tried unsuccessfully in 1974 in Greenland.

The design is shown in figure 5.05, and the end unit, which detects the strain, in figure 5.06. The instrument is supplied with

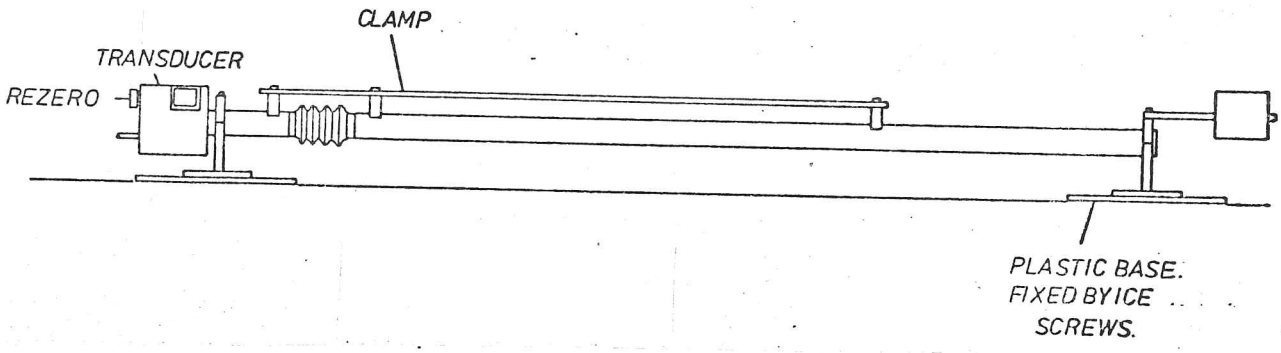

Figure 5.05 The 1 m Strainmeter

a wooden cover that keeps the wind off. Installation time is about ten minutes. The instrument is placed on the ice, the base plates fixed by ice screws, the clamp removed, and the transducer core moved to the centre of the transducer body. A special recording package was designed to provide power for the transducer (in this case an AC-AC LVDT was used), and to record the signal onto magnetic tape (Goodman and Neal, 1977).

When strain occurs, the rod pushes, or pulls the core out of the transducer body. The core is kept away from the transducer by three steel springs at right angles to the end of the rod. These are slightly buckled to give an overall movement of about

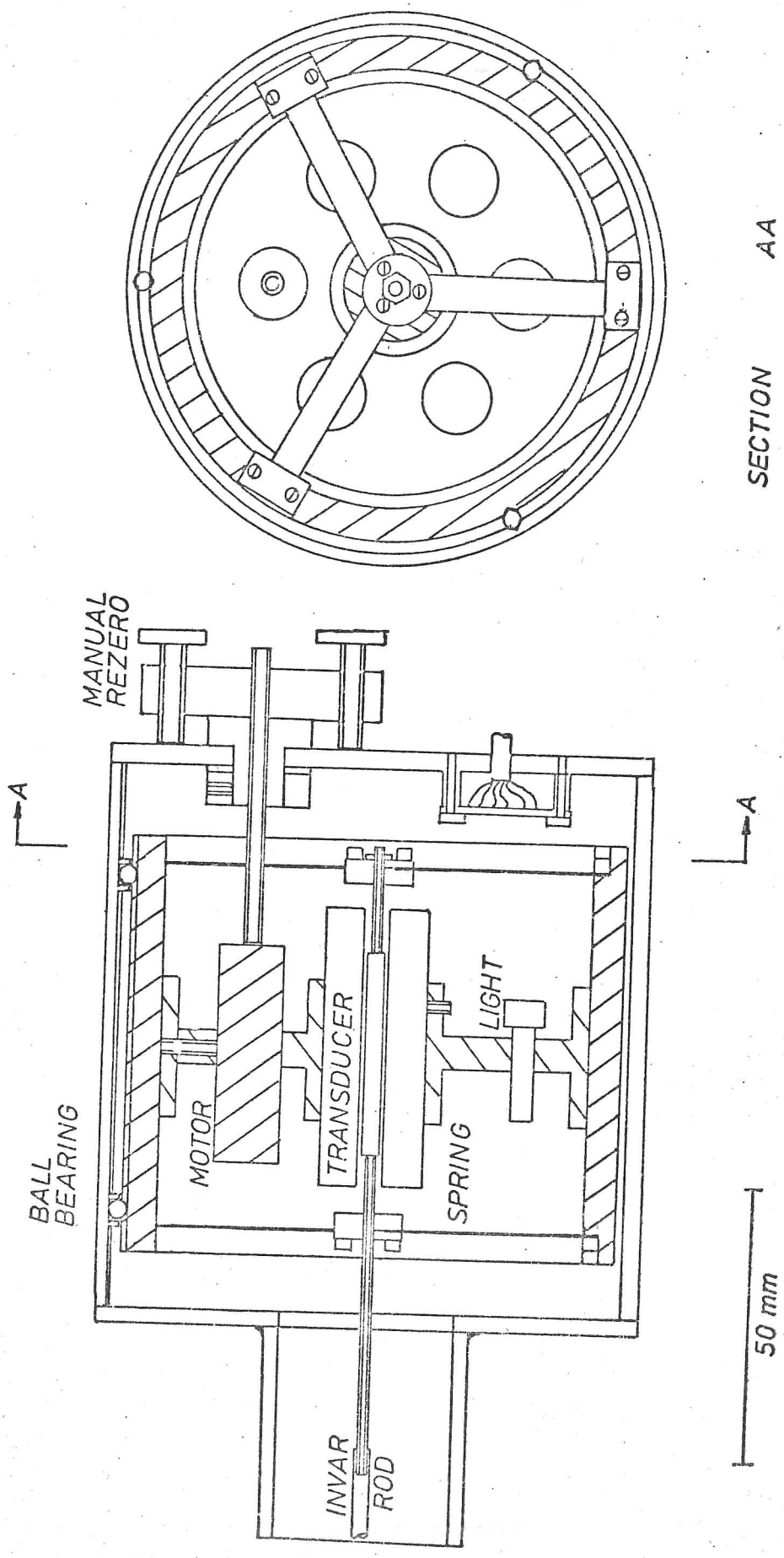

Figure 5.06; End unit of the 1 m strainmeter.

5 mm (the actual movement required is only a few microns). If the core is moved beyond a preset point in the transducer body, the motor is energised which drives the transducer assembly parallel to its housing (there are captured ball bearings in V grooves between the assembly and the housing, see figure 5.06) until the core is in the null position. When the instrument is first set up, the core can be positioned at the centre of the transducer by rotating the manual rezero screw.

The sensitivity is an order of magnitude less than the wire strainmeter, but it is easily enough to observe the strains due to the action of sea waves passing under the ice; the resolution is about 10^{-7} strain, and the temperature dependence was measured to be $1.5 \times 10^{-6}\ ^{\circ}C^{-1}$ (at $-10^{\circ}C$).

2.3 Calibration.

The instrument can be no better than its calibration; if sensible conclusions are to be drawn from the results then there must be no doubt in the calibration of the strainmeters.

The wire strainmeters were calibrated by the same procedure described by King and Bilham (1976) for their strainmeters. Each strainmeter is calibrated relative to a standard, whose absolute calibration is known. The two strainmeters were arranged directly opposite each other, and connected by a length of Invar wire (two different lengths, 2 and 10 m were used). The standard was driven through its range with a motorised micrometer, and the difference signal recorded. This was repeated until the difference was as small as possible over most of the range by attenuating the signal from one of the strainmeters. From the attenuation factor the absolute calibration of the strainmeter can be deduced. It is quite clear from the difference signal if non-linearities are present. King and Bilham estimate that the absolute calibration of the standard instrument is accurate to 2 per cent. All the calibrations were carried out at room temperature.

The 1 m instruments were calibrated in the cold rooms of the Scott Polar Research Institute. One base plate was clamped to a bench, while the other end was fixed to an ordinary X-Y milling machine

moving table. Small movements could then be applied to the instrument, and these were measured with a 0.0001 inch (2.54 μm) dial gauge. The output from the transducer amplifier was fed directly into a digital voltmeter and the readings recorded. A typical calibration is shown in figure 5.07.

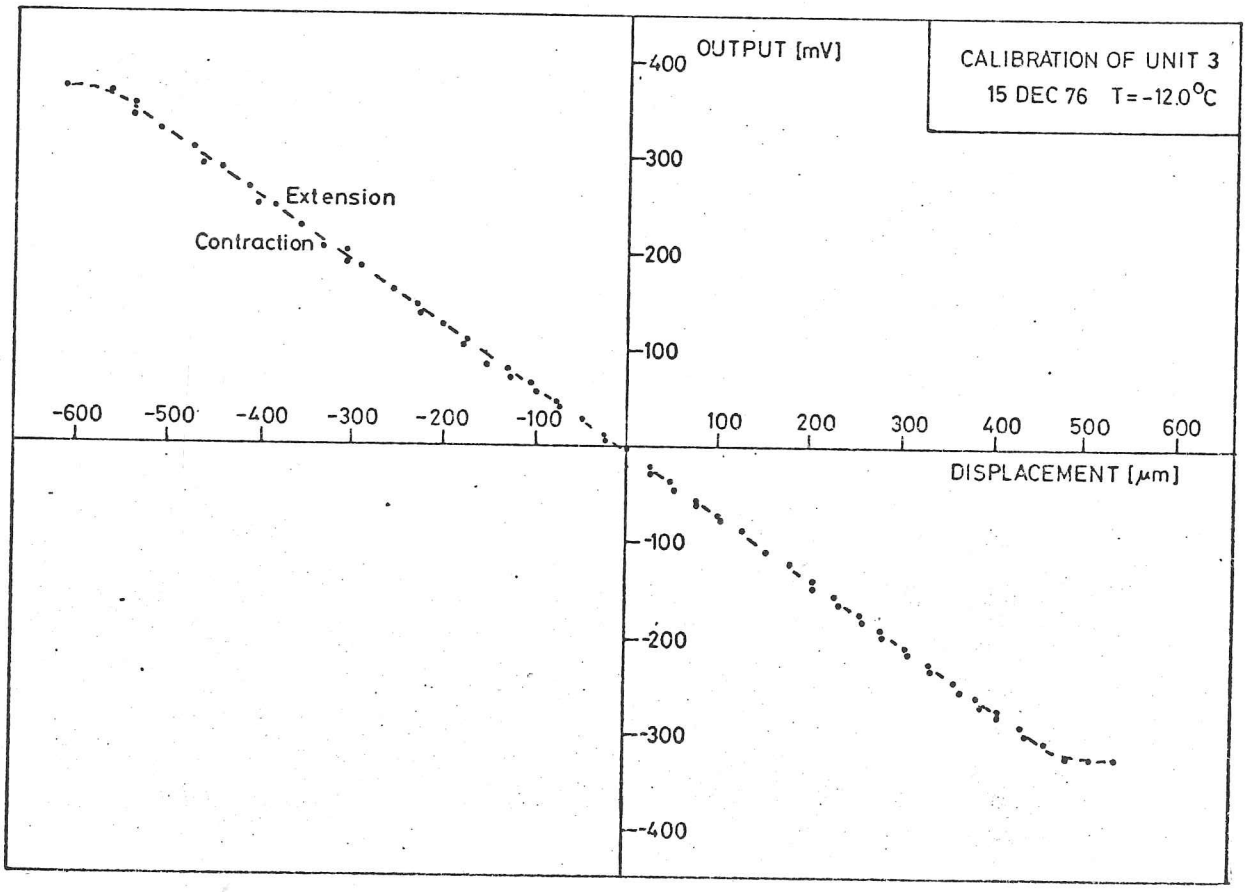

Figure 5.07; A typical calibration of the 1 m strainmeter.

In all the experiments to date, it has not been possible to calibrate the instruments in the field (except for checking the voltage levels in the electronics); this is a serious drawback. In all future experiments a field calibration system will be used. It is important to calibrate the instrument when the wire is in place because bending moments at the clamp can affect the calibration. The simplest method would be to use a standard tensioning unit, which has a motorised micrometer to move the lever, and can replace the end

clamp in any installation.

Time calibrations were made in two ways. When the Chessell chart recorder was in use, it was assumed that the chart ran at a constant speed (the chart drive was a pulse driven stepping motor, and the speed was checked to be constant within 0.1%). In the Barnes Ice Cap, and Argentière experiments Rustrack and Miniscript recorders were used; timing marks, derived from a crystal controlled clock, were made on the chart every three hours in the Ice Cap experiment, and every twenty-four hours under the glacier d'Argentière.

3. SEA ICE EXPERIMENTS.

3.1 Bylot Sound, NW Greenland.

To find out whether a wire strainmeter could detect the strain changes in sea ice as waves pass underneath, a single instrument was taken to Bylot Sound, near Thule, NW Greenland (Goodman, Allan, and Bilham, 1975). A simplified chart of the area is shown in figure 5.09; the position of the fast ice edge, and the density of pack ice beyond are marked. The site was chosen because it was easy to get to from the airstrip at Thule, and it was thought that there would be a flux of swell generated on the North Water between Greenland and Ellesmere Island which could penetrate the pack ice and deform the fast ice in the bay. The method used to fix the strainmeter to the sea ice is shown in figure 5.08.

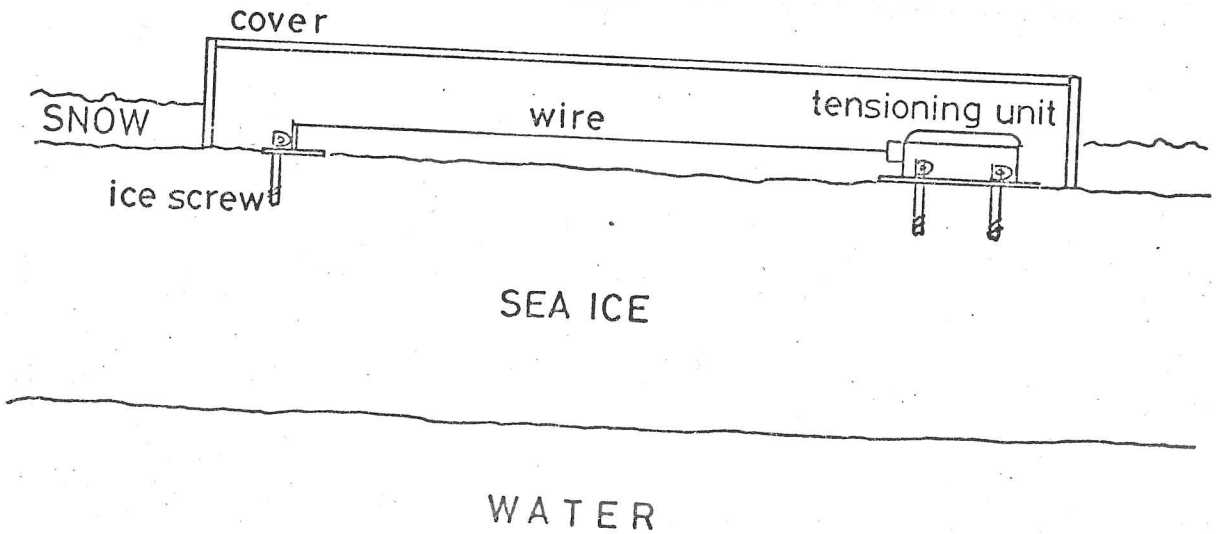

Figure 5.08; The method used to fix the strainmeter to the sea ice.

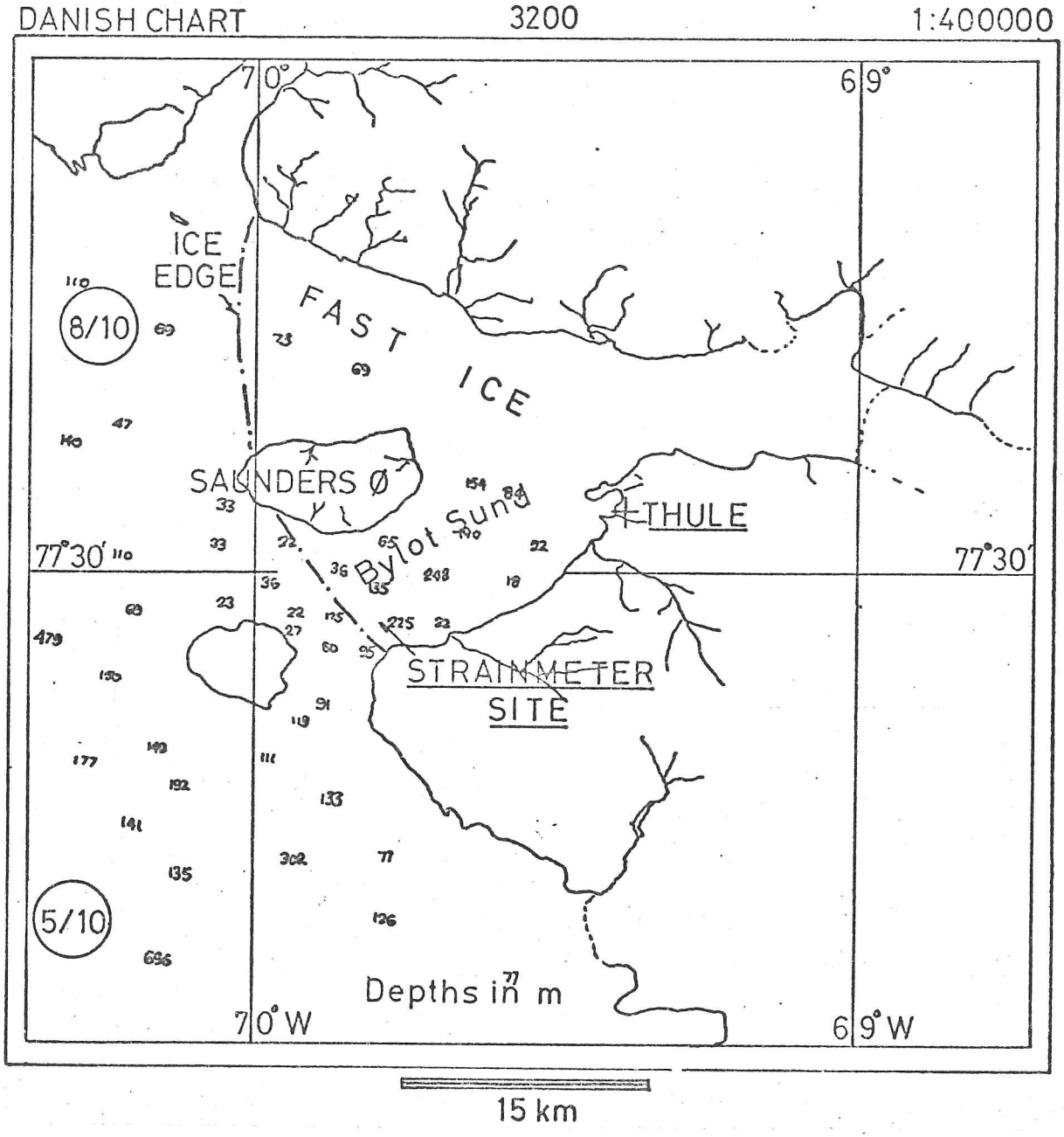

Figure 5.09; The Strainmeter Site at Bylot Sound, NW Greenland.

The strainmeter was set up 75 m from the ice edge (where the ice thickness was 0.85 m). The strainmeter axis was set parallel to what was thought to be the direction of the swell (it would have been better to use three instruments and deduce the principal strain rate axes but only one was available). A record, lasting 52 minutes, was successfully obtained of cyclic strain changes which were almost certainly due to the action of waves. In Cambridge the chart was digitised on a D-Mac table (accurate to 0.1 mm), and the resultant time series processed using programs developed by McKenzie and Beavan (personal

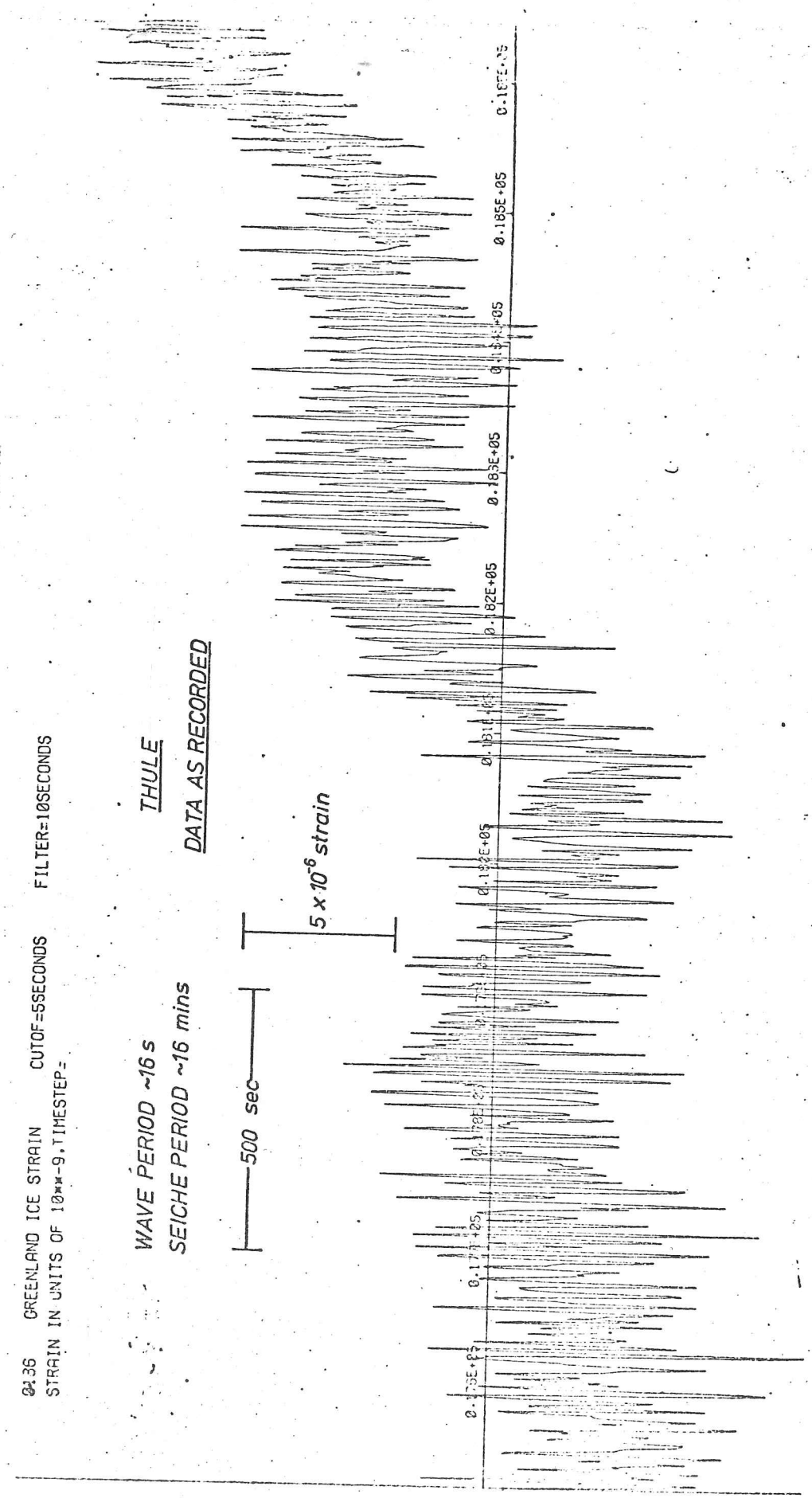

Figure 5.10; The strain record obtained from the sea ice in Bylot Sound.

communication) for the analysis of Earth tide strain data. The record with offsets (put in by the automatic rezeroing system) removed is shown in figure 5.10.

Several interesting features are apparent from the record. Firstly the strain amplitude is about 2.5×10^{-6} strain with a mean period of about 16 s. If the sea conforms to the ice (there are no air pockets), these values can be used to deduce the wave amplitude, and the surface stress in the ice (if elastic behaviour is assumed). To find an order of magnitude estimate of these quantities, it can be assumed firstly that the ice sheet is equally deformed parallel to the ice edge so that plane strain conditions exist, and secondly that the ice is elastic with the neutral axis in the centre of the ice thickness and no shear takes place so that planes perpendicular to the neutral axis remain as planes. With these assumptions simple beam theory can be used; the geometry is shown in figure 5.11.

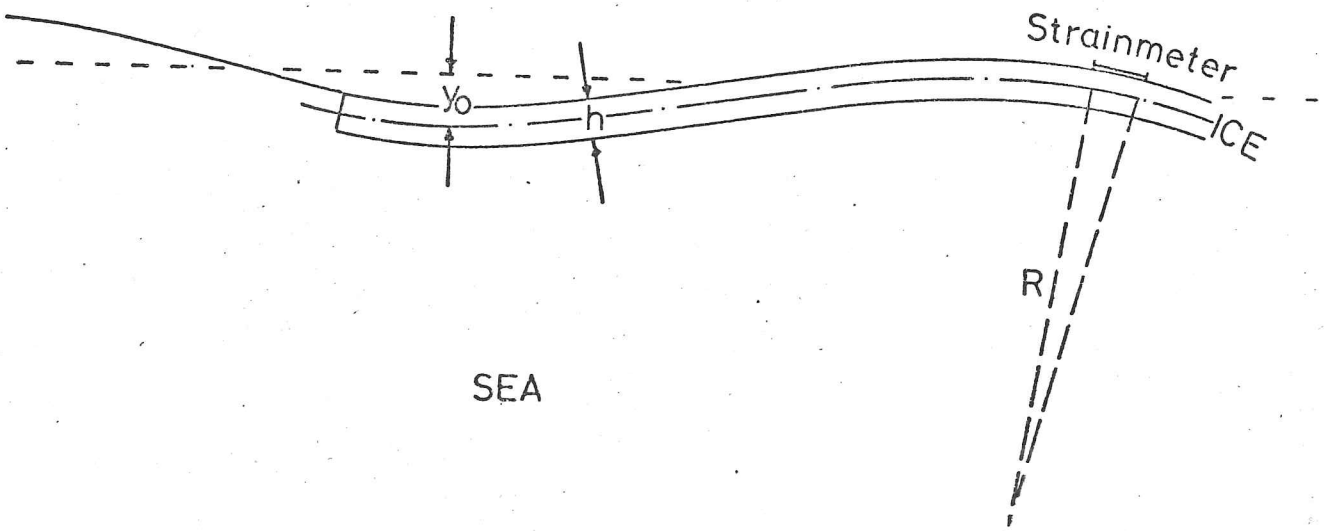

Figure 5.11; The geometry used to estimate the amplitude of the wave and the surface stress in the ice.

If the ice is bent by a simple sine wave $y = y_o \sin(kx-wt)$ (where y is the vertical deflection, x the horizontal position, and the

other symbols have their usual meaning), the surface strain is given by

$$\epsilon = \frac{1}{2}\frac{h}{R} = \frac{1}{2} h y_o k^2 \sin(kx-wt) \qquad 5.01$$

where h and R are defined in figure 5.11, and k is the wave number ($2\pi/\lambda$, λ is the wavelength). The maximum strain is given by

$$\epsilon_{max} = \frac{1}{2} h y_o k^2 \qquad 5.02$$

The wavelength can be deduced from the curves given by Wadhams (1973a); the water depth is just deep enough to make the deep water approximation (the depth is about 200 m) (Kinsman, 1965). For a wave of 16 s period, the wavelength is about 400 m. If this value together with the ice thickness of 0.85 m and strain amplitude of 2.5×10^{-6} is inserted in equation 5.02, the wave amplitude is

$$y_o \sim 2 \text{ mm} \qquad 5.03$$

a not unreasonable value. When standing on the ice, the swell could not be felt although a slight movement could be seen in the loose floes by the ice edge.

It is not necessary to know the wavelength or ice thickness to deduce the surface stress in the ice. If it is assumed to be elastic (an assumption we shall see below is reasonable), then in plane strain the surface stress, σ, is given by;

$$\sigma = \frac{E}{1-\nu^2} \epsilon_{max} \qquad 5.04$$

where E is Young's modulus, and ν Poisson's ratio. Lavrov (1969) gives the following values for E and υ , 6 GN m^{-2} and 0.3 respectively. Then the maximum stress is

$$\sigma_{max} = 0.016 \text{ MN } m^{-2} \qquad 5.05$$

for ϵ equals 2.5×10^{-6} strain. The strain rate is roughly 10^{-7} s^{-1}. From the deformation maps given in figure 2.10 in chapter 2, a stress of 0.016 MN m^{-2} ($\tau/\mu \sim 3 \times 10^{-6}$), the creep rate would be as low as 10^{-10} s^{-1}, and so we would expect the response to be almost all elastic.

A second feature of the record is the few cycles of a long period wave superimposed on the 16 s waves with a period of about 16 mins. The strain amplitude due to this wave is considerably larger, 5×10^{-6}. It is almost certainly the result of a seiche or standing wave in the bay of which Bylot Sound is the entrance. The period of a seiche is given by Merian's formula (Rossiter, 1971),

$$T = \frac{2L}{\sqrt{gd}} \qquad 5.06$$

where T is the seiche period, L the size of the bay, d the mean depth, and g the acceleration due to gravity. Reasonable values for L and d are L equals 15 km and d equals 150 m which yield a value for T of 13 mins.

3.2 Forteau Bay, Labrador.

The success of the experiment in Bylot Sound, led to a further experiment in Forteau Bay, Strait of Belle Île, Labrador by A. Allan of the Scott Polar Research Institute (Allan, 1975). Three strainmeters were used in a variety of configurations, and at different distances from the ice edge. In all 79 charts were brought back (about 40 hrs of strain data).

Only the result of the analysis of one chart will be given here to support the argument that wire strainmeters can yield useful data when installed on sea ice. The Forteau Bay site was very similar to the Bylot Sound experiment, although the bay was more open. Fast ice remained in the bay, with loose floes and eventually open water off the ice edge.

The time series from chart 73 is shown in figure 5.13. The strainmeters were arranged parallel to each other and perpendicular to the ice edge as illustrated in figure 5.12.

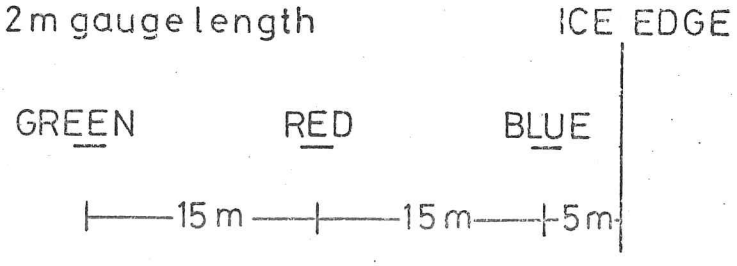

Figure 5.12; The arrangement of the strainmeters for the data given in figure 5.13.

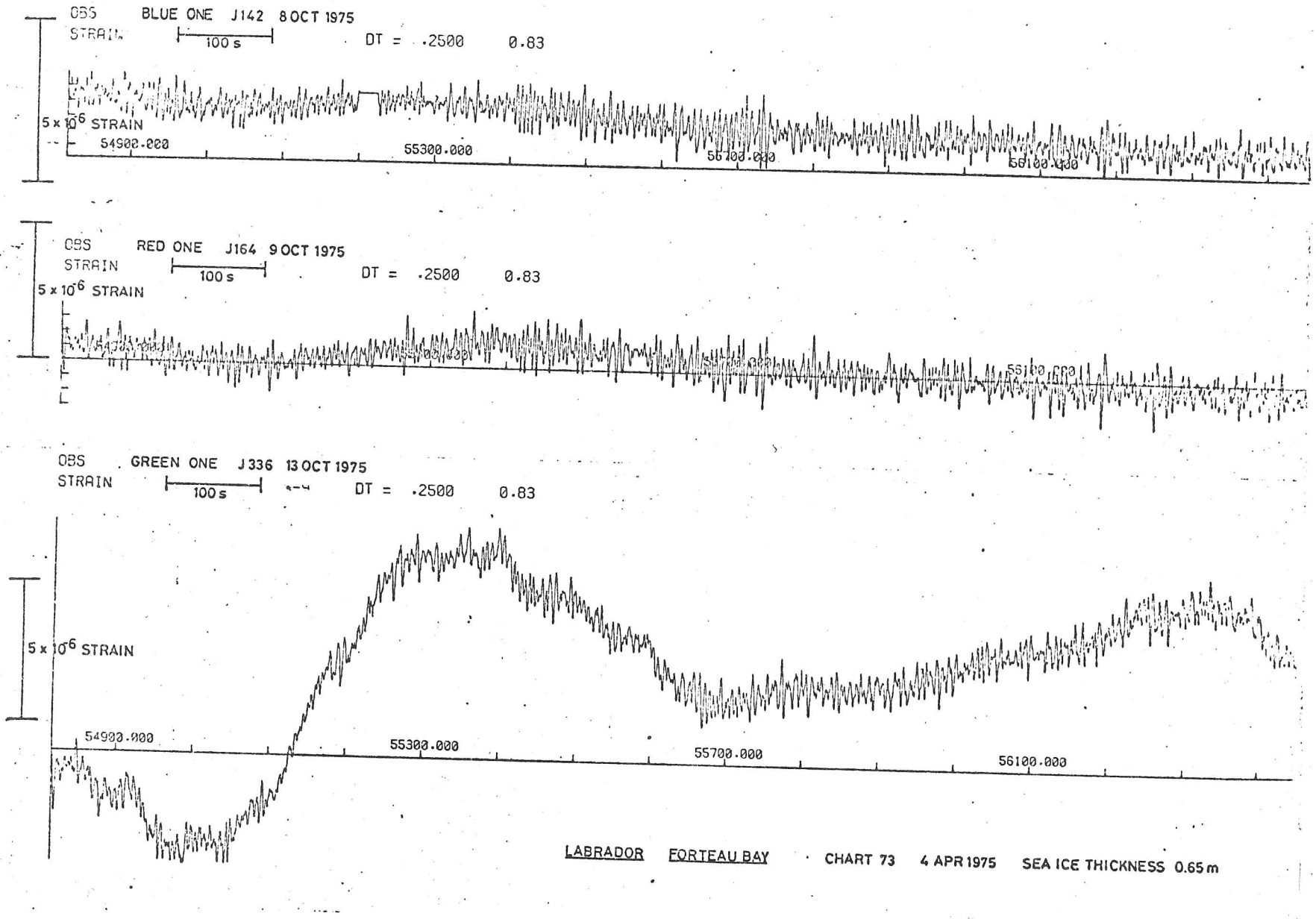

Figure 5.13; The time series from three strainmeters at different distances from the ice edge (see figure 5.12).

The time series are quite different, which indicates that the free surface at the ice edge markedly affects the response of the sea ice to the waves. The long period wave in Green is again probably due to a seiche, and appears only to couple with the ice at distances greater than 30 m from the ice edge. Also it is not easy to follow wave trains from one time series to the next (the phase velocity is about 10 m s^{-1} for the centre frequency of 6.3 s) perhaps because the waves are not incident normally on the ice edge and complicated diffraction patterns have been set up. However when the time series for Blue and Red were spectrally analysed, the two spectrums are almost identical (see figure 5.14; note that the large peak in Blue at 1.5 Hz is a complete artifact due to aliasing of the natural oscillations of the lever - these could be removed by filtering but do not affect the central peak). The spectra are similar to typical wave energy spectrums (Bretshneider, 1963); they have a central period of 6.3 s. This is considerably less than the period observed for the waves in Bylot Sound (16s). Such variations in distributions of energy are quite common; in this case the difference is due to the areas of sea in which the waves are generated - the North Water is much larger than the straits of Belle Île. The strain amplitude is also much smaller (although the seiche amplitude is about the same). From Wadhams (1973a) the corresponding wavelength for 6.3 s is 100 m, which when inserted into equation 5.02 with a strain amplitude of 5×10^{-7}, and ice thickness of 0.65 m, gives a wave amplitude of 0.4 mm.

The stress corresponding to the 6 s waves is 0.003 MN m^{-2}, but for the seiche amplitude of about 3×10^{-6} it is 0.02 MN m^{-2} (where again the figures for E and ν have been taken from Lavrov (1969).

An inspection of all the charts brought back from Forteau Bay indicates that the wave amplitude rapidly increases as the final break-up is approached. This could be simply due to an increase of incident wave height, although the increase seems too great for this. It is possible however that, because of cyclic damage and consequent crack growth, the modulus will fall. A lower modulus allows a bigger transmission coefficient; this enables bigger waves to penetrate the fast ice, which produces more damage, and reduces the modulus even further. It is possible that the final catastrophic break-up occurs when the modulus is sufficiently reduced to allow

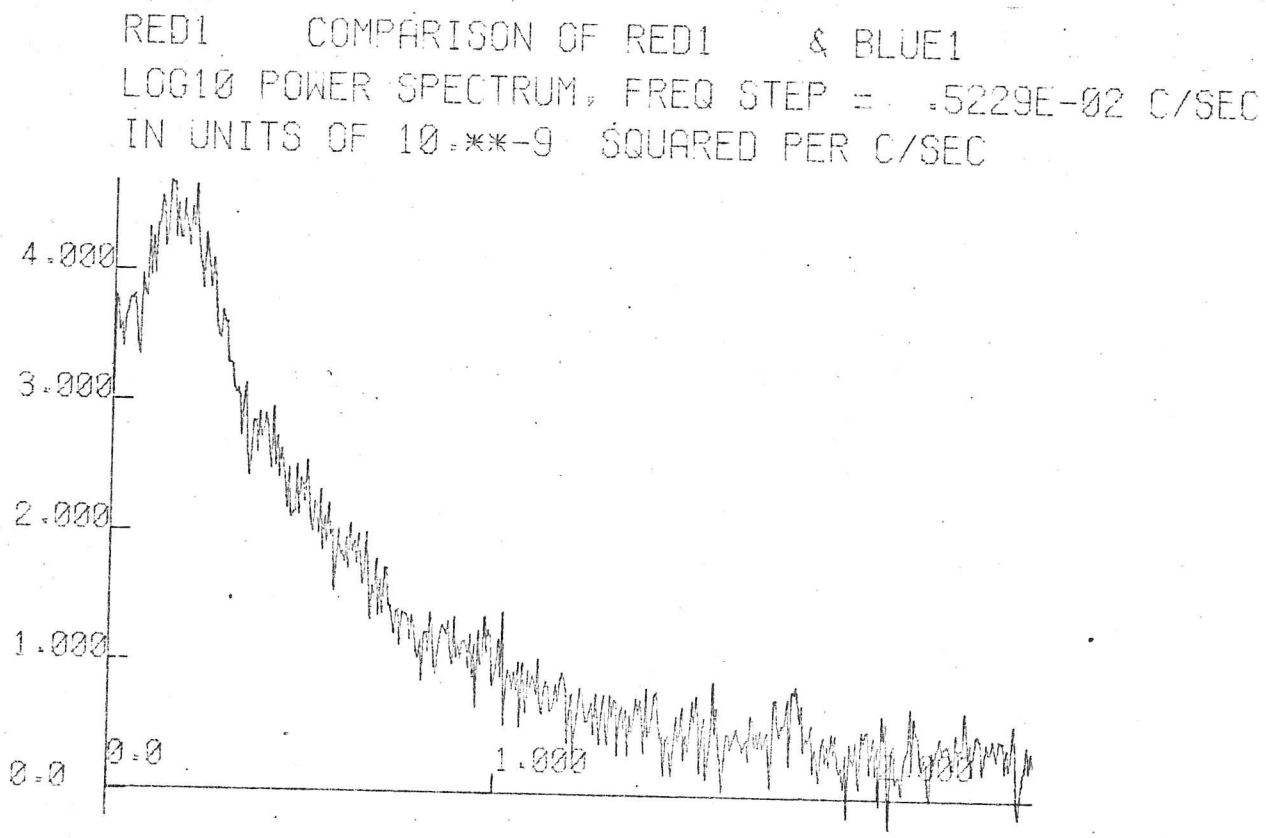

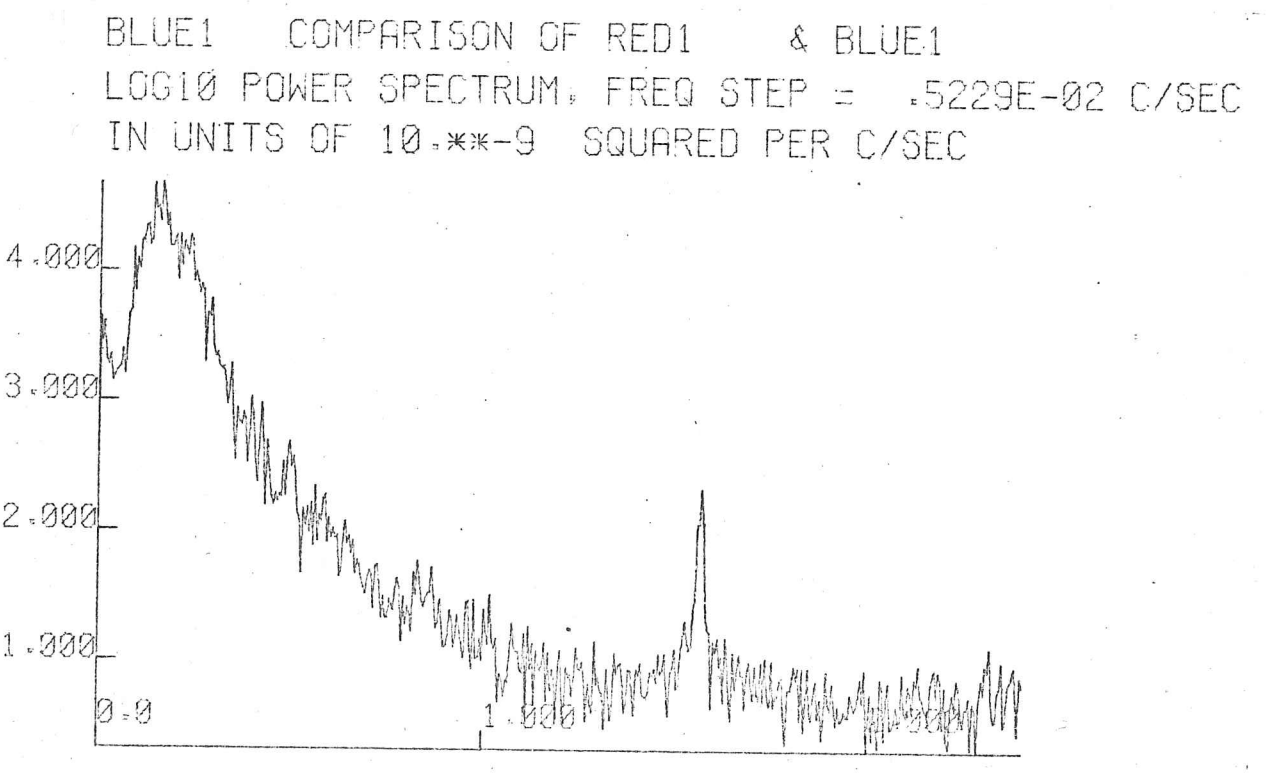

Figure 5.14; The frequency spectrums of Red one and Blue one (figure 5.13). The Nyquist frequency is 2.4 Hz. The peak at 1.5 Hz in Blue spectrum is a complete artifact due to the aliasing of the natural vibrations of the lever which were insufficiently damped.

waves of large amplitude to enter and fracture the ice. This should be investigated further.

The flexural strength of sea ice depends on both the salinity and the temperature (Weeks and Assur, 1967) but for the argument here we have taken the flexural strength to be about 0.3 MN m^{-2} from Butkovich's results (Butkovich, 1956). The stresses observed in the Bylot Sound data, and in the Forteau Bay data are about a factor of ten less than this value, but in both cases the weather was calm. It is therefore quite likely, when the incident wave amplitude is greater, that the surface stress can reach an appreciable fraction of the fracture stress, and will be large enough to nucleate and propagate cracks (this observation motivated the study of fracture in chapter 4). It is interesting to note that if six second waves propagate under the ice for four months (the typical age of the oldest ice in Forteau Bay), the ice is cycled 1.6 million times. In most materials fatigue damage leads to failure after about a million cycles at a stress which is an appreciable fraction of the yield strength (McClintock and Argon, 1966). Attempts were made in the laboratory to examine the fatigue properties of ice but were unsuccessful. However experiments are in progress in Newfoundland, using the 1 m strainmeter, to measure the modulus of in situ beams, and observe the effects of wave action on the beam (Squire, 1978).

Wadhams (1973a) suggests that creep in sea ice is responsible for the attenuation of wave height in the pack ice zone. He assumes that stresses in the ice can be deduced from an elastic response, and the stress changes due to the creep are only a pertubation on top of these stresses. The small stresses observed in Bylot Sound and Forteau Bay, together with the creep rates deduced from the deformation map in figure 2.10, suggest that this assumption is justified. Wadhams suggests in his paper that direct measurement of flexing and attenuation in the sea ice would soon determine how large the attenuation due to creep is. This strainmeters could easily do; they would need to be placed at least 0.5 km apart. Coherence analysis between the time series would give the attenuation as a function of frequency, and hence strain rate. The coherence of the time series in figure 5.13 has been investigated but the work is not yet complete; with closely spaced strainmeters, the

more interesting quantity is the variation with frequency of the phase change between the strain records. The best way to test a model of the response of sea ice to sea waves is to compare the predicted phase spectrum with that observed. The ideal experiment would be to measure the incident wave energy with a wave buoy, the water velocity profile beneath the ice with a current meter, the pressure just beneath the ice, and the surface strain-rate axes with an array of strainmeters. This will be partly accomplished in an experiment to be carried out later this year with a wave buoy and an array of strainmeters on the sea ice in McMurdo Sound.

Strainmeters can also be usefully used on sea ice to detect static deflections due to loads on the surface, or forces from ice which is pushing against a structure. With the advent of exploration in the Arctic, it has become very necessary to know what the load bearing capacity of a sea ice floe is or to have for design purposes the force ice exerts against a structure. There is a danger that the unusual properties of ice, its low creep resistance and low fracture toughness, will be forgotten in the rush to extract the oil. Strain measurements close to an installation can give prior warning of failure, but it should again be emphasised that strainmeters should be arranged in arrays of three. In this way principal strain rate axes can be deduced.

4. GLACIER EXPERIMENTS.

4.1 Roslin Glacier, east Greenland.

In July and August of 1974 strainmeters of various designs were taken to the Roslin glacier, east Greenland ($71^{\circ}51'N$, $24^{\circ}59'W$). The glacier is sub-polar, and it was hoped that surface temperatures would be well below $0^{\circ}C$ to decrease regelation problems. The glacier had been visited in four consecutive years, the depth profile had been measured by radio-echo sounding, and surface velocity measurements had been made across the glacier from stakes (Miller, 1974; MacKeith, 1973). Perhaps the only disadvantage was the 100 km walk to reach the glacier from the coast (the RAF kindly air-dropped all the supplies). Various methods were tested to find the best way to install the wire strainmeter on the glacier surface. Ice screws were again found to be the most convenient (see figure 5.04). A trench was dug in the

ice surface to a depth of 0.5 m, the strainmeter fixed to the ice at the bottom, and the trench covered over to keep the sun off. The arrangement is illustrated in figure 5.15.

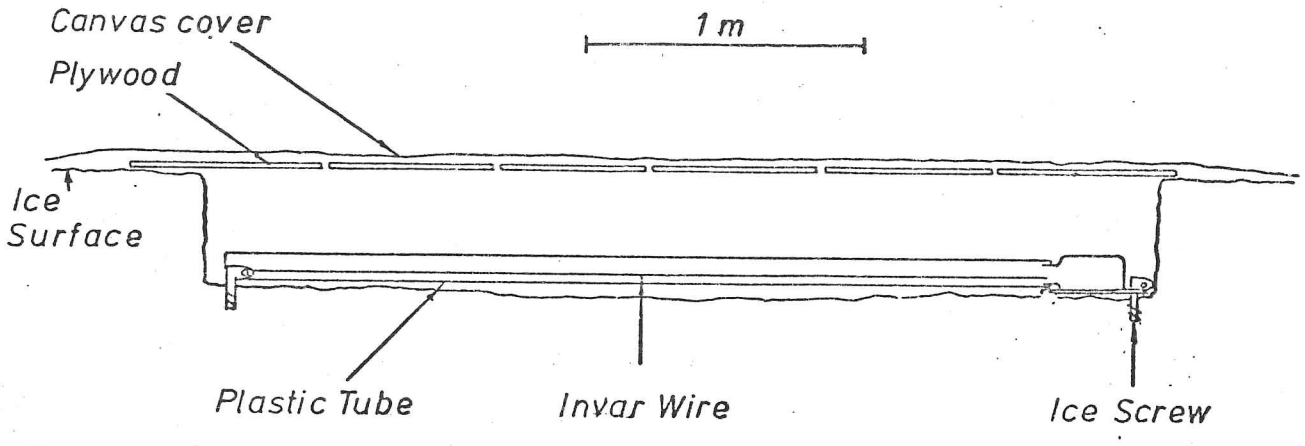

Figure 5.15; The Wire Strainmeter Installed on the Glacier.

Some difficulties were encountered because the ablation rate on the Roslin in 1974 was unusually high, and although the site was snow covered when the party first arrived, the snow rapidly disappeared, and the covered trench soon became a mound on the surface as the surrounding ice (which was not protected from the sun) melted. This would be a major problem in any installation of a strainmeter below the firn line; it would be necessary to dig a trench deeper than the total expected summer surface ablation.

The results obtained were not good, but were sufficiently encouraging to make a second experiment worthwhile. This was made possible by the offer of free logistic support by G. Holdsworth of the Department of the Enviroment, Ottawa to put three wire strainmeters on the Barnes Ice Cap, Baffin Island in the centre of two strain rosettes which had been measured over a number of years. The results are described in the next section.

4.2 Barnes Ice Cap, Baffin Island.

In April and May 1976 three wire straimeters were installed on the Barnes Ice Cap, Baffin Island (Evans, Goodman, and Holdsworth; 1977; Evans and Holdsworth carried out the fieldwork). Two sites were

occupied where 1 km strain diamonds had previously been set up in 1974 (see figure 5.16). The sites were chosen because the strain rates, ice depth, and temperatures were already known. The sites at that time of year were covered by 1-2 m of snow and so there were unlikely to be problems from ablation. Lastly the air temperature was well below zero, and the ice sub-polar, which meant there would be no regelation problems. Extra 50 m strain lines were set up and measured every three to four days (the arrangement of the poles at the two sites is shown in figure 5.17).

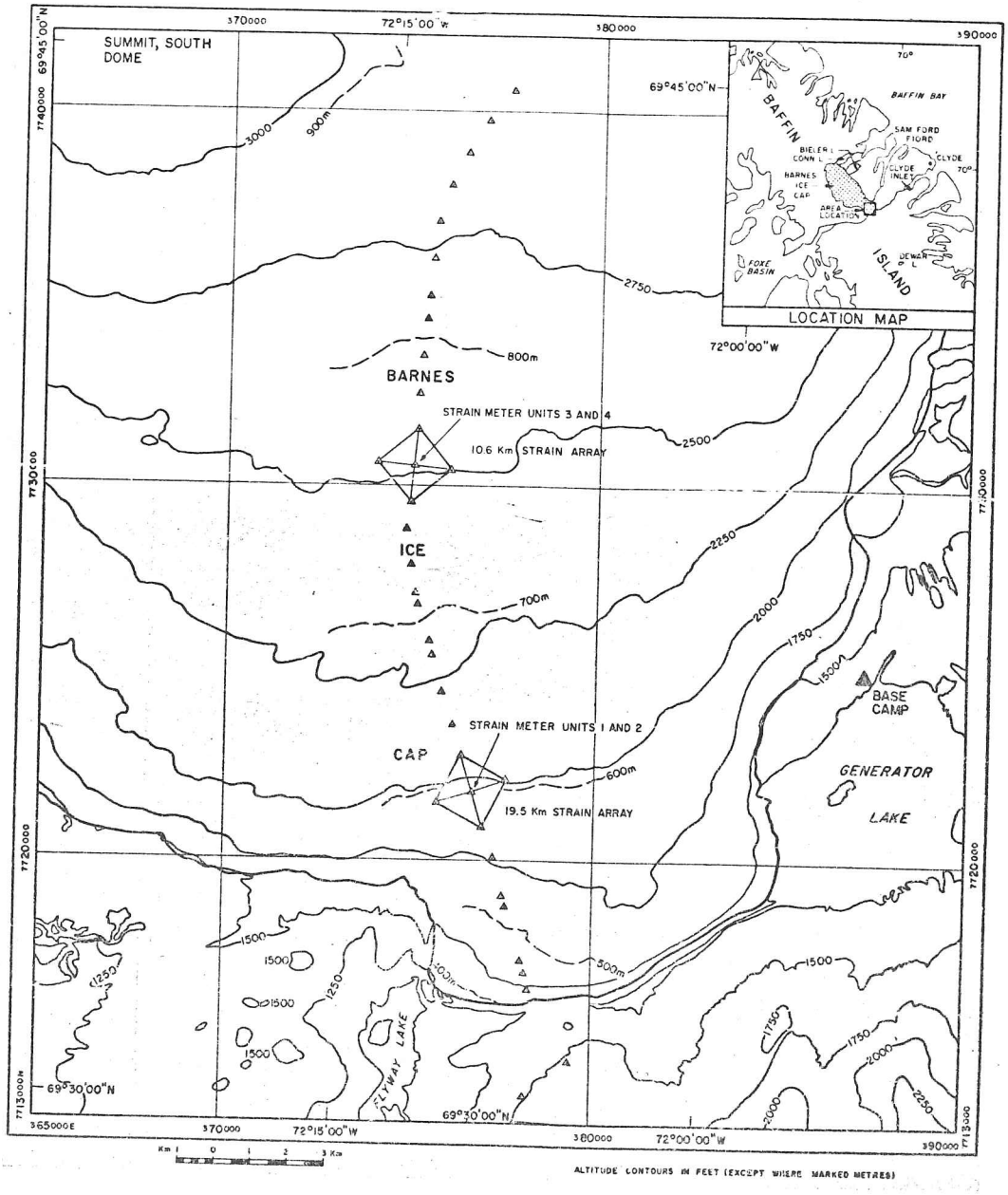

Figure 5.16; The location of the strainmeters on the Barnes Ice Cap, Baffin Island (Courtesy G. Holdsworth).

The distances between the stakes was measured with an INVAR tape over 50 m and with a Wild distomat for the 1 km lengths. The purpose of the experiment was to investigate strain rates averaged over

5 (the strainmeter), 50, and 1000 m, and to see whether wire strainmeters could usefully be used to rapidly determine surface strain rates.

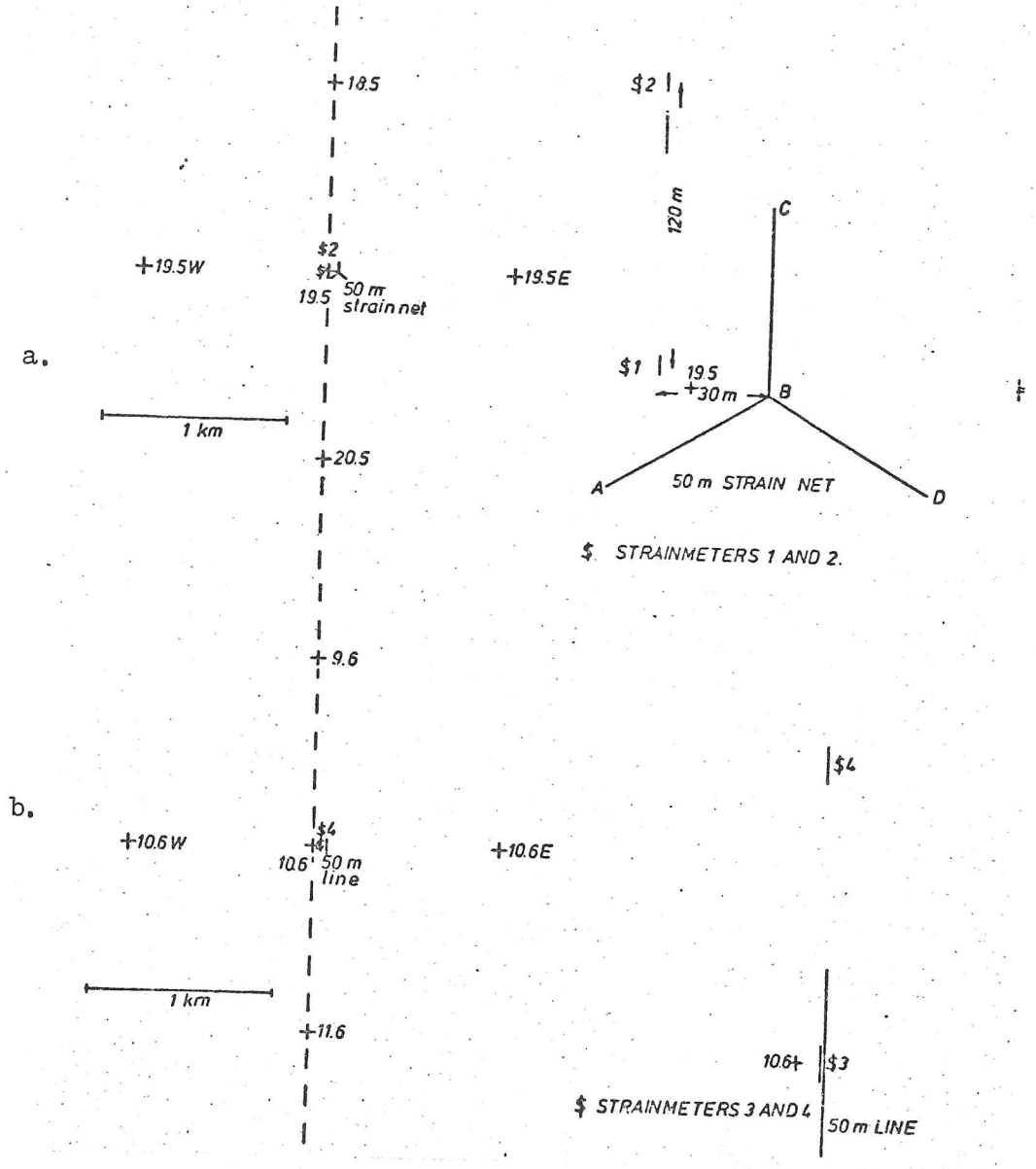

Figure 5.17; The arrangement of the stakes at the two sites (a) 19.5 km and (b) 10.6 km from the ice divide.

There is not space here to discuss the results in detail; the reader is refered to Evans et al (1977). An example of the record from one of the strainmeters is shown in figure 5.18, the time series for the three straimeters in figure 5.19, and the daily mean strain rates calculated from the digitised chart in figure 5.20.

At the 10.6 km strain site, the strain rate observed by the strainmeter agrees quite well with the strain rates deduced from the 50m line, and the 1 km array, if the strain rates along the flow

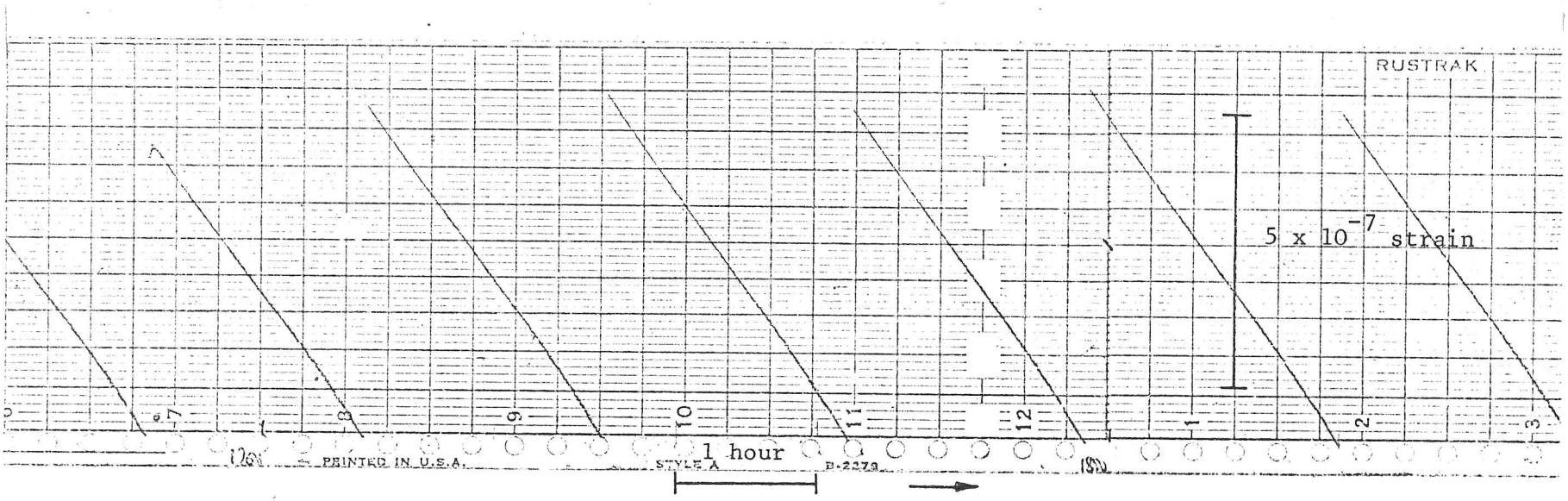

Figure 5.18; An example of the record obtained from the strainmeter on the Barnes Ice Cap. The offsets are put in automatically to keep the signal on the chart.

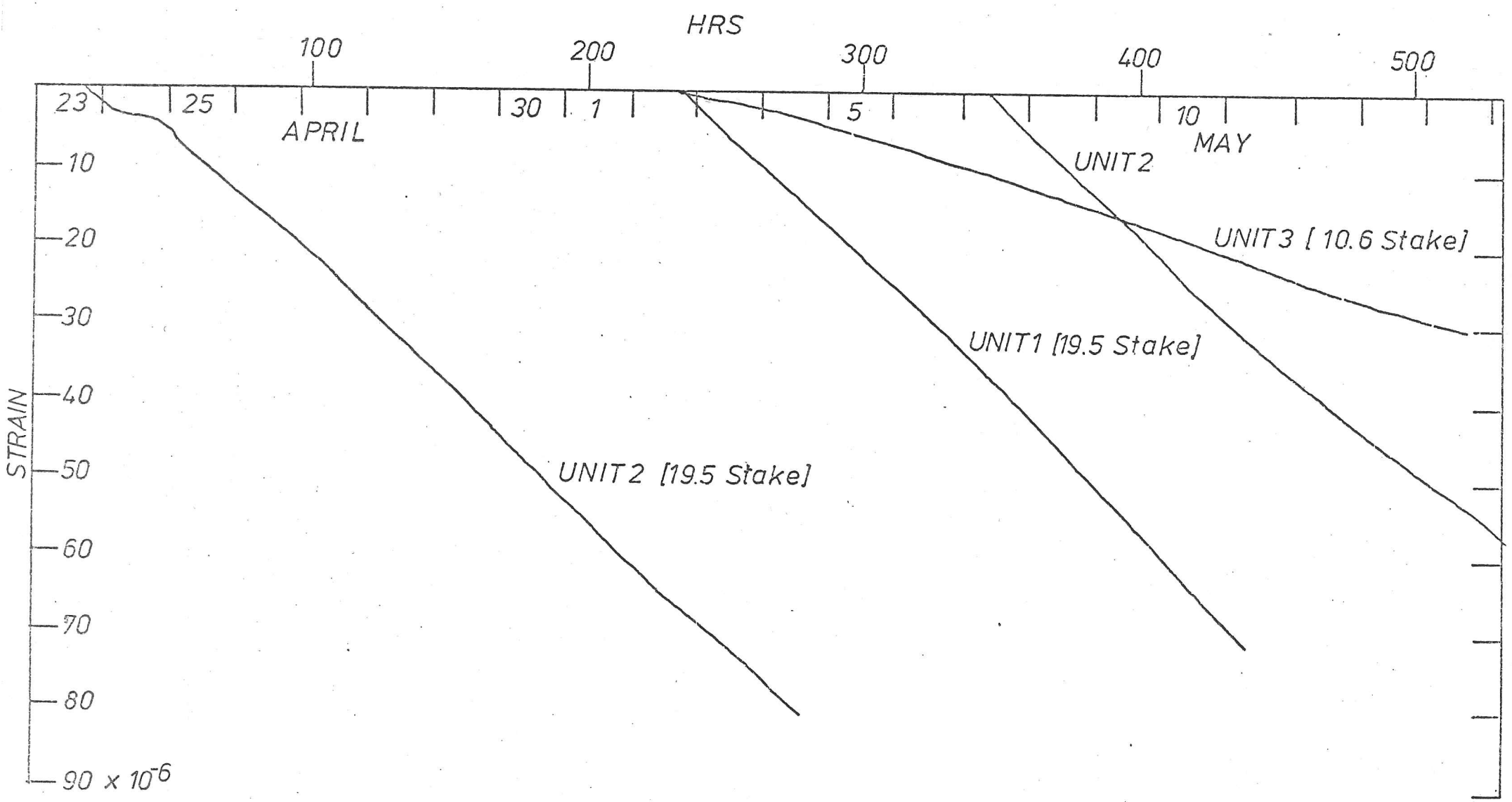

Figure 5.19; The Time Series Obtained from the Three Strainmeters on the Barnes Ice Cap.

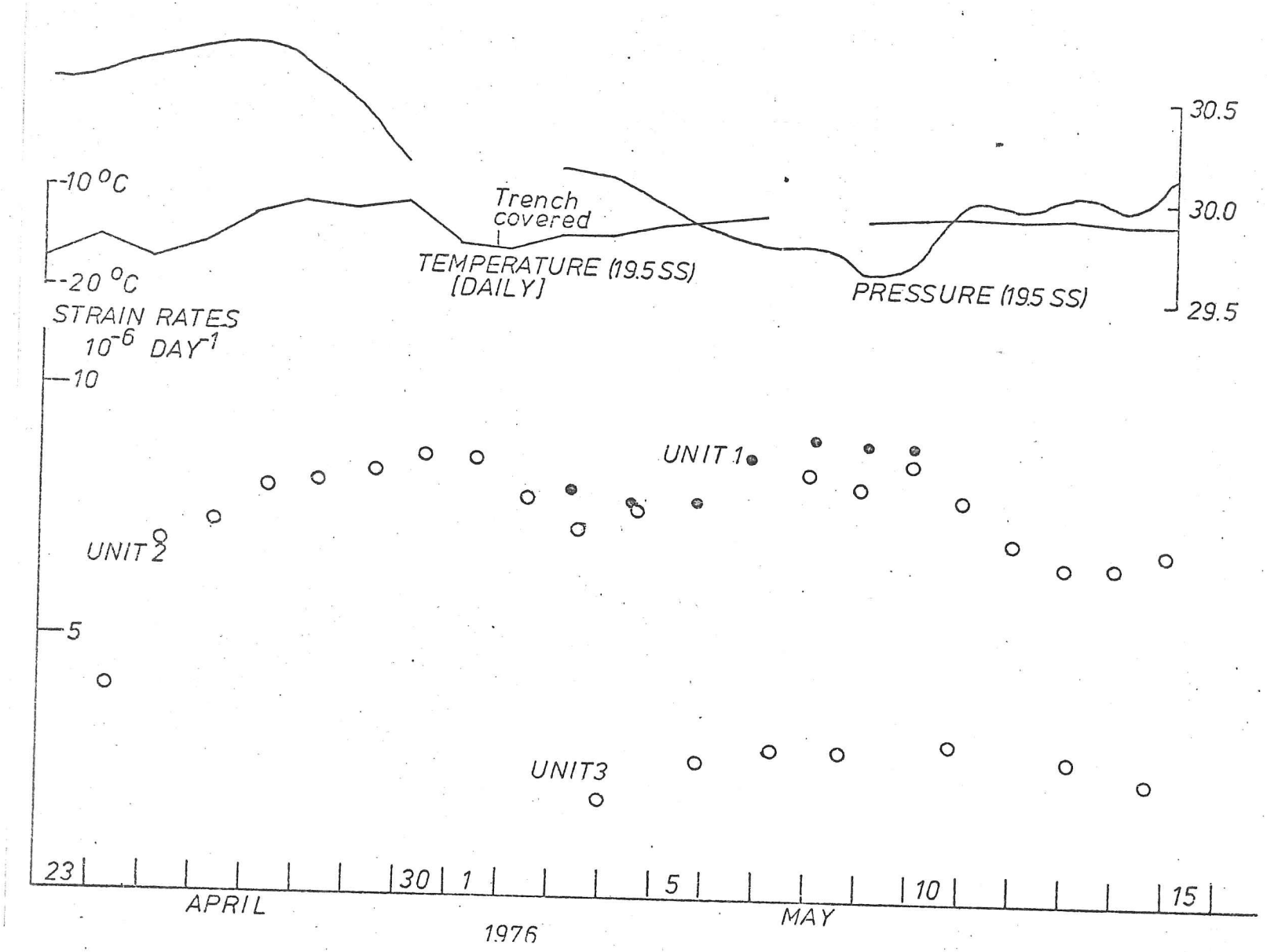

Figure 5.20; Daily Mean Strain Rates Calculated from the time series for the three strainmeters.

Table 5.01

Barnes Ice Cap Strain Results.

	Strain 10^{-6} day^{-1}	Period over which data is averaged.
10.6 km Site;		
Strainmeter (Unit 3)	2.6 ± 0.4	2 May to 14 May 76
9.6-10.6 line	5.74 ± 0.06	May 74,75,76
10.6-11.6 line	2.63 ± 0.06	
9.6-10.6 line	3.5 ± 0.4	April to May 76
10.6-11.6 line	1.4 ± 0.1	
50 m line	1.9 ± 0.2	April to May 76 (last 4 readings)
	3.0 ± 0.3	
19.5 km Site;		
Strainmeter (Unit 1)	8.5 ± 0.6	2 May to 11 May 76
Strainmeter (Unit 2)	7.9 ± 0.6	23April to 4 May 76
	7.6 ± 0.8	7 May to 15 May 76
18.5-19.5 line	3.14 ± 0.03	May 74,75
19.5-20.5 line	1.37 ± 0.01	
50 m line (BC, parallel to the strainmeter)	2.78 ± 0.3	April to May 76

All strain rates are calculated for distances parallel to the slope.

line are assumed to be linear. The results for all the techniques used are given in table 5.01.

At the 19.5 km site the strain rates measured by the strainmeters agree with each other but disagree with the strain rates calculated from the stake arrays. When the principal strain rate axes are calculated for the 1 km diamond, and the 50 m three-legged array, the axes are found to be within 1^{o} of each other (although they differ in magnitude by 20 per cent). This implies that the 50 m data are satisfactory even though large fluctuations, which are not seen on the strainmeter records, appear in the calculated strain rates. However there is no reason to suspect the strains calculated from the 1 km diamond. It is therefore thought that the discrepancy is real and results from the more complicated topography at the 19.5 km site.

In the graph of daily mean strain rates shown in figure 5.20 the error is no greater than the circles drawn. The means appear to have a periodic variation, although the data length is too short to be certain. The variation (which does not correspond to a temperature or pressure change in the trench) might be due to a thermal wave in the ice (Doake, personal communication) or perhaps due to the passing of a kinematic wave (Nye, 1958).

The results show that useful data can be obtained from a wire strainmeter installed on a glacier surface above the firn line. The strainmeter can easily detect strain changes of the order of 10^{-6} per day. Previously laser systems have been used to detect strain rates of this order (Holdsworth, 1975); the strainmeter is less expensive, and can be installed in a shorter time than a laser system (2-3 hours).

Strainmeters should always be used in arrays of three, or if possible four so there is some redundancy. When this is done it is possible to determine the directions and magnitudes of the principal strain axes. This would have been done on the Barnes Ice Cap if more instruments had been available.

4.3 Glacier d'Argentière, Mont Blanc, France.

The last application of wire strainmeters in glaciology is quite different from those described so far. Three wire strainmeters have been installed in two tunnels under the glacier d'Argentière in the French Alps. The rock tunnels, which have been dug as part of a scheme to extract water from the glacier for hydroelectric power, pass within 10 m of the bed of the glacier. The strainmeters, which were left in the tunnels between August 1975 and July 1976, have detected what is thought to be elastic strain changes in the rock due to changes in the way the glacier is sliding over its bed. Only a brief outline of the experiment and the results will be given here.

The glacier has been studied over many years by Vivian and his co-workers (Vivian, 1975; Vivian and Bocquet, 1973; Bocquet and Ricq, 1977). Vivian has made a special study of a natural ice cavity accessible from the tunnels, where he has installed

a 'cavitometer' to monitor the sliding velocity of the glacier (the cavitometer is a wheel held against the glacier by a counterbalanced lever). He finds very large variations in the sliding velocity (± 10 %). There has been some dispute (Theakstone, 1967; Galloway, 1967; Reynaud, 1975; Lliboutry, 1975; Goldthwait, 1973; the last reference summarises observations of jerks to 1967) as to whether a glacier slides smoothly or in jerks. Many difficulties have resulted from confusion of jerks in the glacier motion with stick-slip effects in the measuring apparatus (often a wire connected to the glacier, and held in tension by a spring loaded drum). The purpose of this experiment was to look for indirect evidence of jerky motion. The glacier d'Argentière is particularly suitable because it is sliding at about a metre a day, and therefore is likely to show such effects. Vivian's cavitometer samples the position too infrequently to detect short term 'jerks'. A plan of the tunnel network appears in figure 5.21

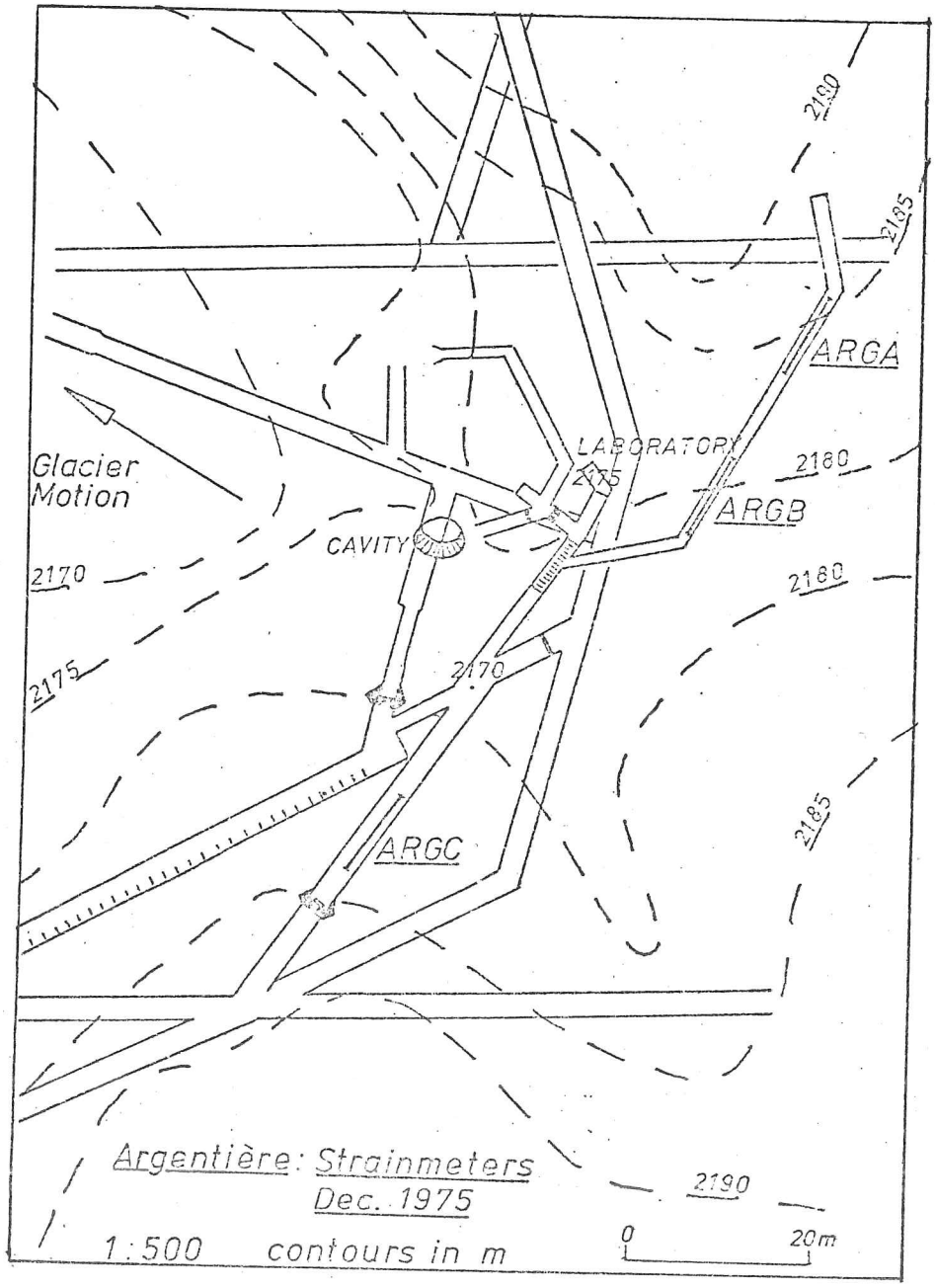

Figure 5.21.

and the relation of the tunnels to the rest of the glacier is shown in figure 5.22.

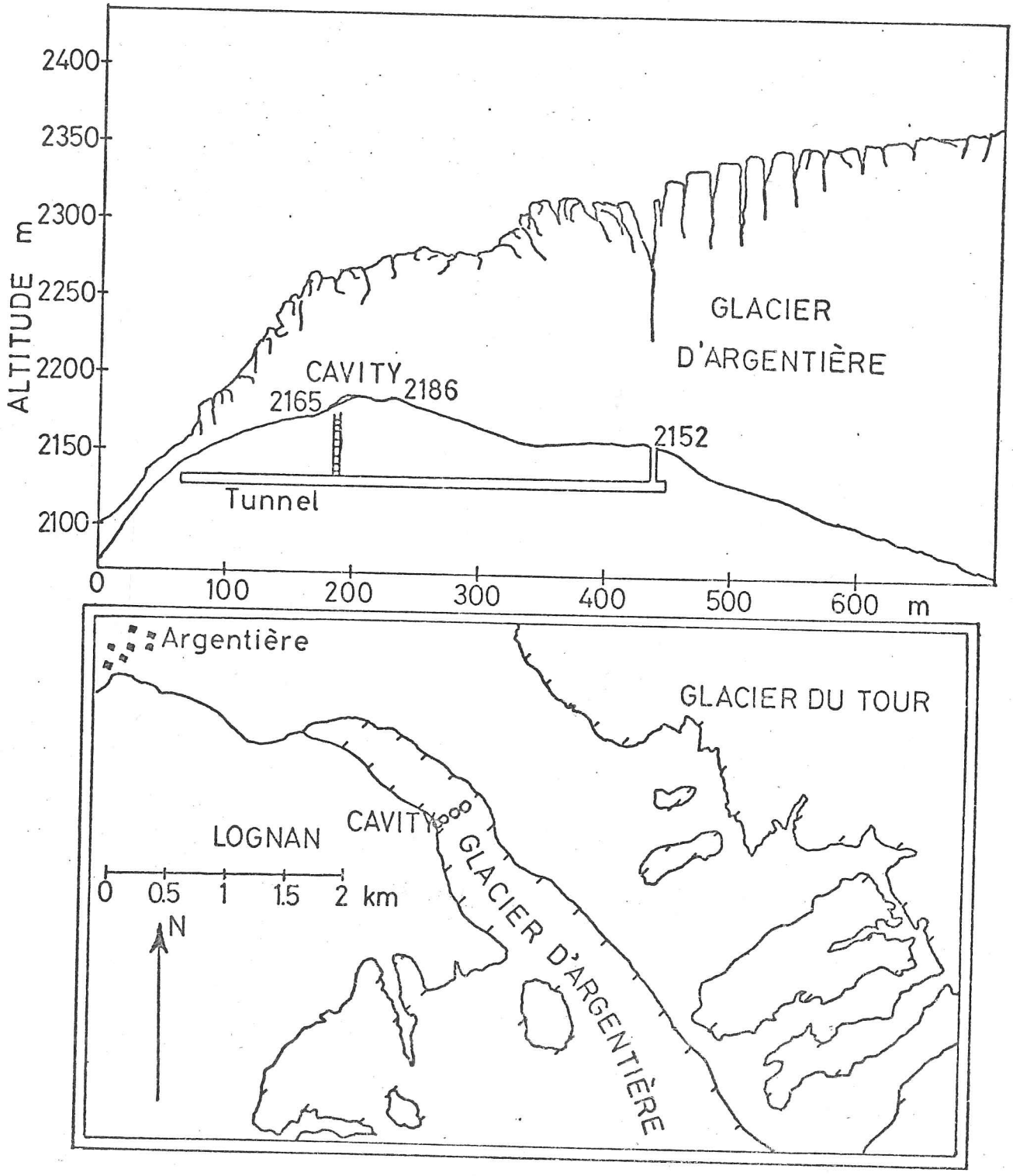

Figure 5.22; The glacier d'Argentière. The tunnels where the strainmeters were installed, are very close to the cavity (see figure 5.21) The diagram is taken from Vivian (1975).

Spans of data lasting about three weeks were obtained in August 75, January 76, and April 76. They all showed long period strain changes,

probably due to the Earth tides, but also frequent (about every two hours) but not regular strain excursions. They lasted about twenty minutes with a very rapid rise time (about 30 s), and then a slow decay back to the original strain value. Some examples are shown in figure 5.24. The events observed in August were about three time larger than those observed in April. Vivian (1975) gives a table of the glacier sliding speed in the years 1971 to 1973. In April and May, the sliding speed at 1.74 cm hr^{-1} was the slowest of the year, while August had the slowest sliding speed of the summer months of 2.36 cm hr^{-1} - 36 % faster.

In April 1976 some time was spent in the tunnels in an effort to obtain good records to make comparisons between the three strainmeters, and a seismometer (Teledyne Geotech with a 1 Hz natural frequency). Many more events were observed on the seismometer than on the strainmeters. Not all the seismic events were from the glacier, but some had signatures which were similar to those previously observed by Neave and Savage (1970), VanWormer and Berg (1973) or Weaver and Malone (1976) from geophones or seismometers close to glaciers. The seismic data obtained requires more analysis, but events which were observed on the strainmeters had corresponding events on the seismic records (the signal from the seismometer was recorded on magnetic tape over two and four periods). Events could be correlated between strainmeters; a comparison for one of the records is shown in figure 5.23.

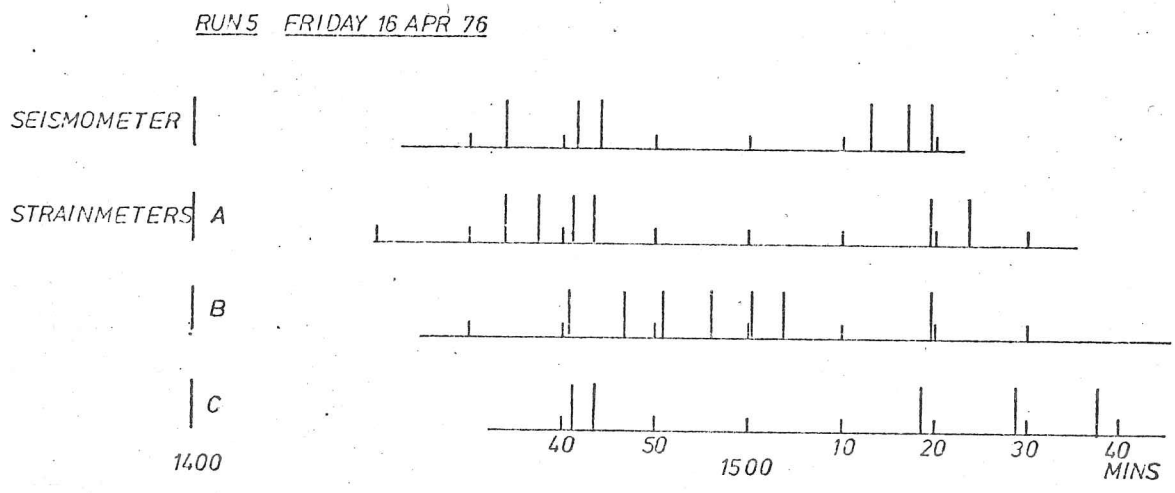

Figure 5.23; Comparison of times events recorded in Argentière.

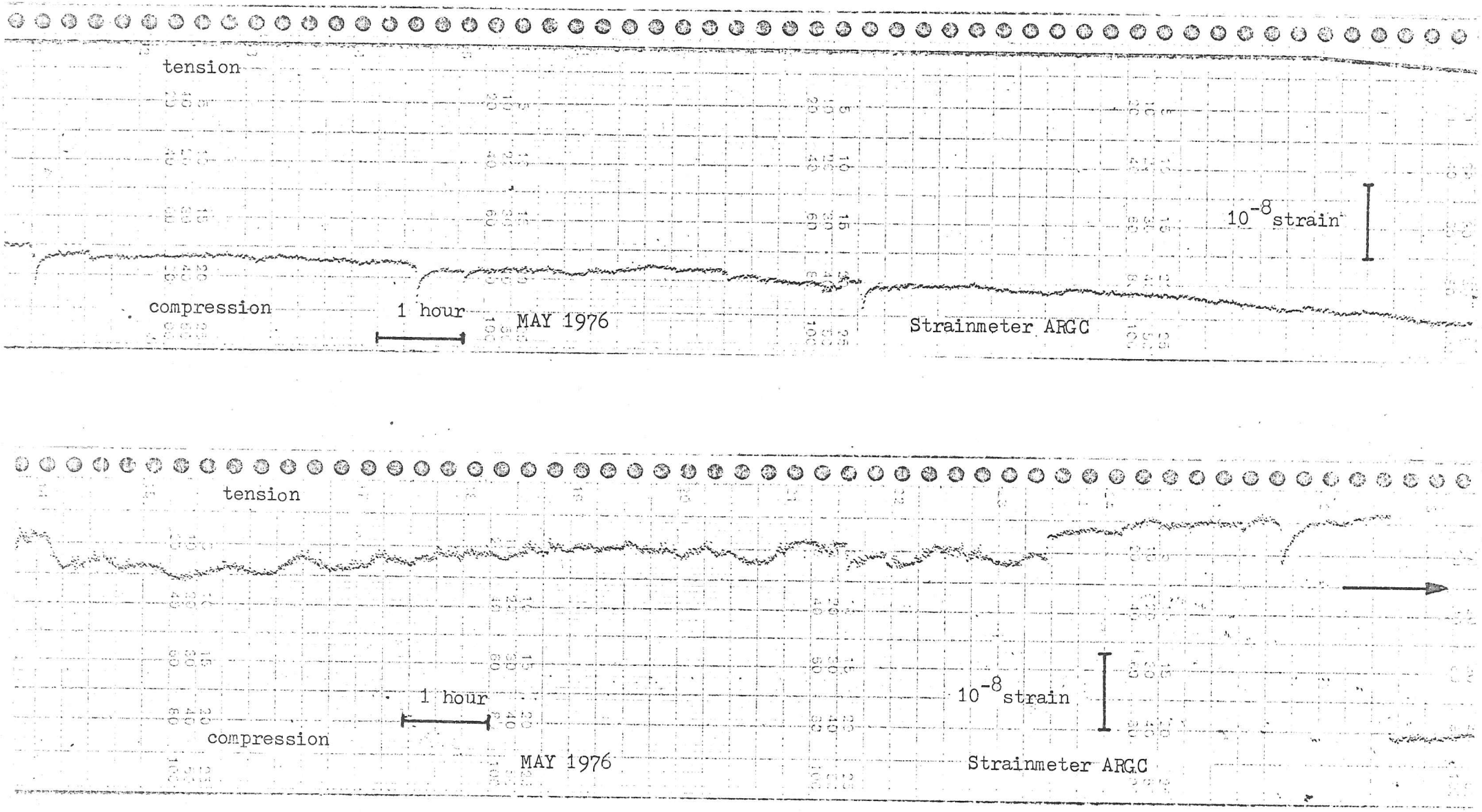

Figure 5.24; Some examples of the strain events observed in Argentière.

It is clear from figure 5.23 that events seen on one strainmeter can be seen on the other two. The strainmeters had a common mains supply but the stabilising circuit is unlikely to show such a slow response to a transient, and events had previously been observed with a strainmeter powered by an accumulator. The events were not observed when the strainmeters were run in Cambridge.

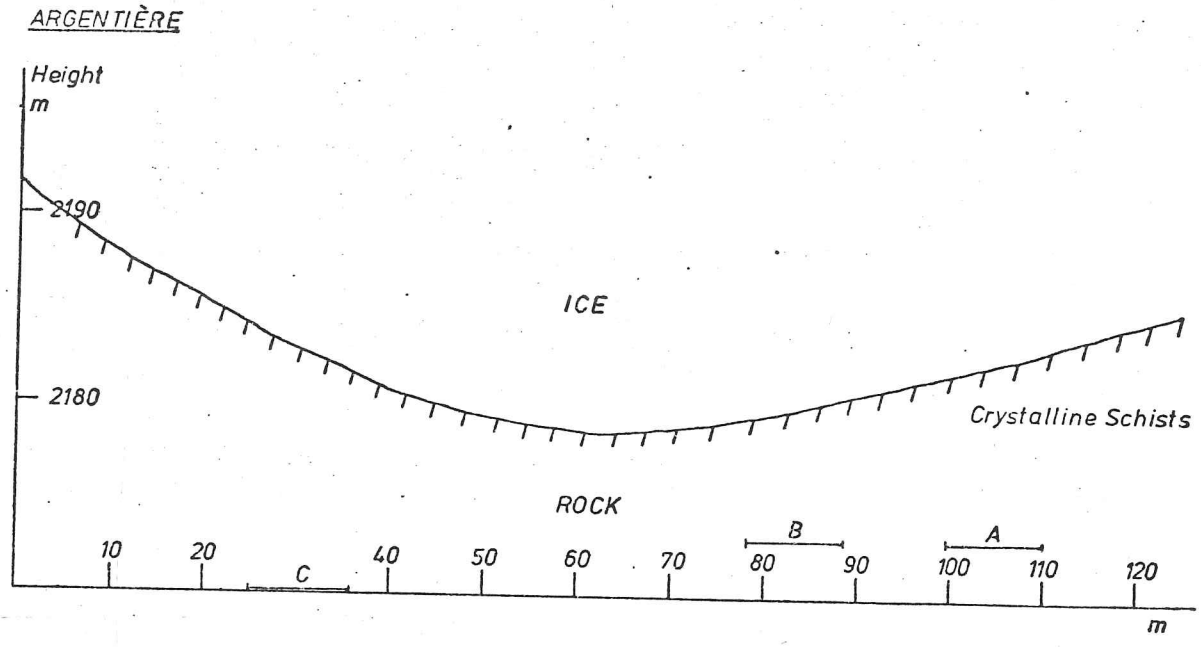

Figure 5.25; A cross-section in the plane of the strainmeters.

The Invar wire was protected by a steel tube (decoupled by rubber bellows from the tensioning and end units), and the tensioning and end units protected from water dripping from the tunnel roof by plastic sheeting. Therefore it is likely that the events were real, and they almost certainly emanated from the glacier.

A possible, but not the only, explanation for the events is the change of tractions on the glacier bed when cracks propagate across frozen patches. The slow decay, and return to the original strain would then be the glacier refreezing to the bed. That frozen patches might exist was first suggested by Robin (1976). He supposes that as the glacier moves over a bump in its bed, water is pushed out of the ice on the glacier side. When the ice reaches the down stream side of the bump, it is at a lower hydrostatic pressure, and has a different equilibrium temperature. To reach the new equilbrium temperature, the down stream ice extracts heat from the surrounding ice (the heat would normally have come from the water

It is clear from figure 5.23 that events seen on one strainmeter can be seen on the other two. The strainmeters had a common mains supply but the stabilising circuit is unlikely to show such a slow response to a transient, and events had previously been observed with a strainmeter powered by an accumulator. The events were not observed when the strainmeters were run in Cambridge.

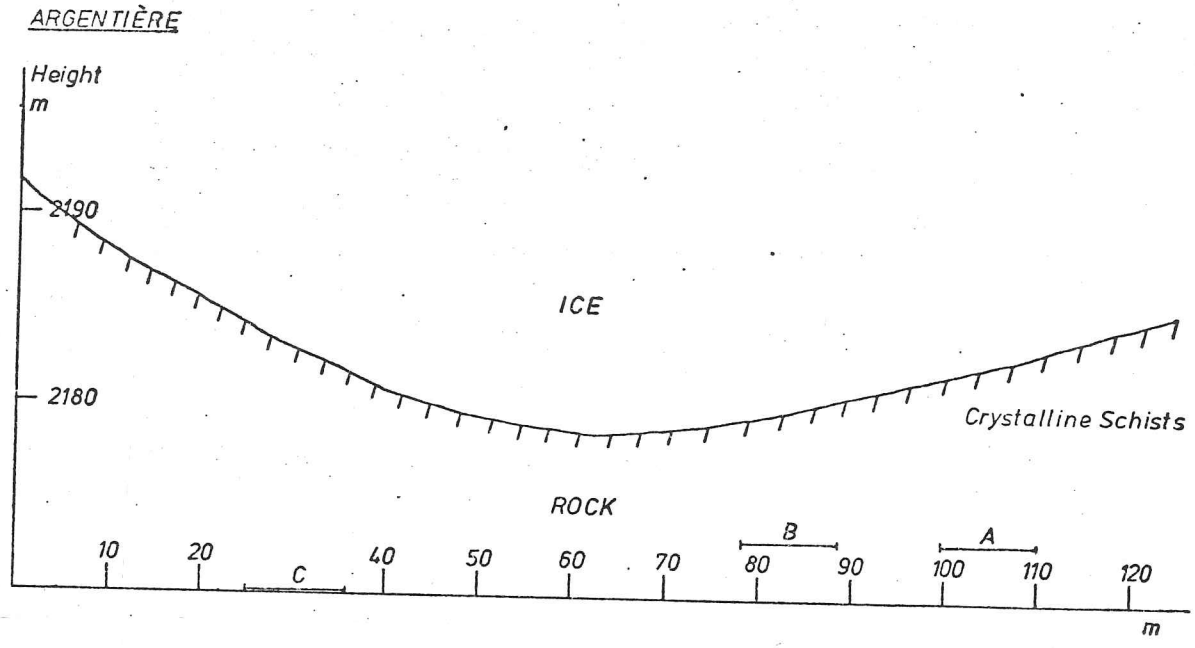

Figure 5.25; A cross-section in the plane of the strainmeters.

The Invar wire was protected by a steel tube (decoupled by rubber bellows from the tensioning and end units), and the tensioning and end units protected from water dripping from the tunnel roof by plastic sheeting. Therefore it is likely that the events were real, and they almost certainly emanated from the glacier.

A possible, but not the only, explanation for the events is the change of tractions on the glacier bed when cracks propagate across frozen patches. The slow decay, and return to the original strain would then be the glacier refreezing to the bed. That frozen patches might exist was first suggested by Robin (1976). He supposes that as the glacier moves over a bump in its bed, water is pushed out of the ice on the glacier side. When the ice reaches the down stream side of the bump, it is at a lower hydrostatic pressure, and has a different equilibrium temperature. To reach the new equilbrium temperature, the down stream ice extracts heat from the surrounding ice (the heat would normally have come from the water

which has been pushed out). Sufficient heat may be removed to freeze the water film between the glacier and the downstream side of the bump.

A very crude calculation can be made to estimate the size of and tangential stress on a frozen patch which gives the strain changes observed in the events. Figure 5.25 on the previous page gives the shape of the glacier bed in the plane of the strainmeters (it is unfortunate that the only tunnels available to instal the strainmeters were almost perpendicular to the direction of glacier flow). Love (1944) gives the results for the displacements in a semi-infinite Poisson solid (λ equals μ) when a point traction is applied to a surface. The displacement, v, perpendicular to the traction (the geometry is given in figure 5.26) is given by;

$$v = \frac{\sigma\delta a}{4\pi\mu}\left[\frac{xy}{r^3} - \frac{1}{2}\frac{xy}{r(r+z)^2}\right] \qquad 5.07$$

where $\sigma\delta a$ is the magnitude of the point tangential traction, the shear modulus, and x, y, and r are defined in figure 5.26.

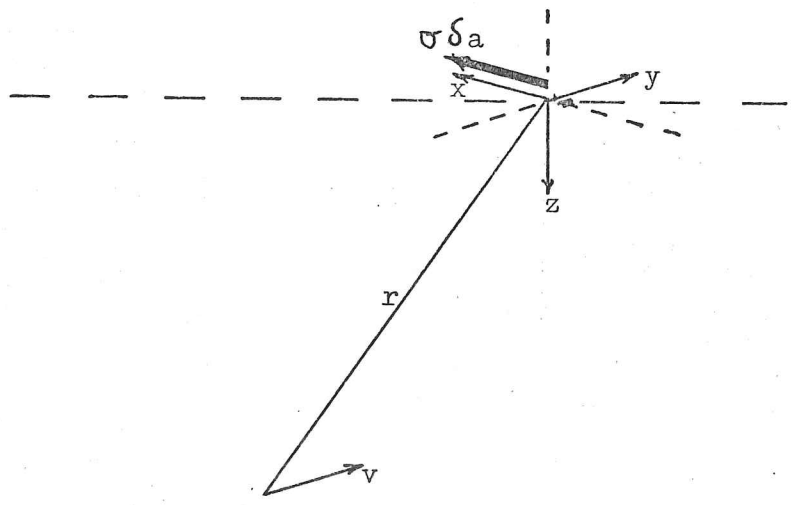

Figure 5.26; The geometry of equation 5.07.

The strain can be calculated from the rate of change of the displacement.

$$\epsilon_{yy} = \frac{\partial v}{\partial y} \qquad 5.08$$

If we consider the case of a frozen patch which is in the plane of the strainmeters, and mid-way between A and B, with , say, z equals

10 m, y equals 40 m, and x equals 0 m. The traction is assumed to be down glacier and perpendicular to the plane of the strainmeters. It is further assumed that there is only one frozen patch close to the strainmeters, (the worst assumption) that the rock surface can be regarded as a free surface (this is plausible because the shear modulus of the ice is a factor of 4 less than the rock) and that the tunnel does not change the strain significantly, then

$$\epsilon_{yy} = \frac{\sigma \delta a}{4\pi\mu} \quad 3 \times 10^{-4} \qquad 5.09$$

The size of an event is about 5×10^{-9} strain, and a reasonable value for the shear modulus of the rock is 12 GN m^{-2} (Jaeger and Cook, 1969). This gives

$$\sigma \delta a = 2.5 \times 10^{6} \text{ N} \qquad 5.10$$

If σ is between 0.1 and 1 MN m^{-2} (Paterson, 1969), then the area over which the stress would act is 25 to 2.5 m^2, or a patch size of 5 m to 1.6 m (if it is square). This is approximately the size of the bumps which are expected to control the sliding speed of the glacier (Nye, 1970).

It is also interesting to note that in VanWormer and Berg's (1973) observations of seismicity, they calculated from the energy of an observed event that sufficient energy would be released if the patch size, δa, multiplied by the forward motion of the glacier, d, were about $\delta a d \simeq 3000$ m^3. They needed to assume that δa was 1 km^2 to get a reasonable forward displacement, d, of 3 mm, (a lower limit). This was calculated for the energy from a large event.

If the mean speed of the glacier in May 1976, was the same as its value given for May 1971 by Vivian (1975) of 1.74 cm hr^{-1}, then the Argentière glacier moves forward about 5 mm during each event.

Thus much needs to be resolved in the data collected from Argentière. It is thought that the events are real elastic changes in the rock, but it is by no means certain that they result from frozen patches on the glacier bed. The tunnels are under a complicated ice-fall, and movement, or collapse, of seracs may cause events (but it would be difficult then to explain why the strain record returns to its

orginal value). Other features have been observed on the charts including simple offsets and oscillations (examples of which can be seen on the charts in figure 5.24). There is no doubt, however, that the installation of a wire strainmeter in a rock tunnel close to a glacier bed does detect glacial processes. With more instrumentation (a strainmeter to measure the vertical strain in the tunnels and array of seismometers to locate the position of events) it would be possible to make a better interpretation of the events seen. Because of the large number of schemes to extract water from beneath a glacier, there are a large number of sites where a similar experiment to the one described could be carried out.

5. SUMMARY AND CONCLUSIONS.

Results from five field experiments have been described. Wire strainmeters were successfully used to observe the bending of sea ice when waves pass underneath, to measure surface strain rates on a glacier and an ice cap, and to observe elastic strain changes in the rock very close to a sliding glacier.

The strainmeter is sufficiently sensitive to easily resolve normal strain rates found in glaciers and sea ice (10^{-7} per day), and, with the addition of an automatic rezeroing system, the instrument can be left unattended for long periods. The device is inexpensive (~£400-00 with electronics), and simple to instal. Alternative instruments such as a laser (Holdsworth, 1975) or resistance wire gauges (Meier et al, 1957; Warner and Cloud, 1974) are not as convenient to use or instal, and in the case of the laser costly.

Strainmeters could be used to detect deflections due to static loads, or forces created as sea ice is pushed against a structure. A problem which is especially pertinent because of recent exploration for oil in the Arctic.

Later this year strainmeters will be installed on Erebus Glacier Tongue, McMurdo Sound, Antarctica to investigate the way the glacier, which is floating, oscillates. It is hoped from this to deduce the forces acting on the glacier, and if it eventually calves, to estimate the fracture toughness in a large ice mass.

The design for a new 1 m strainmeter was also given.

6. APPENDIX.

6.1 Linear Strain.

Many textbooks describe the concepts of the strain tensor (Landau and Liftshiftz, 1959; Jaeger and Cook, 1969). Only the results and the assumptions made to derive them will be given here.

When a body is deformed, every point within it is generally displaced. The displacement can be represented by a vector field, if u_i is the displacement components of a point x_i which has moved to x_i' $(i=1,2,3)$, then

$$u_i = x_i' - x_i \qquad 5.11$$

then the strain tensor ϵ_{ij} is defined by

$$\epsilon_{ij} = \frac{1}{2}\left|\frac{\partial u_i}{\partial x_j} + \frac{\partial v_j}{\partial x_i}\right| \qquad 5.12$$

when the displacements are small.

The strain tensor relates the rate of change of $\underline{u}$ to the rate of change of $\underline{x}$, so that

$$du_i = \epsilon_{ij}\, dx_j \qquad 5.13$$

If a strainmeter is placed in a direction with direction cosines l_i to an arbitary axes set, then the strain, e, measured by the strainmeter is given by

$$e = \frac{|\underline{dx} + \underline{du}| - |\underline{dx}|}{|\underline{dx}|} = \frac{dx_i + \epsilon_{ij} dx_j}{dx_i} - 1 \qquad 5.14$$

$$e = |l_i + \epsilon_{ij} l_j| - 1$$

$$e = \epsilon_{ij} l_i l_j + O(\epsilon_{ij}\epsilon_{ik}) \qquad 5.15$$

So that provided $O(\epsilon_{ij}\epsilon_{ik})$ can be neglected, the linear strain can be related to the strain tensor by;

$$e = \epsilon_{ij}\, l_i\, l_j \qquad 5.16$$

Which, when written out in full, is

$$e = (l_1\ l_2\ l_3)\begin{bmatrix}\epsilon_{11}\ \epsilon_{12}\ \epsilon_{13}\\ \epsilon_{21}\ \epsilon_{22}\ \epsilon_{23}\\ \epsilon_{31}\ \epsilon_{32}\ \epsilon_{33}\end{bmatrix}\begin{bmatrix}l_1\\ l_2\\ l_3\end{bmatrix} \qquad 5.17$$

In the special case of a free surface, it can be shown that the boundary conditions on the strain tensor are (Beavan, 1976);

$$\epsilon_{13} = \epsilon_{23} = 0 \qquad 5.18$$

$$\epsilon_{33} = -\frac{\lambda}{\lambda+2\mu}(\epsilon_{11}+\epsilon_{22}) \qquad 5.19$$

where λ and μ are Lamé's constants. There are then only three independent strain components ϵ_{11}, ϵ_{22}, and ϵ_{12} (if the 3 axis is normal to the free surface). Three strain determinations in the 1-2 plane will determine these, if none of the strain measurements are collinear.

In this special case the linear strain, e , is related to ϵ_{11}, ϵ_{22}, and ϵ_{12} by;

$$e = \epsilon_{11}\cos^2\vartheta + 2\epsilon_{12}\sin\vartheta\cos\vartheta + \epsilon_{22}\sin^2\vartheta \qquad 5.20$$

where ϑ is the angle between the angle made by the strainmeter and the 1 axis.

CHAPTER SIX

CONCLUSIONS

Chapter 6.

CONCLUSIONS.

1. SUMMARY AND CONCLUSIONS.

It was intended that each chapter should be self-contained. This brief chapter summarises, and reiterates some of the conclusions already made.

Chapters two and three discussed possible creep mechanisms in polycrystalline ice. Deformation maps were constructed to illustrate the creep data. These showed a number of interesting features. First, when the map was compared with the creep data plotted on the same axes, better agreement with the low temperature hardness data were obtained by the introduction of the Peierls barrier, or lattice resistance controlled, glide mechanism. Secondly, diffusional mechanisms were shown to be feasible. But the strain rates predicted were so low that a laboratory creep experiment, in normal circumstances, will not be able to detect linear flow (which a diffusional mechanism predicts). If it were possible, however, to stop grain growth, and manufacture ice with a very small grain size (less than 0.1 mm), it might then be feasible to look for diffusional creep at low stresses. Some evidence was given from fabric development that diffusional flow occurs in the upper layers of the Antarctic ice sheet at Byrd station. The effects of diffusional creep are masked by sintering and transient phenomena.

Full support was given for Glen's model of proton rearrangement controlled glide. The statistical model developed in chapter three suggested that a simple quantification of Glen's ideas does not predict the observed dislocation velocities. It is necessary to suppose, as Whitworth et al (1976) also observe, that the mean time between proton rearrangements is shorter close to the dislocation than the average in the lattice. This makes further quantification difficult, because in general models of dislocation cores are not good.

In chapter four, the concept of a critical stress intensity factor, K_{1c}, at a crack tip was discussed. It was shown that K_{1c} can only be defined if a true singularity exists at the crack tip. Wide scale creep would invalidate this assumption. By carrying out tests at high strain rates and low temperatures, it was possible to suppress

Chapter 6.

CONCLUSIONS.

1. SUMMARY AND CONCLUSIONS.

It was intended that each chapter should be self-contained. This brief chapter summarises, and reiterates some of the conclusions already made.

Chapters two and three discussed possible creep mechanisms in polycrystalline ice. Deformation maps were constructed to illustrate the creep data. These showed a number of interesting features. First, when the map was compared with the creep data plotted on the same axes, better agreement with the low temperature hardness data were obtained by the introduction of the Peierls barrier, or lattice resistance controlled, glide mechanism. Secondly, diffusional mechanisms were shown to be feasible. But the strain rates predicted were so low that a laboratory creep experiment, in normal circumstances, will not be able to detect linear flow (which a diffusional mechanism predicts). If it were possible, however, to stop grain growth, and manufacture ice with a very small grain size (less than 0.1 mm), it might then be feasible to look for diffusional creep at low stresses. Some evidence was given from fabric development that diffusional flow occurs in the upper layers of the Antarctic ice sheet at Byrd station. The effects of diffusional creep are masked by sintering and transient phenomena.

Full support was given for Glen's model of proton rearrangement controlled glide. The statistical model developed in chapter three suggested that a simple quantification of Glen's ideas does not predict the observed dislocation velocities. It is necessary to suppose, as Whitworth et al (1976) also observe, that the mean time between proton rearrangements is shorter close to the dislocation than the average in the lattice. This makes further quantification difficult, because in general models of dislocation cores are not good.

In chapter four, the concept of a critical stress intensity factor, K_{1c}, at a crack tip was discussed. It was shown that K_{1c} can only be defined if a true singularity exists at the crack tip. Wide scale creep would invalidate this assumption. By carrying out tests at high strain rates and low temperatures, it was possible to suppress

the creep. A value of K_{1c} of about 100 kN $m^{-3/2}$ was found from laboratory experiments. This agrees with the results of Liu and Loop (1976, personal communication). The corresponding value of the crack extension force, G, is about 3 J m^{-2}. This is considerably more than twice the surface energy (0.2 J m^{-2}) that the simple Griffith theory would predict, and suggests that some energy is lost in plastic work at the crack tip. The best way to examine the effect of creep at the crack tip is to determine the value of K_{1c} over as wide a temperature range as possible. The experiment could easily be done using the median crack test which was described in the chapter. It would also be fruitful to replicate the crack surfaces, and examine the surfaces in a scanning electron microscope. The appearance of the crack surface should suggest the microscopic processes occuring at the crack tip.

The ultimate goal is to combine the work presented in chapters two, three and four to produce a 'fracture map' (Ashby, personal communication). A fracture map is very similar to a deformation map but represents both the brittle and ductile mechanisms of failure.

Finally in Part II five field experiments were described. Wire strainmeters were successfully used to observe the bending of sea ice when waves pass underneath, to measure the surface strain rates on a glacier, and an ice cap, and to observe strain changes in the rock underneath a glacier.

The strain experiments were carried out with the dual aim of perfecting a new method for the rapid determination of surface strain rates, and to collect field data on the creep and fracture of ice. Interesting results, from the sea ice in particular, were obtained. Sea ice may be fatigued by the cycling action of waves (a wave with a 10 s period puts a million cycles into the sea ice in one season).

In December of this year, an array of strainmeters will be installed on Erebus Glacier Tongue, McMurdo Sound, Antarctica. The glacier is nearing the end of a thirty year cycle when 5-6 kms of ice will calve off the end. The glacier grows, gets too long, and then the seaward end breaks off (the glacier is floating). It is

hoped that sufficient data will be collected to deduce the forces the sea exerts on the glacier. If calving does subsequently occur, some knowledge of the way a large ice mass breaks up should be obtained.

Work continues on the action of sea waves on sea ice. The 1 m strainmeter described is operating in Newfoundland at this moment. It is hoped that by combining knowledge about the way sea ice fractures with an oceanographic model of what is happening under the ice to get some insight into the way waves break-up sea ice.

I hope the reader has enjoyed his perusal of my work. I have enjoyed writing the thesis. One does not find out how little one knows until forced to write about it. The work is open to the criticism that I have spread my interests too widely, and so cannot hope to understand any part of it in detail. However I have gained much by working between different disciplines, and hope my viewpoint is sufficiently different to have made some contribution to glaciology.

If nothing else (all research students reading this take heed) I have proved to my own satisfaction the law summarised in the quotation 'Work expands to fill the time available' (Parkinson).

ERTS 1 SATELLITE PICTURE

OF THE STAUNINGS ALPS

3RD SEPTEMBER 1972

Modern glaciology ?

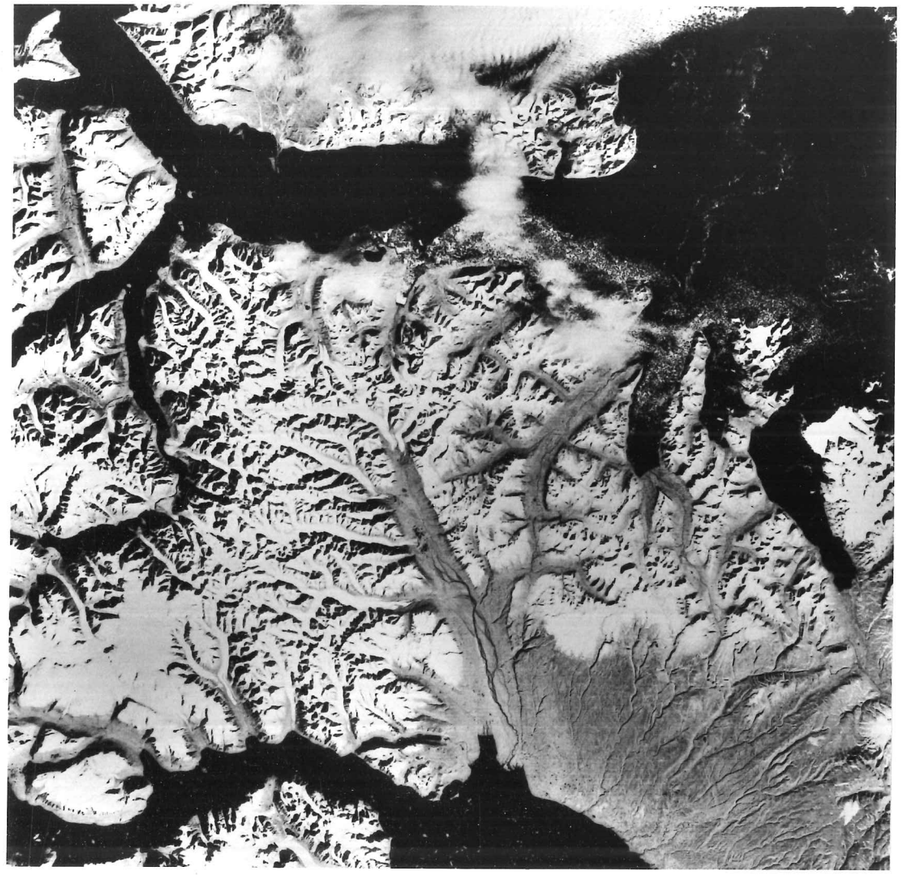

REFERENCES

REFERENCES

Allan, A.J., 1975, The breaking of sea ice by ocean waves. Scott Polar Research Institute Internal Report, p.1-12.

Ashby, M.F., 1972, A first report on deformation mechanism maps. Acta Met., Vol. 20, p.887-897.

Ashby, M.F. and Verrall, R.A., 1973, Diffusion accommodated flow and superplasticity. Acta Met., Vol. 21, p.149-163.

Atkins, A.G., Silvério, A., and Tabor, D., 1966, Indentation hardness and the creep of solids. J. Inst. Met., Vol. 94, p.369-378.

Barnes, P., 1968, Plastic flow, pressure melting, and other mechanisms in the deformation of ice 1. Unpublished Ph.D. thesis, University of Cambridge, p.1-173.

Barnes, P., Tabor, D., and Walker, J.C.F., 1971. The friction and creep of polyscystalline ice. Proc. Roy. Soc. Lond. A, Vol. 324, p. 127-155.

Beavan, R.J., 1976, Earth strain: ocean loading and analysis. Unpublished. Ph.D. thesis, University of Cambridge.

Bilham, R.G., 1970, The measurement of Earth strain. Unpublished Ph.D. thesis, University of Cambridge.

Bilham, R.G., and King, G.C.P., 1970, Strain-gauges for geophysics. XIIe Assemblée Générale de la Commission Séismologique Européenne Luxembourg, 21-29 Sept. 1970.

Bishop, J.F.W. and Hill, R., 1951. A theory of the plastic distortion of a polycrystalline aggregate under combined stresses. Phil. Mag. Ser. 7, Vol. 42, p.414-427.

Bocquet, G. and Ricq, J.C., 1977, Measurement of ice movement in subglacial cavities: a new cavitometer beneath the Glacier d'Argentière. J. Glaciol., Vol. 18, No. 78, p.137-142.

Blicks, H., Dengel, O., and Riehl, N, 1966, Diffusion von Protonen (Tritonen) in reinen und dotierten Eis-Einkristallin. Phys. Kondens. Mater, Vol. 4, p.375-381.

Bretschneider, D.L., 1963, A one-dimensional gravity wave spectrum. Proc. of Conf. on Ocean Wave Spectra. Pub. Prentice Hall. U.S. N.O.O. and Nat. Acad.Sci., Maryland, 1961.

British Standards Institute, 1971, Plane strain fracture toughness (K_{1c}) testing. Draft for Development, p.1-20.

Bromer, D.J. and Kingery, W.D., 1968. Flow of polycrystalline ice at low stresses and small strains. J. App. Phys., Vol. 39, No. 3, p.1688-1691.

References

Budd, W.F., 1966, The dynamics of the Amery Ice Shelf. J. Glaciol. Vol. 5, No. 45, p.335-338.

Budd, W.F., 1969, The dynamics of ice masses. ANARE Sci. Rep., Ser. A(1V) Glaciology, Pub. No. 108, p.1-216.

Budd, W.F., 1972, The development of crystal orientation fabrics in moving ice. Zeitschrift für Gletscherkunde, Bd. 8, Ht. 1-2, p.65-105.

Budd, W.F., Jenssen, D., and Radok, U., 1971, Derived physical characteristics of the Antarctic ice sheet. Melbourne, University of Melbourne, Meteorology Dept. Pub. No. 18.

Bullough, R., 1964, The cracked dislocation under tension. Phil. Mag., Ser. ', Vol. 9, p.917-925.

Burdekin, F.M. and Stone, D.E.W., 1966, J. Strain Analysis, Vol. 1, No. 2, p.145.

Butkovich, T.R., 1954. Hardness of single ice crystals. Snow, Ice and Permafrost Research Establishment (SIPRE) Res.Rep. 56.

Butkovich, T.R., 1956, Strength studies of sea ice. Snow, Ice and Permafrost Research Establishment (SIPRE) Res. Rep. 20, p.1-15.

Butkovich, T.R. and Landauer, J.K., 1960, Creep of ice at low stresses. Snow, Ice and Permafrost Research Establishment (SIPRE) Res. Rep. 72, p. 1-6.

Coble, R.L., 1963, A model for boundary diffusion controlled creep in polycrystalline materials. J.App. Phys., Vol. 34, No.6.

Colbeck, S.C. and Evans, R.J., 1969, Experimental studies related to the mechanics of glacier flow. Trend in Engineering, Vol. 21, No. 2, p.8-14.

Colbeck S.C. and Evans, R.J., 1971, Small-scale strain measurements on a glacier surface. J. Glaciol., Vol. 10, No. 59, p.237-243.

Dantl, G., 1968, Die elastischen Moduln von Eis-Einkristallen. Phys. Kondens. Materie, Vol. 7, p.390-397.

Dengel, O. and Riehl, N., 1963, Diffusion von Tritonen in NH_4F-dotierten Eis-Einkristallen. Phys. Kondens. Materie., Vol. 1, p.58-59.

Dillon, H.B., and Andersland, O.B., 1967, Deformation rates of polycrystalline ice. In: Physics of Snow and Ice (Ed. H. Ôura), Inst. Low Temperature Science, Hokkaido Univ., Sapporo, p 313-327.

Dorrer, E. 1971, Movement of the Ward Hunt Ice Shelf, Ellesmere Island, N.W.T., Canada. J. Glaciol. Vol. 10, No. 59, p.211-225.

Duval, P., 1972, Fluage et recristallisation dynamique de la glace polycristalline. Comp. Ren. Acad. Sci. Paris, T. 275, p337-339.

Evans, R.E., 1975, Spatial inhomogeneity of the Earth strain tide. Unpublished Ph.D. thesis, University of Cambridge.

Evans, K, Goodman, D.J. and Holdsworth, G., 1977, The installation of three continuously recording wire strainmeters on the Barnes Ice Cap, Baffin Island. to be submitted to J. Glaciol.

Fletcher, N.H., 1970, The Chemical Physics of Ice. p.1-271. Cambridge University Press.

Frank, F.C. and Nye, J.F., 1973, Hydrology of the intergranular veins in a temperate glacier. Symposium on the Hydrology of Glaciers, Cambridge 1969. I.A.S.H. Pub. No. 95, p.157-161.

Frost, H.J., Goodman, D.J., and Ashby, M.F., 1976, Kink velocities on dislocations in ice. A comment on the Whitworth, Paren and Glen model. Phil. Mag. Vol. 33, No. 6, p.951-961.

Fukuda, A. and Higashi A. X-ray diffraction topographical studies of the deformation behaviour of ice single crystals. Physics of Ice (Eds. N. Riehl, B. Bullemer, and H. Engelhardt), p239-250.

Fukuda, A. and Higashi, A., 1973, Dynamical behaviour of dislocations in ice crystals. Crystal Lattice Deffects, Vol. 4, No. 3.

Galloway, R.W., 1967, Mechanical measurement of glacier motion. J. Glaciol., Vol. 6, No. 48, p.805-816.

Gerard, V.B., 1971, An INVAR wire earth strainmeter. J. Phys. Earth: Sci. Instrum., Vol. 4, p. 689-692.

Glen, J.W., 1955, The creep of polycrystalline ice. Proc. Roy. Soc. A, Vol. 228, p. 519-538.

Glen, J.W., 1968a, The effect of hydrogen disorder on dislocation movement and plastic deformation of ice. Phys. Kond. Mater., Vol. 7, p.43-51.

Glen, J.W. 1968b., The importance of the hydrogen atom arrangement in determining how ice can deform plastically. Commission of Snow and Ice General Assembly, Bern, Sept.-Oct., 1967, p.352-355.

Glen, J.W., 1974, The Physics of Ice. U.S. Army Cold Regions Research and Engineering Laboratory, MonographII-C2a, p.1-79.

Gold, L.W., 1960, The cracking activity in ice during creep. Canadian J. Phys., Vol.38, p.1137-1148.

Gold, L.W., 1961, Formation of cracks in ice plates by thermal shock. Nature, Vol. 192, No. 4798, p.130-131.

Gold, L.W., 1963, Crack formation in ice plates by thermal shock. Canadian J. Phys., Vol. 41, p.1712-28.

Gold, L.W., 1965, The initial creep of columnar grained ice. Pt. I and Pt. II, Canadian J. Phys., Vol. 43, p.1414-34.

Gold, L.W., 1966, Dependence of crack formation on crystallographic orientation for ice. Canadian J.Phys., Vol. 44, p.3757-3764.

Gold, L.W., 1967, Time to formation of first cracks in ice. In: Physics of snow and ice (Ed. H. Oura) Inst. Low Temperature Science, Hokkaido University, Sapporo, p.359-370.

Gold, L.W., 1969, Crack formation in ice during creep. Scr. Met., Vol. 3, p.367-370.

Gold, L.W., 1972a, The process of failure of columnar-grained ice. Phil. Mag., Vol. 26, No. 2, p311-328.

Gold, L.W., 1972b, The failure process in columnar-grained ice. Nat.Res.Council of Canada, Div.BuildingResearch, NRCC 12637, p.1-108.

Gold, L.W., 1973, Activation energy for the creep of columnar-grained ice. In: Physics and Chemistry of Ice (Ed. E. Whalley, S.J. Jones, and L.W. Gold) p.362-364. Ottawa: Roy. Soc. Canada.

Goldthwait, R.P., 1973, Jerky glacier motion and melt water. Cambridge conference on Hydrology of Glaciers, IASH Pub. No. 95, p.183-188.

Goodman, D.J., Allan, A., and Bilham, R.G., 1975. Wire strainmeters on ice. Nature, Vol. 255, No.5503, p.45-46.

Goodman, D.J. and Neal, C., 1977, A 1 m strainmeter for use on sea ice. Scott Polar Research Institute Report III.

Gow, A.J., 1963, The inner structure of the Ross Ice Shelf at Little America V, Antarctica, as revealed by deep core drilling. General Assembly at Bern. IASH Pub. No. 61, p.272-284.

Gow, A.J., 1968, Preliminary results of studies of ice cores from the 2164 m deep drill hole, Byrd Station, Antarctica. ISAGE (Ed. A.J. Gow, C.Keeler, C.C. Langway and W.F. Weeks.) IASH Pub. No. 86, p.78-92.

Gow, A.J., 1970. Deep core studies of the crystal structure and fabrics of Antarctic glacier ice. U.S. Army Cold Regions Research and Engineering Laboratory Res. Rept. 282, p.1-20.

Gow, A.J. and Williamson, T., 1976, Rheological implications of the internal structure and crystal fabrics of the West Antarctic ice sheet as revealed by deep core drilling at Byrd Station. Geol. Soc. of Amer. Bull., Vol. 87, p.1665-1677.

Gow, A.J., Ueda, H.T. and Garfield, D.E., 1968, Antarctic ice sheet: Preliminary results of first core hole to bedrock. Science, Vol. 161, p.1011-1013.

Griffith, A.A., 1920, The phenomena of rupture and flow in solids. Phil. Trans. Roy. Soc. Lond. A. Vol. 221, p.1-163.

Guyot, P. and Dorn, J.E., 1967, A critical review of the Peierls Mechanism. Canadian J. Phys., Vol. 45, p983-1016.

Haefeli, R., Jaccard, D., and Quervain M. de, 1968, Deformation of polycrystalline ice under combined uniaxial and hydrostatic pressure. General Assembly at Bern. IASH Pub. 79.

Harper, J.G. and Dorn, J.E., 1957, Acta Met., Vol. 5, p. 654.

Hawkes, J. and Mellor M., 1972, Deformation and fracture of ice under uniaxial stress. J. Glaciol., Vol. 11, No. 61, p.103-131.

Herring, C., 1950. Diffusional viscosity of a polycrystalline solid. J. Appl. Phys., Vol. 21, p.437-445.

Higashi A. and Sakai, N., 1961, Movement of small angle boundary of ice crystal. J. Phys. Soc. Japan, Vol. 16, p.2359-2360.

Higashi, A., Mae S., and Fukuda, A., 1968, Strength of ice single crystals in relation to the dislocation structure. Int. Conf. Strength of Met. and Alloys, Tokyo, Japan. Sept., 1967., in Trans. Japan Inst. Met., Vol. 9, p.784-789.

Hirth, J.P. and Lothe, J., 1968, Theory of dislocations. McGraw-Hill, USA, p.1-780.

Hobbs, P.V., 1974, Ice physics. Oxford: Clarendon Press, p.1-837.

Holdsworth, G., 1975, Measurement of small strain-rates over short time periods. J. Glaciol., Vol. 14, No. 71, p. 317-328.

Hunkins, K., 1962, Waves on the Arctic Ocean. J. Geophys. Res., Vol. 67, No. 6, p.2477-2489.

Hutchinson, J.W., 1977, Creep and plasticity of hexagonal polcrystals as related to single crystal slip. Div. of Eng. and App. Phys., Harvard Univ., Cam., Mass. Rep. Mech. I, p.1-12.

Itagaki, K., 1966, Self-diffusion in ice single crystals. SIPRE, Res. Rep., No. 178, p.1-14.

Jaeger, J.C. and Cook, N.G.W., 1969, Fundamentals of Rock Mechanics. Science Paperbacks and Chapman and Hall, Lond., p1-515.

Johnston, W.G., 1962, Yield points and delay times in single crystals. J. App. Phys., Vol. 33, No. 9, p2716-2730.

Johnston, T.L. and Parker, E.R., 1957, Preliminary investigation of surface effects in flow and fracture. Min. Res. Lab. TR. Ser. 27, No. 16, Univ. of Cal., Berkeley, p.1-21.

Jones, D.R.H., 1973, The measurement of solid-liquid interfacial energies from the shapes of grain boundary grooves. Phil. Mag. Vol. 27, No. 3, p.569-584.

Jones, S.J. and Gilra, N.K., 1972, Increase of dislocation density in ice by dissolved hydrogen fluoride. App. Phys. Lett., Vol. 20, p.319-

Jones, S.J. and Gilra, N.K., 1973a, X-ray topographical study of dislocations in pure and HF doped ice. Phil. Mag., Vol. 27, No. 2, p.457-472.

Jones, S.J. and Gilra, N.K., 1973b, Dislocations in ice observed by X-ray topography. Physics and Chemistry of Ice (Ed. Whalley, Jones, S.J. and Gold, L.W.) Roy. Soc. Can.,Ottawa, p.344-349.

Jones, S.J. and Glen, J.W., 1968. The mechanical properties of single crystals of ice at low temperatures. Gen. Ass. Berne, IASH, Pub. 79, p.326-40.

Jones, S.J. and Glen, J.W., 1969a, The mechanical properties of single crystals of pure ice. J. Glaciol., Vol. 8, No. 54, p.463-473.

Jones, S.J. and Glen, J.W., 1969b, The effect of dissolved impurities on the mechanical properties of ice crystals. Phil. Mag. Vol. 19, No. 157, p.13-24.

Kamb, W.B., 1958, Theory of prefered crystal orientation developed by crystallization under stress. J. of Geology, Vol. 67, No. 2, p. 153-170.

Kamb, B., 1972, Experimental recrystallization of ice under stress. Geophys. Monograph Series, Vol. 16, (Ed. Heard, H.C., Borg, I.Y., Carter, N.L., and Raleigh, C.B.)

Kelly, A., 1966, Strong solids. Oxford Univ. Press.

Kelly, A., and Groves, G.W., 1970, Crystallography and crystal defects. Longman, London, p.1-428.

Kenny, P., and Campbell, J.D., 1967, Fracture toughness: an examination of the concept in predicting the failure of materials. Prog. in Mat. Sci., Vol. 13, No. 3., p.137-181.

Ketcham, W.M. and Hobbs, P.V., 1969, An experimental determination of the surface energies of ice. Phil. Mag., Vol. 19, p.1161-73.

King, G.C.P. and Bilham, R.G., 1973, Strain measurements instrumentation and technique. Phil. Trans. of the Roy. Soc. Lond., Ser. A, Vol. 274, p.209-17.

King, G.C.P. and Bilham, R., 1976, A geophysical wire strainmeter. Bull. Seism. Soc. of Amer., Vol. 66, No. 6, p2039-2047.

Kinsman, B., 1965, Wind waves. Pub. Prentice-Hall, NJ, p1-675.

Knott, J.F., 1973, Fundamentals of fracture mechanics. Butterworths, Lond. p.1-273.

Kocks, U.F., 1970, Met. Trans., Vol. 1, p1121.

Kocks, U.F., 1970, Polyslip in polycrystals. Acta. Met., Vol. 6, p.85-94.

Kocks, U.F., Argon, A.S., and Ashby, M.F., 1973, Thermodynamics and kinetics of slip. Progress in Materials Science, Vol. 19, p.1-262.

Kuon, L.G. and Jonas, J.J., 1973, Effect of strain rate and temperature on the microstructure of polycrystalline ice. Physics and Chemistry of Ice (Ed. E. Whalley, S.J. Jones, and L.W. Gold). Roy. Soc. Can. Ottawa, p.370-376.

Landau, L.D. and Lieshitz, E.M., 1959, Theory of elasticity. Pergamon, Oxford, p.1-165.

Langdon, T.G., 1973, Creep mechanisms in ice. Physics and Chemistry of Ice. (Ed. E. Whalley, S.J. Jones, and L.W. Gold). Roy. Soc. of Canada, Ottawa.

Lavrov, V.V., 1969, Deformation and strength of ice. Gidrometeorologicheskoe Izdatel'stvo, Leningrad, 1969 (Eng. transl. by Israel Prog. for Sci. Trans., Jerusalem).

Lawn, B.R. and Wilshaw, T.R., 1975, Fracture of brittle solids. C.U.P., p.1-204.

Le Schack, L.A. and Haubrich, R.A., 1964, Observations of waves on an ice-covered ocean. J. Geophys. Res., Vol. 69, No. 18, p.3815-3821.

Liebowitz, H. (Ed), 1969, Vol. I, Fracture, Academic Press, N.Y.

Liebowitz, H. (Ed), 1971, Vol. II, Fracture, Academic Press, N.Y.

Liebowitz, H. (Ed), 1972, Vol. VII, Fracture, Academic Press, N.Y.

Liu, H.W. and Loop, L.W., 1976, Fracture toughness of fresh-water ice. Personal Communication (may appear as CRREL report).

Lliboutry, L., 1975, Hydrol. Sci. Bull., XX, Vol. 3, No. 9, p.365-366.

Love, A.E.H., 1944, Mathematical theory of elasticity. Dover, N.Y. 4th Edition.

MacKeith, P., 1973, Cambridge and Imperial College expeditions to Greenland. Polar Record, Vol. 16, No. 103, p.580-81.

Maï, C., 1976, Physique des Solides - Etude de topographie X du comportement dynamique des dislocations dans la glace I_h. Comp. Rendu. Acad. Sci. Paris, T. 282, Séree B, p515-518.

McClintock F.A., and Argon, A.S., 1966, Mechanical Behaviour of Materials. Addison-Wesley, Ontario, p1-770.

Meier, M.F., Carel, J.E., Hoerni, J.A., Melbourne, W.G., Pines, C.J. and Walker, P.T., 1957, Preliminary study of crevasse formations, Blue Ice Valley, Greenland, 1955. SIPRE TR 38, No. 38, p.1-80.

Mellor, M., and Smith, J.H., 1966, Creep of snow and ice. CRREL RR 220, p.1-12.

Mellor, M. and Testa, R., 1969a, Effect of temperature on the creep of ice. J. Glaciol., Vol. 8, No. 52, p.131-152.

Mellor, M. and Testa, R., 1969b, Creep of ice under low stress. J. Glaciol., Vol. 8, No. 52, p.147-152.

Miller, K.J.M., 1974, Cambridge Staunings Expedition, 1972. Eng. Dept., Univ. Cam. Internal Reports.

Morgan, P.J., 1970, Ice surface movement in Marie Byrd Land. Ohio State Univ. Inst. of Pol. Stud. Report No. 38, p.1-43.

Muguruma, J. and Higashi, A., 1963, Observations of etch channels on the (0001) plane of ice crystals produced by non-basal glide. J. Phys. Soc. of Japan, Vol. 18, No. 9, p.1261-1269.

Nabarro, F.R.N., 1948, Report on the Bristol Conf. on the Strength of Solids. p.75.

Nakamura, T. and Jones, S.J., 1973, Mechanical properties of impure ice crystals. Physics of Ice, Ottawa. p.365-369.

Neave, K.G. and Savage, J.C., 1970, Icequakes on the Athabasca Glacier. J. Geophys. Res., Vol. 75, No. 8, p.1351-1362.

Nye, J.F., 1957, Physics of crystals. Oxford, Clarendon Press, p.1-322.

Nye, J.F., 1958, Surges in glaciers. Nature, Vol. 181, p.1450-1451.

Nye, J.F., 1970, Glacier sliding without cavitation in a linear viscous approximation. Proc. Roy. Soc. Lond. A., Vol. 315, p.381-403.

Onsager, L. and Runnels, L.K., 1969, Diffusion and relaxation phenomena in ice. J. Chem. Phys., Vol. 50, No. 3, p.1089-1103.

Paris, P. and Sih, G.C., 1965, Stress analysis of cracks. Fracture Toughness Testing, ASTM STP 381, Amer. Soc. Test. & Mat.

Parmeter, R.R., 1975, On the fracture of ice with part through cracks. AIDJEX Bull., No. 30, p.94-118.

Paterson, W.S.B., 1969, The physics of glaciers. Pergamon, p.1-250.

Perez, J., Tatibouët, J., Vassoike, R., and Gobin, P.F., 1975, Comportement dynamique des dislocations dans la glace. Phil. Mag., Vol. 31, p.985.

Raj, R. and Ashby, M.F., 1971, Grain boundary sliding and diffusional creep. Trans. Met. Soc. AIME, Vol. 2, p.1113.

Ramseier, R.O., 1967, Self-diffusion of tritium in natural and synthetic ice monocrystals. J. Appl. Phys., Vol. 38, No. 6, p2553-6.

References

Reynaud, L., 1975, Mouvements du glacier en surface sur une courte echelle de temps. Hydrological Sciences, Bull. 20, Vol. 3, No. 9, p.329-339.

Rice, J.R., 1968, Mathematical analysis in the mechanics of fracture. Fracture: an advanced treatise (Ed. H. Liebowitz, Vol. II, Acad. Press, N.Y.) p.191-311.

Rigsby, G.P., 1958, Effect of hydrostatic pressure on velocity of shear deformation of single ice crystals. J. Glaciol. Vol. 3, p. 273-278.

Rigsby, G.P., 1960, Crystal orientation in glacier and experimentally deformed ice. J. Glaciol, Vol. 3, No. 27, p.589-606.

Robin, G. de Q., 1963, Ocean waves and pack ice. Polar Record, Vol. 11, No. 73, p.389-393.

Robin, G. de Q., 1966, Wave propagation through fields of pack ice. Phil. Trans. Roy. Soc. Lond. Ser. A., Vol. 255, No. 1057, p.313-339.

Robin, G. de Q., 1976, Is the basal ice of a temperate glacier at the pressure melting point? J. Glaciol., Vol. 16, No. 74, p.183-195.

Rossiter, J.R., 1971, Long period sea waves: Seiches, surges and tides in coastal waters. Seiches in dynamic waves in civil engineering (Ed. Howells, D.A., Haigh, J.P., and Taylor, C.), Wiley Interscience, New York, p.155-168.

Schulz, H.H. and Knappwost, A., 1968, Die festkörperreibung des eises als relaxationseffekt. Wear, Vol. 11, p.3-20.

Schytt, V., 1958, C: The inner structure of the ice shelf at Ma dheim. Glaciology II: Norwegian-British-Swedish Antarctic Expedition, 1949-52. Sci. Res., Vol. 4, Norsk Polarinstitut, Oslo, p.181.

Shumskiy, P.A., 1958, The mechanism of ice straining and its recrystallisation. IUGG, IASH, Chamonix Sym., Pub. 47, p.244-248.

Sih, G.C., 1973, Handbook of stress intensity factors for researchers and engineers. Inst. of Fracture and Solid Mechanics, Lehigh Univ., Penn., USA.

Shirnov, V.N. and Lin'Kov, E.M., 1971, Studies in ice physics and ice engineering, Ed. G.N. Yakovler. Gidrometeorologicheskoe Izdatel'stvo, Leningrad.

Smith, R.A., 1976, The application of fracture mechanics to the problem of crevass penetration. J. Glaciol., Vol. 17, No. 76, p.223-28.

Squire, V., 1978, Ph.D. thesis, to be completed. University of Cambridge

Steinemann Von S., 1958, Experimentelle untersuchungen zur plastizität von eis. Beiträge zur Geologie der Schweiz. Hydrologie Nr. 10. p.1-70.

References

Stroh, A.N., 1954, The formation of cracks as a result of plastic flow. Proc. Roy. Soc. A., Vol. 223, p.404-414.

Sydenham, P., 1969, A tensioned wire strainmeter. J. Phys. Earth: Sci. Instrum. Ser. 2, Vol. 2, p.1095-1097.

Sytinskiy, A.D. and Tripol'nikov, V.P., 1964, Some results of investigations of the natural vibrations of ice fields of the central Arctic. Izv. Acad. Nank. SSSR, Ser. Geofiz., Vol. 4, p.615-621.

Swain, M.V. and Lawn, B.R., 1976, Indentation fracture in brittle rocks and glasses. Martin Marietta Laboratories, Tech. Rep. 75-12C, p.1-29.

Tabor, D., 1951, The hardness of metals. Oxford Univ. Press.

Tabor, D., 1970, The hardness of solids. Reviews in Physics in Technology, Vol. 1, No. 3, p.145.

Taylor, G.I., 1956, Strains in crystalline aggregates. Proc. of Coll. on Deformation and Flow of Solids, Madrid, 1955. Berlin: Springer, 1956, p.3-12.

Tegart, W.J. McG., 1964, Non-basal slip as a major deformation process in the creep of polycrystalline ice. J. Glaciol., Vol. 5, p.251-254.

Theakstone, W.H., 1967, Basal sliding and movement near the margin of the glacier Østerdalsisen, Norway. J. Glaciol., Vol. 6, No. 48, p.805-816.

Thomas, R.H., 1973a, The creep of ice shelves: interpretation of observed behaviour. J. Glaciol., Vol. 12, No. 64, p.55-70.

Thomas, R.H., 1973b, The creep of ice shelves: theory. J. Glaciol., Vol. 12, No. 64, p.45-53.

Turner, C.E., 1975, Yielding fracture mechanics. J. Strain Analysis, Vol. 10, No. 4, p.207-216.

Van Wormer, D. and Berg, E., 1973, Seismic evidence for glacier motion. J. Glaciol., Vol. 12, No. 65, p.259-265.

Vivian, R., 1975, Les glaciers des Alpes Occidentales. Pub. Allier, Grenoble, p.1-513.

Vivian, R. and Bocquet, G., 1973, Subglacial cavitation phenomena under the Glacier d'Argentière, Mont Blanc, France. J. Glaciol., Vol. 12, p.439-51.

Wadhams, P. 1973a, Attenuation of swell by sea ice. J. Geoph. Res., Vol. 78, No. 18, p.3552-3563.

Wadhams, P., 1973b, The effect of a sea ice cover on ocean surface waves. Unpublished, Ph.D. thesis, Univ. of Cambridge.

Wakahama, G., 1964, On the plastic deformation of ice V. Plastic deformation of polycrystalline ice (In Japanese with English summary). Low Temp. Sci., Ser. A., Vol. 22, p.1-24.

Walker, J.C.E., 1970, The mechanical properties of ice at high homologous temperatures. Unpublished. Ph.D. thesis, Univ. of Cambridge.

Warner, G. and Cloud, G., 1974, Measurement of surface strain rates in glaciers using embedded wire strain gauges. Proc. of Third SESA Int. Congress on Experimental Mechanics, Los Angeles, Ca., May, 1973. Experimental Mechanics, Vol. 14, No. 1, p.24-28.

Watanabe, O., and Ôura, H., 1968, Experimental studies on orientation of polycrystalline ice by unconfined compression. Low Temp. Sci., Ser. A., No. 26, p.1-28 (in Japanese with extended English summary).

Weaver, C.S., and Malone, S.D., 1976, Mt. St. Helens seismic events: volcanic earthquakes or glacial noises. Geophs. Res. Letts., Vol. 3, No. 3, p.197-200.

Webb, W.W. and Hayes, C.E., 1967, Dislocation and plastic deformation of ice. Phil. Mag., Vol. 16, p.909-25.

Weeks, W.F. and Assur, A., 1967, The mechanical properties of sea ice. Cold Regions Research Engineering Laboratory, Rep. II-C3, p.1-80.

Weertman, J., 1957, Deformation of floating ice shelves. J. Glaciol., Vol. 3, p.38-42.

Weertman, J., 1963, The Eshelby-Schoek viscous dislocation damping mechanism applied to the steady-state creep of ice. Ice and Snow (Ed. W.D. Kingery), MIT Press.

Weertman, J., 1969, The stress dependence of the secondary creep rate at low stresses. J. Glaciol., Vol. 8, No. 54, p.494-5.

Weertman, J., 1973, Creep of ice. Physics and Chemistry of Ice. Ed. E. Whalley, S.J. Jones and L.W. Gold. Roy. Soc. of Canada, Ottawa, p.320-337.

Weertman, J., 1977, Penetration depth of closely spaced water free crevasses. J. Glaciol., Vol. 18, No. 78, p.37-46.

Whitworth, R.W., Paren, J.G., and Glen, J.W., 1976, The velocity of dislocations in ice - a theory based on proton disorder. Phil. Mag. Vol. 33, p.409-426.

Wu, H.C., Chang, K.J. and Schwarz, J., 1976, Fracture in the compression of columnar grained ice. Eng. Fract. Mech., Vol. 8, p.365-372.

PLATES

I

A MODEL OF AN ICE 1_h LATTICE

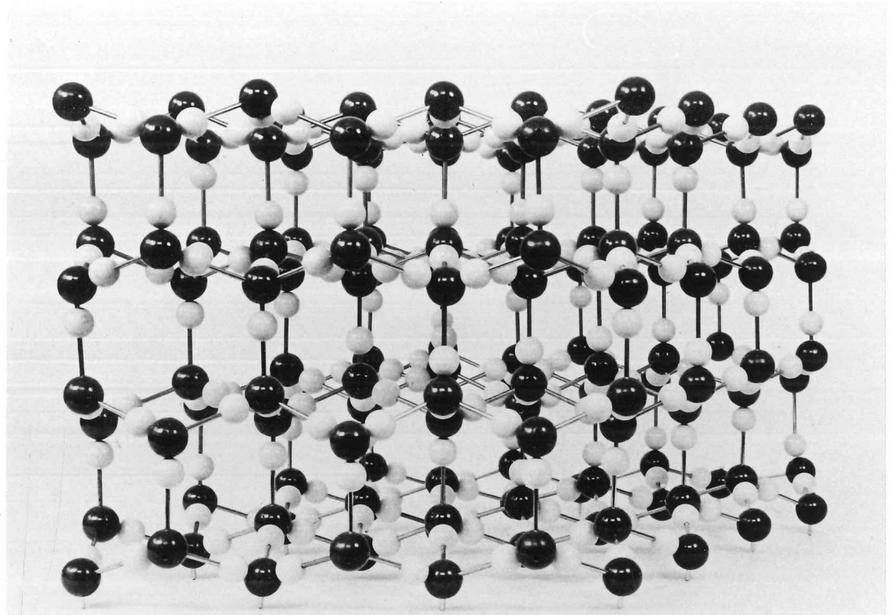

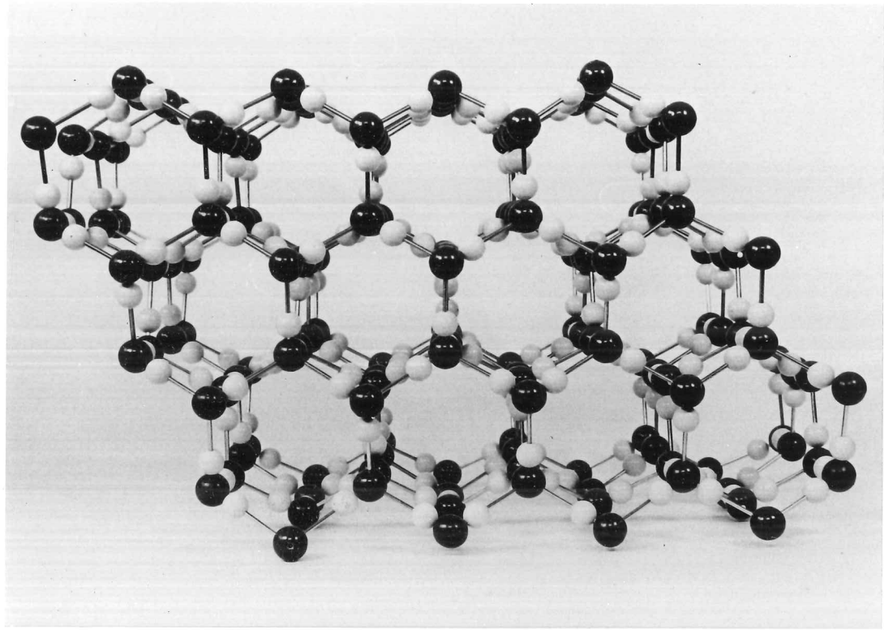

II

FRACTURE APPARATUS

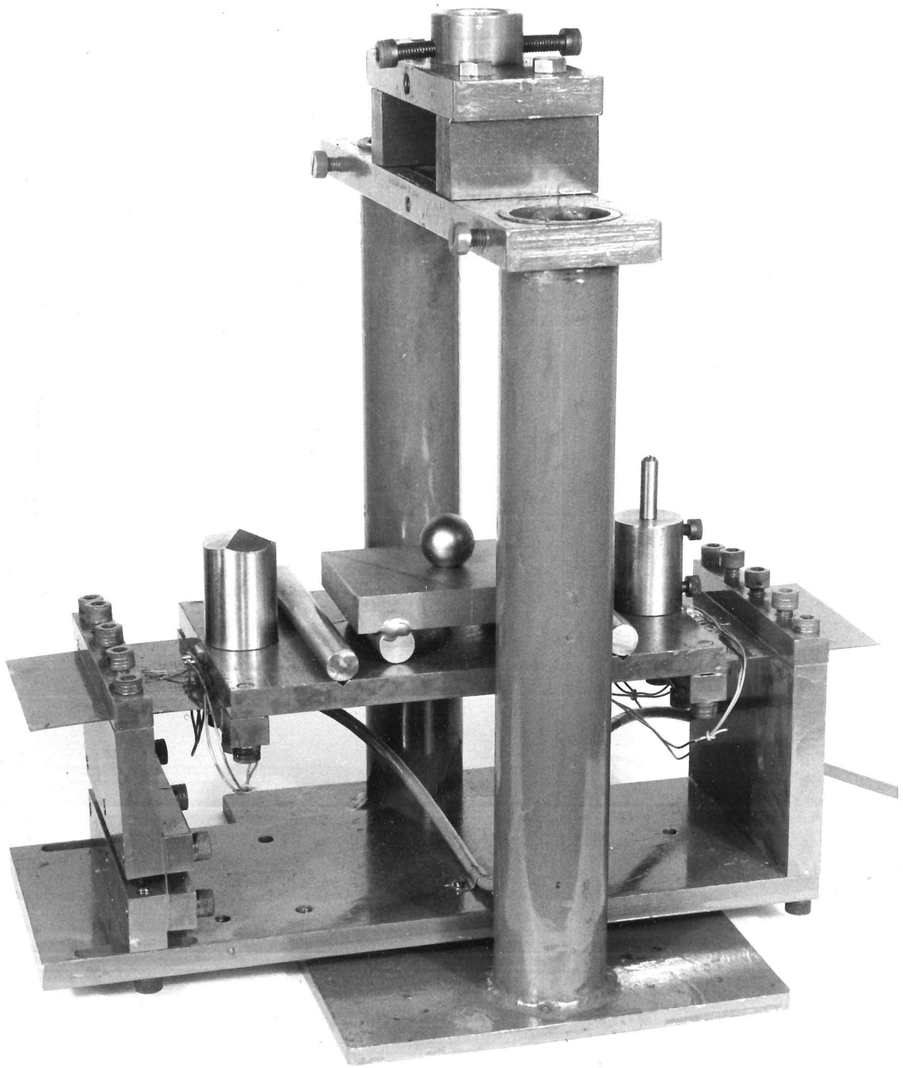

III

THE WIRE STRAINMETER INSTALLED ON A GLACIER

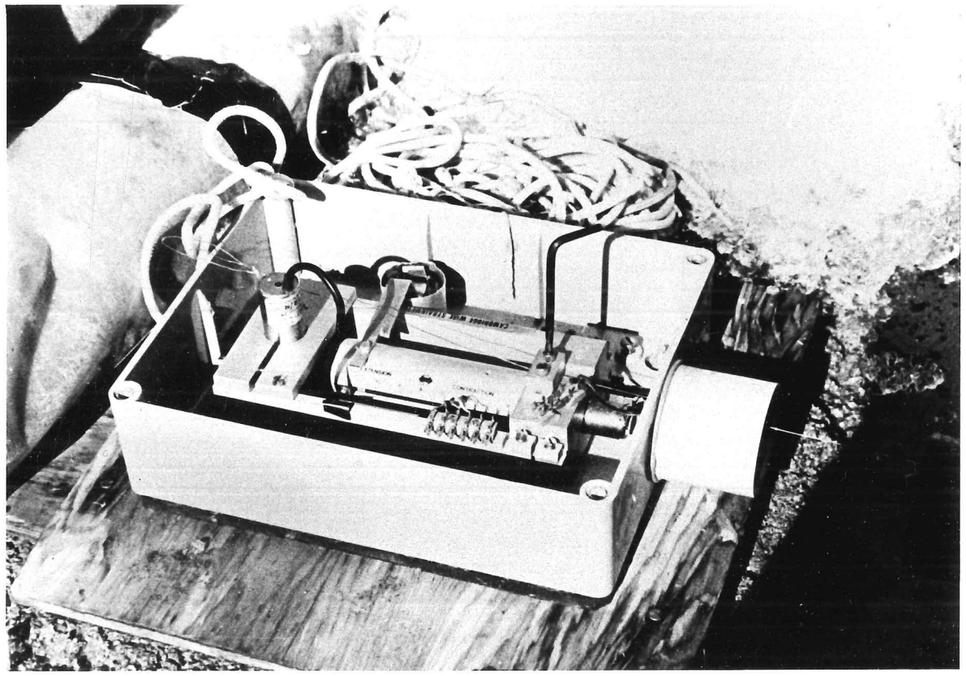

IV

THE 1 m STRAINMETER ON SOME SEA ICE NEAR THE NORTH POLE

HMS SOVEREIGN IN THE BACKGROUND

V

A STRAINMETER INSTALLED ON

THE FLOOR OF A TUNNEL IN ARGENTIÈRE